In compliance with the
Canadian Privacy Legislation
some supporting forms
may have been removed from
this dissertation.

While these forms may be included
in the document page count,
their removal does not represent
any loss of content from the dissertation.

UNIVERSITY OF ALBERTA

Numerical Modelling of the Evolution of Oblate Hailstones in Alberta Storms

by

Colleen Gayle Ranger ©

A thesis submitted to the Faculty of Graduate Studies and Research in partial fulfillment of the requirements for the degree of Master of Science

Department of Earth and Atmospheric Sciences

Edmonton, AB

Fall 2003

National Library
of Canada

Acquisitions and
Bibliographic Services

395 Wellington Street
Ottawa ON K1A 0N4
Canada

Bibliothèque nationale
du Canada

Acquisisitons et
services bibliographiques

395, rue Wellington
Ottawa ON K1A 0N4
Canada

Your file Votre référence
ISBN: 0-612-87865-1
Our file Notre référence
ISBN: 0-612-87865-1

The author has granted a non-exclusive licence allowing the National Library of Canada to reproduce, loan, distribute or sell copies of this thesis in microform, paper or electronic formats.

L'auteur a accordé une licence non exclusive permettant à la Bibliothèque nationale du Canada de reproduire, prêter, distribuer ou vendre des copies de cette thèse sous la forme de microfiche/film, de reproduction sur papier ou sur format électronique.

The author retains ownership of the copyright in this thesis. Neither the thesis nor substantial extracts from it may be printed or otherwise reproduced without the author's permission.

L'auteur conserve la propriété du droit d'auteur qui protège cette thèse. Ni la thèse ni des extraits substantiels de celle-ci ne doivent être imprimés ou aturement reproduits sans son autorisation.

Canada

UNIVERSITY OF ALBERTA

LIBRARY RELEASE FORM

Name of Author: Colleen Gayle Ranger

Title of Thesis: Numerical Modelling of the Evolution of Oblate Hailstones in Alberta Storms

Degree: Master of Science

Year this Degree Granted: 2003

Permission is hereby granted to the University of Alberta Library to reproduce single copies of this thesis, and to lend or sell such copies for private, scholarly, or scientific purposes only.

The author reserves all other publication and other rights in association with the copyright in the thesis, and except as hereinbefore provided, neither the thesis nor any substantial portion thereof may be printed or otherwise reproduced in any material form whatever without the author's prior written permission.

Aug. 26/03

UNIVERSITY OF ALBERTA

FACULTY OF GRADUATE STUDIES AND RESEARCH

The undersigned certify that they have read, and recommended to the Faculty of Graduate Studies and Research for acceptance, a thesis entitled *Numerical Modelling of the Evolution of Oblate Hailstones in Alberta Storms* submitted by Colleen Gayle Ranger in partial fulfillment of the requirements for the degree of Master of Science.

A. B. G. Bush

Approved: 25 August '2003

ABSTRACT

The mass growth and heat budget equations of a hailstone model were extended to allow for oblate forms with a rough surface. This hail growth model was coupled with a one-dimensional steady-state cloud model to predict the maximum hail size for Alberta hailstorms. Model runs were initialized with proximity soundings recorded during the Alberta Hail Project (AHP) area for the summers of 1983, 1984 and 1985.

The results showed that oblateness of stones can be included with virtually no additional computational resources. Comparing model sizes of typically oblate hailstones with spherical ones indicates that the oblateness added about 10% to final hailstone equivalent diameter. In general, we found a monotonic relationship between hail size and oblateness. The effects of hailstone surface roughness were comparable to those of hailstone oblateness. Comparison of model predicted hail sizes with AHP surface observations suggests that the model for rough oblate stones is suited to assist in forecasting maximum hail sizes.

TABLE OF CONTENTS

Page

1 INTRODUCTION 1

1.1 Hailstones and Models 1
1.2 Oblate Hailstones 2
1.3 Theory of Hail Growth and Growth Environment 4
1.4 Numerical Hail Models 8
1.5 The Alberta Hail Project 10
1.6 Statement of Research Objectives 12

2 MODEL DESCRIPTION 15

2.1 Introduction 15
2.2 The Hail Model 15
2.3 The Cloud Model 29
2.4 Coupling the Microphysical Model with the Cloud Model 30
2.5 Choice of Initial Embryo Diameter 31

3 DEPENDENCE OF MICROPHYSICAL PARAMETERS ON DEGREE OF OBLATENESS 33

3.1 Introduction 33
3.2 Terminal Velocity 35
3.3 Mass Growth Rate 36
3.4 Heat Transfer 39
3.5 Summary 41

4 MODELLING THE EFFECTS OF OBLATENESS 42

4.1 Introduction 42
4.2 11 July 1985 42
4.3 6 July 1984 48
4.4 Effects of Oblateness on 20 Severe Hail Days 54
4.5 Effects of Aspect Ratio on Model Output 56
4.6 Summary 58

5 EFFECTS OF ROUGHNESS AND FACTOR SEPARATION ANALYSIS 59

5.1 Introduction 59
5.2 Simulating the Evolution of a Smooth-Surfaced Hailstone 60

5.3 The Factor Separation Method 64
5.4 Factor Separation Analysis for the Case Study Days 65
5.5 Factor Separation Analysis for 20 Severe Hail Days 67
5.6 Summary 70

6 MODEL SENSITIVITY AND OTHER CONSIDERATIONS 71

6.1 Hail Model Sensitivity Tests 71
6.2 Cloud Model Sensitivities and Considerations 79
6.3 Summary and Discussion 82

7 EVALUATION OF THE MODEL PREDICTED MAXIMUM HAIL SIZE 85

7.1 Introduction 85
7.2 Assigning Size Categories to Oblate Hailstones 85
7.3 Forecast Skill Scores 87
7.4 Summary 91

8 CONCLUSIONS AND SUGGESTIONS FOR FUTURE WORK 92

8.1 Conclusions 92
8.2 Suggestions for Future Work 94

REFERENCES 97

APPENDIX A: List of Symbols 109

APPENDIX B: Deriving the Rate of Change of the Major Diameter of a Growing Hailstone 112

APPENDIX C: Deriving the Nusselt and Sherwood Numbers 114

APPENDIX D: Selection of Embryo Diameter for Severe Hail Days 117

APPENDIX E: Dependence of Collection Efficiency and the Onset of Shedding on Aspect Ratio 118

APPENDIX F: Forecast Skill Scores 123

FIGURES 124

TABLES 142

LIST OF TABLES

Table **Page**

4.1 Observed cloud parameters and maximum observed hail size along with cloud and hail model output from the control runs for our two case study days: 11 July 1985 and 6 July 1984. 142

4.2 Differences between the final maximum equivalent hailstone diameter (D_{eq}) and total growth time (τ) predicted by the oblate model (designated by D_{eq} and τ, respectively) and the corresponding parameters predicted by the model if the hailstone is assumed to remain spherical (designated by D_S and τ_S, respectively). The percent increases in equivalent diameter, total growth time, and kinetic energy (based on $\mathrm{K.E.} \propto \mathrm{D}_{\mathrm{eq}}^{4}$) are also shown. These percent increases are calculating by taking the differences between the oblate and spherical results and dividing by the spherical value. 143

4.3 Final equivalent diameter (D_{eq}) at ground and total evolution time (τ) as a function of minimum aspect ratio (α_c) for (a) 11 July 1985 and (b) 6 July 1984. Also shown are the percent increase in D_{eq} compared to that of the final diameter attained by a spherical hailstone ($\%\mathrm{D}_{\mathrm{eq}} = (\mathrm{D}_{\mathrm{eq}}(\alpha_{\mathrm{c}}) - \mathrm{D}(\alpha = 1))/\mathrm{D}(\alpha = 1)$), the percent increase in τ compared to that of the growth time of a spherical hailstone ($\%\tau = (\tau(\alpha_{\mathrm{c}}) - \tau(\alpha = 1))/\tau(\alpha = 1)$), and the percent increase in kinetic energy (K.E.) compared to that of a spherical hailstone, assuming $\mathrm{K.E.} \propto \mathrm{D}_{\mathrm{eq}}^{4}$. Control values are in boldface. 144

4.4 Average final equivalent diameter at ground ($<D_{eq}>$) and average total evolution time ($<\tau>$) as a function of minimum aspect ratio (α_c) for all 20 severe hail days from 1983 to 1985. Also shown are the average percent increase in D_{eq} compared to that of the final diameter attained by a spherical hailstone ($\langle \%\mathrm{D}_{\mathrm{eq}} \rangle = \langle (\mathrm{D}_{\mathrm{eq}}(\alpha_{\mathrm{c}}) - \mathrm{D}(\alpha = 1))/\mathrm{D}(\alpha = 1) \rangle$) and the average percent increase in τ compared to that of the growth time of a spherical hailstone ($\langle \%\tau \rangle = \langle (\tau(\alpha_{\mathrm{c}}) - \tau(\alpha = 1))/\tau(\alpha = 1) \rangle$). The average percent increase in kinetic energy, K.E., has also been calculated (in the same manner as the other averages) assuming $\mathrm{K.E.} \propto \mathrm{D}_{\mathrm{eq}}^{4}$. Control values are in boldface. 144

5.1 Comparison of selected results for experiments *RO*, *SO*, *RS* and *SS*. Final equivalent diameter (D_{eq}) and total growth time (τ) are shown for the two case study days (11 July 1985 and 6 July 1984). 145

5.2 Contributions of the total effect, the effect of roughness, the effect of oblateness, and the mutual interaction effect towards the final maximum equivalent diameter (D_{eq}) of a hailstone for each of the 20 severe hail days between 1983 and 1985. Values are in percentages and were derived using the factor separation technique. The averages of each of the four effects for all 20 severe hail days are also shown. 145

5.3 Contributions of the total effect, the effect of roughness, the effect of oblateness, and the mutual interaction effect towards the total growth time (τ) of a hailstone for each of the 20 severe hail days between 1983 and 1985. Values are in percentages and were derived using the factor separation technique. The averages of each of the four effects for all 20 severe hail days are also shown. 146

6.1 Sensitivity experiments showing the effect of changing the major diameter at which the hailstone's aspect ratio begins to decrease (D_1) and the major diameter beyond which the hailstone's aspect ratio remains constant at 0.77 (D_2) for each of two severe hail days: 11 July 1985 and 6 July 1984. The averages for all severe hail days are also shown. Control values are in boldface. 147

6.2 Sensitivity experiments showing the effect of varying the collection efficiency of ice (E_i) on final equivalent diameter (D_{eq}) and total growth time (τ) of an average oblate hailstone for the two case study days (11 July 1985 and 6 July 1984) and for the averages of all severe hail days. Control values are highlighted in boldface. 147

6.3 Sensitivity experiments showing the effect of varying the median volume cloud droplet radius (r_d) on final equivalent diameter (D_{eq}) and total growth time (τ) of an average oblate hailstone for the two case study days (11 July 1985 and 6 July 1984) and for the averages of all severe hail days. Control values are highlighted in boldface. 148

6.4 Sensitivity experiments showing the effect of varying the hailstone ice density (ρ_H) on final equivalent diameter (D_{eq}) and total growth time (τ) of an average oblate hailstone for the two case study days (11 July 1985 and 6 July 1984) and for the averages of all severe hail days. Control values are highlighted in boldface. 148

6.5 Sensitivity experiments showing the effect of varying the initial embryo diameter (D_0) on final equivalent diameter (D_{eq}) and total growth time (τ) of an average oblate hailstone for the two case study days (11 July 1985 and 6 July 1984) as well as for 28 July 1984. The chosen control values for each case are highlighted in boldface. The embryo diameter for each severe hail day was chosen to both maximize final equivalent diameter while minimizing total growth time. 148

6.6 Comparison of the final diameter at ground (D), hailstone size category and total growth time (τ) for (spherical) hailstones evolving under the HAILCAST shedding and terminal velocity schemes and for spherical hailstones evolving under the HC2 shedding and terminal velocity schemes. All HC2 runs were done using the control parameter values for HAILCAST in order to facilitate easy comparison. The observed hail size category and corresponding representative diameter are also shown for each severe hail day. (P = PEA, GR = GRAPE, W = WALNUT, G = GOLFBALL, >G = >GOLFBALL). 149

6.7 The difference in final hail diameter and total growth time of the HC2 and HAILCAST terminal velocity/shedding schemes. The abbreviation H2 refers to HC2 predictions and H1 refers to HAILCAST predictions. Also shown are the percent increases in final diameter and total growth time when our model (HC2) is used compared with the original HAILCAST. The averages for all 20 severe hail days are shown, and our case study days are highlighted in boldface. 150

7.1 Fractional difference, f_D, between a hailstone's major diameter and its equivalent diameter, as a function of aspect ratio, α. 151

7.2 Differences in hailstone size category that result when major diameter, *D*, is used to classify hailstones instead of equivalent diameter, D_{eq}. For an oblate hailstone with an aspect ratio of 0.77 and for one with an aspect ratio of 0.50, the major diameter is calculated for hailstones with equivalent diameters that represent the average of each size category, and then again for those with equivalent diameters that represent the upper limit of each size category. Then, a new size category is assigned to each oblate hailstone, based on its major diameter. 151

7.3 Summary of maximum equivalent diameter at ground predicted by the spherical and oblate versions of HC2 compared to the actual size categories (given as ranges of equivalent diameter values in cm) observed on the 20 severe hail days between 1983 and 1985. 152

7.4 2 × 2 contingency tables used to derive the skill scores of hail forecasts for the oblate and spherical versions of HC2 for 62 hail days. 152

7.5 Skill scores the HC2 spherical and oblate hail models for 62 hail days and for 20 severe hail days between 1983 and 1985. 152

7.6 Hail-size forecast performance of the HC2 spherical and oblate model versions for 62 hail days and 20 severe hail days between 1983 and 1985. 153

LIST OF FIGURES

Figure **Page**

1.1 Schematic diagram of a smooth, oblate hailstone, presented from two different views: looking down its minor axis (left) and looking along its major axis (right). The length of its minor axis is its minor diameter, D_{min}, and the length of its major axis is its major diameter, D. 124

1.2 Sample of walnut-sized hailstones from a storm on 19 July 2002 near Eckville, AB (courtesy of J. Brimelow). Notice the oblate hailstone next to the bottom right of the knife (this hailstone is viewed looking along its major diameter). 124

1.3 The Alberta Hail Project's principal target area between Edmonton and Calgary and centred on the radar site located at the Red Deer Industrial Airport. 125

2.1 Schematic diagram of the tumbling motions of an oblate hailstone. The view of the hailstone is looking down its major axis (i.e. a "side view"), and is falling in the negative Z direction. The oblate hailstone spins about its minor axis (labelled "spin axis"), which in turn precesses/nutates, describing a horizontal (circular) cone ("gyration cone") with its apex located at the centre of the particle. Adapted from García-García and List (1992). 126

3.1 Ratio of terminal velocity of an oblate hailstone to that of a spherical hailstone of the same mass. 127

3.2 Ratio of the mass growth rate of an oblate hailstone to that of a spherical hailstone. Calculations are done for 3 cases: 1) Collection efficiency is constant (this case occurs when the hailstone is in a region where all cloud water is in the form of ice); 2) The hailstone is in a region where there is no cloud ice present and is not shedding (it may be undergoing either wet or dry growth); 3) The hailstone is assumed to be in the wet shedding growth regime, and there is no cloud ice present. In case 3, the following ambient conditions are assumed: $T_a = -15°\text{C}$, $\rho_a = 0.6$ kg m^{-3}, $\chi_w = 6$ g m^{-3}. The hailstone for which this calculation is done (case 3) is assumed to have a density of 900 kg m^{-3} and a mass of 3.77 g. 127

3.3 Ratio of rate of heat transfer by convection/conduction of an oblate hailstone to that of a spherical hailstone of the same mass. 128

4.1 Upper-air sounding released from Penhold at 1715 LT on 11 July 1985 plotted on a tephigram. The dashed line represents the dewpoint profile, the solid line is the environmental temperature, and the curved solid line is the pseudoadiabat (based on the observed surface temperature and dewpoint). 129

4.2 Upper-air sounding released from Penhold at 1715 LT on 6 July 1984 plotted on a tephigram. The dashed line represents the dewpoint profile, the solid line is the environmental temperature, and the curved solid line is the pseudoadiabat (based on the observed surface temperature and dewpoint). 129

4.3 Model derived profiles of updraft velocity for 11 July 1985 (solid line) and 6 July 1984 (dashed line). 130

4.4 Model derived profiles of liquid water content (LWC) for 11 July 1985 (solid line) and 6 July 1984 (dashed line). 130

4.5 Growth time history of an oblate hailstone on 11 July 1985 for 3 different aspect ratios: $\alpha_c = 1$ (dotted line), $\alpha_c = 0.77$ (heavy black line), and $\alpha_c = 0.50$ (dash-dotted line). Depicted are (a) Height (Z); (b) Hailstone temperature (T_S); (c) Equivalent diameter (D_{eq}); (d) Mass growth rate (dM/dt); (e) Terminal velocity ($V_{T)}$; (f) Growth regime (1 = dry, 2 = wet, 3 = wet shedding). 131

4.6 Growth time history of an oblate hailstone on 6 July 1984 for 3 different aspect ratios: $\alpha_c = 1$ (dotted line), $\alpha_c = 0.77$ (heavy black line), and $\alpha_c = 0.50$ (dash-dotted line). Depicted are (a) Height (Z); (b) Hailstone temperature (T_S); (c) Equivalent diameter (D_{eq}); (d) Mass growth rate (dM/dt); (e) Terminal velocity ($V_{T)}$; (f) Growth regime (1 = dry, 2 = wet, 3 = wet shedding). 132

4.7 Percent increase in final equivalent diameter (a) and total growth time (b) as a function of aspect ratio for the two case study days: 11 July 1985 (crosses) and 6 July 1984 (diamonds). The corresponding average percent increases for all 20 severe hail days (triangles) are also shown. 133

5.1 Nusselt number as a function of Reynolds number for 4 different types of hailstones: a rough oblate (RO) hailstone ($\alpha = 0.77$), a smooth oblate (SO) hailstone ($\alpha = 0.77$), a rough spherical (RS) hailstone and a smooth spherical (SS) hailstone. A Reynolds number of 10000 corresponds to an equivalent diameter of 1.2 cm for an ambient temperature of - 15°C, while a Reynolds number of 60000 corresponds to an equivalent diameter of 3.7 cm for the same ambient temperature. 134

5.2 Growth time history of an oblate hailstone on 11 July 1985 for 4 cases: rough oblate (heavy solid line), rough spherical (dotted line), smooth oblate (dash-dotted line) and smooth spherical (dashed line). Depicted are (a) Height (Z); (b) Hailstone temperature (T_S); (c) Equivalent diameter (D_{eq}); (d) Mass growth rate (dM/dt); (e) Terminal velocity ($V_{T)}$; (f) Growth regime (1 = dry, 2 = wet, 3 = wet shedding). For the oblate cases, hailstones are assumed to evolve to a constant aspect ratio of 0.77. 135

5.3 Growth time history of an oblate hailstone on 6 July 1984 for 4 cases: rough oblate (heavy solid line), rough spherical (dotted line), smooth oblate (dash-dotted line) and smooth spherical (dashed line). Depicted are (a) Height (Z); (b) Hailstone temperature (T_S); (c) Equivalent diameter (D_{eq}); (d) Mass growth rate (dM/dt); (e) Terminal velocity ($V_{T)}$; (f) Growth regime (1 = dry, 2 = wet, 3 =wet shedding). For the oblate cases, hailstones are assumed to evolve to a constant aspect ratio of 0.77. 136

6.1 Aspect ratio as a function of hailstone major diameter for control values of $D_1 = 1$ cm, $D_2 = 2$ cm and $a_c = 0.77$. 137

6.2 Growth time history of an average oblate hailstone on 28 July 1984 for 2 different embryo diameters: $D_0 = 400$ μm (dotted line) and $D_0 = 700$ μm (solid line). Depicted are (a) Height (Z); (b) Hailstone temperature (T_S); (c) Equivalent diameter (D_{eq}); (d) Mass growth rate (dM/dt); (e) Terminal velocity ($V_{T)}$; (f) Growth regime (1 = dry, 2 = wet, 3 = wet shedding). 138

6.3 Growth time history of an oblate hailstone on 28 July 1984 for 3 different aspect ratios: $a_c = 1$ (dotted line), $a_c = 0.77$ (heavy black line), and $a_c = 0.50$ (dash-dotted line). Depicted are (a) Height (Z); (b) Hailstone temperature (T_S); (c) Equivalent diameter (D_{eq}); (d) Mass growth rate (dM/dt); (e) Terminal velocity ($V_{T)}$; (f) Growth regime (1 = dry, 2 = wet, 3 = wet shedding). The embryo diameter is 400 μm and the storm duration is 60 minutes. 139

6.4 Growth time history of an oblate hailstone on 28 July 1984 for 3 different aspect ratios: $a_c = 1$ (dotted line), $a_c = 0.77$ (heavy black line), and $a_c = 0.50$ (dash-dotted line). Depicted are (a) Height (Z); (b) Hailstone temperature (T_S); (c) Equivalent diameter (D_{eq}); (d) Mass growth rate (dM/dt); (e) Terminal velocity (V_T); (f) Growth regime (1 = dry, 2 = wet, 3 = wet shedding). The embryo diameter is 700 μm and the storm duration is 60 minutes. 140

7.1 Summary of skill scores for the spherical and oblate versions of HC2 for 62 hail days ("All") and 20 severe hail days ("Severe") between 1983 and 1985. 141

1 INTRODUCTION

1.1 Hailstones and Models

Precipitation occurs in various forms, including drizzle, raindrops, snowflakes, ice pellets, graupel and freezing rain. High-density ice particles that are 5 mm or more in diameter are referred to as hailstones. Small hailstones are usually spherical with relatively smooth surfaces. However, as hailstones grow larger, they tend to develop different shapes and rough surfaces with "bumpy" irregularities (e.g. Barge and Isaac, 1973; Knight and Knight, 1970b). Consequently, large hailstones are seldom perfectly smooth spheres. Matson and Huggins (1980) reported that 84% of hailstones within a large sample collected over the High Plains of the USA exhibited a disk-like shape, classified as oblate spheroids, while the other 16% were classified as "cones". Of the conical hailstones, 26% were "close to being labelled oblate spheroids". Moreover, Barge and Isaac (1973) found that the most common shape of hailstones collected from Alberta thunderstorms was oblate (41.3% of hailstones in their sample were oblate spheroids).

Hailstorms have the potential to cause significant damage. Strong and Lozowski (1977) found that hail damage to crops increased logarithmically with increasing kinetic energy of hailstones. The kinetic energy of a falling hailstone is roughly proportional to D^4, where D is the hailstone's diameter. Thus, to forecast the damage potential of hail, it is important to focus on predicting the maximum size of the hailstones, as the biggest stones will cause most of the damage (as long as they are sufficiently dense).

To better understand the evolution of hailstones and to forecast maximum hail size, researchers have developed computer models that quantify the dynamics and thermodynamics of hailstone growth (e.g. Dennis and Musil, 1973; English, 1973). A hailstone's shape and its degree of surface roughness affect the microphysical processes that govern its evolution (such as melting, aggregation, and the heat transfer across a hailstone's surface). These microphysical processes are an integral part of numerical hail models. However, contrary to observed hailstones, most hail models are based on the assumption that the model hailstones remain perfectly spherical throughout their evolution.

The primary objective of this thesis is to develop a numerical model that is capable of simulating the evolution of oblate hailstones. Through use of this model, we will investigate the effects of oblateness on the evolution of hailstones. A secondary objective is to determine the relative influences of hailstone shape (i.e. degree of oblateness) and surface roughness on the growth of hailstones. Our approach is based on an extended version of the numerical hail prediction model originally created by Poolman (1992) and modified by Brimelow et al. (2002b). The model consists of a one-dimensional, steady-state cloud model coupled with a time-dependent hail growth model that is capable of simulating oblate hailstones with either realistically rough surfaces or perfectly smooth surfaces. Before explicitly outlining the objectives of this study, we will discuss some parameters used to describe oblate hailstones, and then present an overview of the theory of hail growth. A review of hail models will be provided next, followed by a description of the Alberta Hail Project.

1.2 Oblate Hailstones

An oblate spheroid is an ellipsoid of revolution; its shape is reminiscent of a sphere that has been flattened. The shape of an ellipsoid can be described by specifying the length of each of its three axes. Two of an oblate spheroid's axes are of equal length (this length is its major diameter, D) and its third axis is smaller than the other two (this length is its minor diameter, $D_{\min}$). Figure 1.1 is a schematic diagram of an oblate hailstone, presented from two different views: looking down its minor diameter, $D_{\min}$, and looking along its major diameter, D. The degree of oblateness of a hailstone can be quantified by its aspect ratio, α, defined as

$$\alpha = \frac{D_{\min}}{D}. \qquad (1.1)$$

A spherical hailstone has an aspect ratio of 1, and aspect ratio decreases as the degree of oblateness of a hailstone increases. Figure 1.2 depicts an assortment of walnut-sized oblate hailstones from an Alberta hailstorm. One of these hailstones is turned on its "side" (bottom right of the red knife); i.e. the view of this hailstone is looking along its major diameter.

Barge and Isaac (1973) measured both the minimum and maximum dimensions of a large number of hailstones from Alberta thunderstorms. Some of these hailstones had maximum dimensions that were as large as 6 cm. They found that the minimum value of aspect ratio was 0.30 and the modal value was between 0.75 and 0.79. Matson and Huggins (1980) conducted similar studies and determined that the mean aspect ratio of their hailstone sample was 0.77, which falls in the middle of the range reported by Barge and Isaac (1973). There is evidence that large hailstones become more oblate as they grow (e.g. Macklin, 1977). From an examination of the internal symmetry of 90 stones, Browning and Beimers (1967) concluded that aspect ratio decreases as maximum hail dimension increases. Field observation studies conducted by Knight (1986) support these findings.

The size of an oblate hailstone is often quantified using a parameter known as the equivalent diameter, D_{eq}. The equivalent diameter is the diameter of a spherical hailstone that is of the same mass and density as an oblate hailstone of aspect ratio α (i.e. it is the diameter that an oblate hailstone of a given mass would have if it were perfectly spherical). D_{eq} is a function of an oblate hailstone's aspect ratio and major diameter:

$$D_{eq} = \alpha^{1/3} D. \tag{1.2}$$

The equivalent diameter is a useful parameter when directly comparing the sizes of oblate hailstones with different aspect ratios.

Interestingly enough, when we were writing this introduction an e-mail was sent to us with a report that claimed an all time world record for the largest officially recorded hailstone in terms of diameter. This monster stone fell on 29 June 2003 in Nebraska, USA. We quote the e-mail report:

> "At 7:05 pm Sunday the National Weather Service in Hastings received reports of large hail in Aurora, Hamilton County Nebraska. Initial reports stated that the hail had penetrated the roof of a home, leaving holes in the structure large enough to crawl through. The stones were saved and placed in a freezer at the residence and two NWS employees were sent to assess the damage and record the size. The Aurora hailstone measured 6.5 inches (17 cm) in diameter with a circumference of 17.3 inches (44 cm) and weighted 1.33 pounds. This compares to the Potter Nebraska hailstone on July 12, 1928. The Potter Nebraska hailstone was 5.4 inches in diameter and weighed approximately 1.5 pounds. Prior to today, the largest hailstone on record occurred in Coffeyville Kansas on September 3, 1970. This stone measured 5.7 inches in diameter, 17.5 inches (44 cm) in circumference and weighed 1.67 pounds."

1.3 Theory of Hail Growth and Growth Environment

In this section, the main physical and dynamical processes of hail growth, and their relation to the degree of oblateness and roughness of a hailstone, are summarised. Much of our current scientific knowledge about the evolution of hailstones was obtained from two major field experiments that focussed on the investigation of hailstorms: the Alberta Hail Project (information available at http://datalib.library.ualberta.ca/AHParchive/) and the National Hail Research Experiment (Knight and Squires, 1982a,b). For a detailed description of the hail growth process, the reader is referred to Macklin (1977).

1.3.1 Hailstone Microphysics

Hailstones form when hailstone embryos accrete supercooled water droplets in clouds with strong updrafts (García-García and List, 1992). These embryos are typically between 1 and 10 mm in diameter (Macklin, 1977), and may be in the form of frozen drops or graupel (e.g. Knight and Knight, 1970a; Knight and Knight, 1978; Knight, 1981). The majority of hailstones grow in the region of the cloud between the 0°C and - 40°C levels, where the cloud water content consists of a nonzero fraction of supercooled droplets. Above the - 40°C level, the cloud water is usually in the form of ice crystals only (Vali and Stansbury, 1965). Hailstones that have made their way to this region grow slowly by accreting these ice crystals, due to the small ice-ice collection efficiency. (When ice crystals collide, they often bounce off each other rather than merge. Orville, 1977 states that the upper limit for the ice-ice collection efficiency is 0.25).

The rate of a hailstone's growth depends on its heat budget: the rate of release of latent heat as accreted supercooled water droplets freeze on its surface, versus the rate at which this latent heat is transferred away from the hailstone's surface. The heat budget of a hailstone (refer to Chapter 2 for details) also depends on its degree of oblateness, as well as its surface roughness (e.g. Greenan and List, 1995; García-García and List, 1992), its size, and in-cloud conditions (Dennis and Musil, 1973).

If the rate of release of latent heat on a hailstone's surface exceeds the rate of heat transfer away from its surface, the hailstone's surface temperature rises to 0°C, which allows liquid water to exist on the surface of the hailstone. This situation is referred to as wet growth, because the hailstone typically has a wet surface when its surface temperature is equal to 0°C. During wet growth, any intercepted ice crystals are accreted, as they easily "stick" to the hailstone's wet surface (English, 1973). Depending on the ambient temperature, liquid water content and size of the hailstone, it may begin to shed water in the form of up to millimetre-sized drops (Levi and Lubart, 1998; Greenan and List, 1995). The amount of water shed by a hailstone is in part determined by its major diameter (Levi and Lubart, 1998), and, through that parameter, its degree of oblateness. If the surface temperature of the hailstone equals 0°C, melting occurs. If the rate of heat transfer away from the hailstone's surface is sufficiently large, the hailstone's surface temperature remains below 0°C. This is known as dry growth, because any accreted supercooled water droplets freeze completely on the hailstone's surface. During this growth regime, only a small fraction of intercepted ice crystals are accreted, as they do not readily "stick" to the hailstone's dry surface (English, 1973).

The mass growth rate of a hailstone by accretion of supercooled cloud droplets and ice crystals is governed by the process of continuous collection. The instantaneous mass growth rate of a hailstone is proportional to its terminal velocity (relative to the cloud droplets that follow the air motion). The instantaneous mass growth rate is also proportional to the cross-sectional area of the hailstone (perpendicular to the flow), the net collection efficiency of cloud water, and the ambient cloud water content (refer to Chapter 2 for details). A hailstone's terminal velocity is partially determined by its aspect ratio and its surface roughness (Böhm, 1989). The net collection efficiency for cloud water is partially influenced by the degree of oblateness of a hailstone, as well (Levi and Lubart, 1998). Depending on how strongly these microphysical parameters depend on aspect ratio, the degree of oblateness of a hailstone may have a significant influence on its mass growth rate.

1.3.2 The Hail Growth Zone

Field studies and numerical modelling of hailstones indicate that there is a preferential region within hailstorms where maximum hail growth occurs (English, 1973; Browning, 1977; Nelson, 1983; Foote, 1984; Miller et al., 1988). This region is referred to as the hail growth zone (HGZ) and occurs at temperatures from about - 20°C to - 40°C. Maximum hail growth occurs in the HGZ for three reasons (Brimelow, 1999): 1) within this zone the maximum cloud water content is located; 2) the ambient temperature is low enough to facilitate dry growth, enabling most (or all) of the accreted water to freeze on the hailstone's surface; 3) according to Vali and Stansbury (1965), the HGZ is composed of a mixture of supercooled water droplets and ice crystals. A hailstone undergoing wet growth within this mixed-phase zone accretes ice crystals, in addition to supercooled water droplets, without adding heat to the hailstone. The collection of ice crystals thus allows the hailstone to grow larger than it would have been able to if all the available accreted mass were liquid (Nelson, 1983).

1.3.3 Storm Scale Features

Two major microphysical criteria required for hail growth in thunderstorms are the presence of hail embryos and high liquid water contents. Storm-scale features also influence hail growth. For maximum growth, the growing hailstone must remain in the HGZ long enough to reach an appreciable size. This can only be realized if the magnitude of the updraft velocity is almost the same as the hailstone's terminal velocity as it grows within the storm (Browning, 1977). If the updraft is too strong, the hailstone is rapidly carried beyond the HGZ and is expelled in the storm's anvil. If the updraft is too weak, the hailstone will fall from the cloud before it attains an appreciable size. Updraft velocities greater than 25 m s^{-1} (approximately the terminal velocity of a 2 cm hailstone) are required in the HGZ to produce severe hail (Brimelow, 1999).

The trajectories most likely to produce large hail are those that entail a single ascent and descent through or around the main updraft (e.g. Nelson, 1983; Foote, 1984; Rasmussen and Heymsfield, 1987c; Miller et al., 1988 and Brandes et al., 1995). The modelling results also show that large hailstones do not undergo recirculation. Based on the findings from field programs and modelling studies, Browning and Foote (1976) developed a conceptual model for the growth of severe hail in a steady-state supercell. In this model, the hail growth consists of three stages (which we paraphrase from Brimelow, 1999):

(1) Hail embryos form upwind of the main updraft, within a region of weak to moderate updrafts. As the embryos are advected towards the updraft core, they have sufficient time to become millimetre-sized particles.

(2) By the time the particles enter the HGZ, they are several millimetres in diameter and have terminal velocities in excess of 15 m s^{-1}, which is large enough to prevent them from being ejected into the anvil. Also, liquid water contents are close to their adiabatic values within and on the periphery of the main updraft, due to the low precipitation efficiency and entrainment commonly observed in the updraft core (Bluestein et al., 1988). These factors enable the hailstones to grow rapidly as they are advected across the updraft core by the storm relative inflow.

(3) The hailstones descend through the updraft when their terminal velocity exceeds that of the updraft. As they descend, they continue to grow until they pass below the freezing level and begin to melt.

Browning and Foote's (1976) conceptual model applies only to steady-state supercell storms and all hailstorms, even supercells, do not necessarily follow these exact growth stages (e.g. Miller et al., 1990). The hail growth process in multi-cell storms is slightly different. In this type of storm, stages 2 and 3 occur within a mature cell, but the hail embryos originate from developing feeder or daughter cells upwind of the mature cell (Heymsfield et al., 1980; Krauss and Marwitz, 1984; Cheng and Rogers, 1988).

1.4 Numerical Hail Models

Brimelow et al. (2002b) discussed the limitations of using weather radar and radar-derived parameters to forecast the occurrence of severe hail:

> "Weather radar is widely employed to monitor the structure, severity and development of thunderstorms. For example, dual polarization radar techniques have been used to identify the presence of hail in thunderstorms (Al-Jumily et al., 1991). Radar-derived parameters, such as the Vertically Integrated Liquid (VIL) and the hail detection algorithm of Witt et al. (1998), are often used to detect and to nowcast hail. However, Edwards and Thompson (1998) found that VIL based parameters currently used to predict hail severity show limited skill. Moreover, Witt et al. (1998) noted that predicting maximum hail diameter was the most challenging aspect of their hail detection algorithm. The most significant caveat of current radar-derived hail algorithms is that they only indicate hail after it has commenced or once it is imminent. Thus, typically little or no lead-time can be achieved when issuing and disseminating severe weather warnings."

Consequently, other means of forecasting maximum hailstone size must be used to alert forecasters to the threat of damaging hail in advance. An alternative to radar is to produce forecasts of hail size using numerical models, with atmospheric sounding data as input.

The following excerpt from Brimelow et al. (2002b) outlines the difficulties associated with 3-D, time-dependent hail models:

> "Multidimensional, time-dependent hail models have been widely used to simulate hailstorms and have contributed to our current understanding of hail growth mechanisms (e.g., Orville and Kopp, 1977; Clark, 1982; Xu, 1983; Farley, 1987; Kubesh et al., 1988). However, these models require extensive computing resources. Brooks et al. (1992) discussed the formidable challenges involving initialization of three-dimensional (3-D) cloud models. Furthermore, field experiments using 3-D cloud models are limited to relatively small areas, and access to the model's output is only available to a select group of clients (Brooks et al., 1993)."

To avoid these shortcomings, many researchers have developed one-dimensional (1-D) cloud models, which are based on the assumption that atmospheric variables are only a function of height. These 1-D models have been used extensively to model hailstone growth (Musil, 1970; Wisner et al., 1972; Dennis and Musil, 1973; Chisholm, 1973; Poolman, 1992).

Modelling and field studies have established that the largest hailstones are formed in the so-called hail growth zone, a region close to the adiabatic core of the thunderstorm updraft. It is, therefore, feasible to model the evolution of the largest hailstones using a simple coupled one-dimensional cloud and hail model that mimics the conditions in the hail growth zone. Brimelow et al. (2002b) employed such a model, which they referred to as "HAILCAST", to predict the maximum hail size on the ground. Their approach was to use a 1-D steady-state cloud model coupled with a time-dependent hail growth model. They tested HAILCAST by running the model for 160 proximity soundings recorded within the Alberta Hail Project area (refer to Section 1.5 for details) for three summers between 1983 and 1985. The forecast skill of the model at predicting the occurrence and maximum size of hail was then evaluated by comparing model output with reports of maximum hail size gathered from a high-density observation network within the Alberta Hail Project area. The comparison between the model and observations indicated significant skill in forecasting hail (Probability of Detection: POD = 0.85, False Alarm Ratio: FAR = 0.26, and Heidke Skill Score: HSS = 0.64). HAILCAST was also used operationally to provide forecasts of maximum hail size for a hail-suppression project in Mendoza, Argentina (Brimelow et al., 2002a). The performance statistics for the hail season from 15 October 1999 to 15 March 2000 were: POD = 0.76, FAR = 0.29, HSS = 0.60. The governing equations of the time-dependent hail growth model were those used by Musil (1970), Dennis and Musil (1973), and Rasmussen and Heymsfield (1987a,b); these microphysical formulations are all based on the assumption that a growing hailstone remains spherical throughout its evolution.

We are aware of only one attempt to model the growth of oblate hailstones. English (1973) developed a hail growth model that allowed for oblate hailstones, which she combined with a cloud model characterized by a sloping updraft. By conducting some experiments that involved modelling oblate hailstones, English (1973) found that, in some cases, oblate hailstones grew larger than spherical hailstones.

1.5 The Alberta Hail Project

The Canadian Prairies are prone to frequent severe thunderstorm outbreaks during the summer months. South-central Alberta is particularly prone to hailstorms, with hail observed on an average of 51 days between 1 June and 31 August (Smith et al., 1998). On average, there are about 20 days per summer with severe hail (hailstone equivalent diameter greater than 2 cm) in central Alberta. It is for these reasons that a major study of hailstorms, the Alberta Hail Project (AHP), was conducted in this region. The following excerpt from Brimelow et al. (2002b) is a summary of the AHP:

> "The Alberta Hail Project was an intensive field study of Alberta hailstorms that lasted from 1957 to 1985 (Admirat et al., 1985; Smith et al., 1998). The project area covered 33 700 km^2 (Figure 1.3) and was centred on the

> Penhold radar site located at 52.2°N, 113.9°W (Smith and Yau, 1993a). Its dual purpose was to conduct research on hailstorms and to assess the potential of reducing hail damage through cloud seeding (Deibert, 1984). Each spring, hail cards were mailed to approximately 20 000 farmers in the project area. On days with hail, between 10% and 20% of the farmers responded, yielding an average of one observer per 16-32 km^2 (Smith et al., 1998). In addition to the hail-card reports, telephone surveys were also conducted on days with hailstorms, resulting in observation densities as high as one report per 3 square kilometres. As a result, it is believed that only a very small percentage of hail reaching the surface went undetected."

The extensive hailstorm data collected during the Alberta Hail Project can be accessed via an online archive: http://datalib.library.ualberta.ca/AHParchive/.

> "Observers within the AHP were requested to report the largest and most common hail sizes. For the duration of the project, six categories were specified to size the observed hailstones: shot, diameter < 0.4 cm; pea, $0.4 \leq D_{eq} < 1.3$ cm; grape, $1.3 \leq D_{eq} < 2.1$ cm; walnut, $2.1 \leq D_{eq} < 3.3$ cm; golfball, $3.3 \leq D_{eq} < 5.3$ cm; and larger than golfball, ≥ 5.3 cm (Strong, 1974). Comparisons with measurements using aluminum hailpads indicated that the observed hail sizes had an error margin of approximately 10% (Admirat et al., 1985)" (Brimelow et al., 2002b).

Unfortunately, with the exception of the collection made by Barge and Isaac (1973), information regarding the shapes of the hailstones was not collected during the AHP.

To capture the atmospheric conditions during thunderstorm outbreaks, upper-air soundings were released from Penhold at 1715 local time (LT). Brimelow et al. (2002b) examined 160 soundings, collected over the summers of 1983 – 1985. Of these soundings, 98 were released on days with no hail, 42 on days with non-severe hail (grape-sized or smaller) and 20 on days with severe hail (walnut-sized or larger). Surface temperature and dewpoint, representative of a storm's inflow, were obtained from a mesonetwork (Brimelow et al., 2002b). Our study focuses mainly on the 20 severe hail days within the dataset of Brimelow et al. (2002b).

1.6 Statement of Research Objectives

1.6.1 Objectives

This study has two objectives. The primary objective is to determine the quantitative effects of the degree of oblateness on the evolution of a hailstone and its final equivalent diameter on the ground. The second objective is to determine the relative importance of hailstone surface roughness compared to oblateness in regards to the evolution of a hailstone.

To investigate the effects of oblateness, we will focus on addressing the following questions:

- How do the microphysical parameters that govern the evolution of a hailstone (terminal velocity, mass growth rate, rate of heat transfer) depend on its degree of oblateness (i.e. aspect ratio)?
- What are the differences in the evolution of model spherical and oblate hailstones?
- How do the final maximum equivalent diameter and total growth time of a model hailstone depend on its aspect ratio?
- Is it desirable to include the effects of oblateness in a time-dependent microphysical hail model used for operational forecasting of maximum hail size?

To investigate the effects of hailstone surface roughness, we will address the following questions:

- What are the differences in the microphysical parameters (terminal velocity, heat transfer rate, etc.) of a realistically rough-surfaced hailstone, versus those of a perfectly smooth hailstone?
- What are the differences in the evolution of rough-surfaced hailstones and smooth-surfaced hailstones as determined by a numerical model?

Are these differences comparable to those between spherical and oblate hailstones?

- How are final maximum equivalent diameter and total growth time of a model hailstone influenced by surface roughness?
- Are there any mutual interaction effects between hailstone roughness and oblateness? If so, what is the magnitude compared to the (pure) individual effects?
- How do the effects of roughness and oblateness compare to the model's sensitivity to other microphysical parameters?

1.6.2 Outline of Thesis

Chapter 2 provides a description of the model, hereafter referred to as HC2 (HAILCAST 2). HC2's background is presented in this chapter, along with the model equations for oblate hailstones. In Chapter 3, we develop simple analytical expressions for key parameters that influence the evolution of hailstones as functions of aspect ratio (terminal velocity, mass growth rate, heat transfer rate). Chapter 4 deals with modelling the effects of oblateness. Two case studies of severe hail days are presented in detail; they illustrate the output of HC2 for the evolution of an oblate hailstone. For each of the two case study days, the simulated evolution of a spherical hailstone is compared to those of two oblate hailstones, each with a different aspect ratio (0.50 and 0.77). For each of the 20 severe days, the differences in final equivalent diameter at ground and total growth time between a spherical and an oblate hailstone with an aspect ratio of 0.77 are discussed. We also determine the effects of varying the aspect ratio within the observed range of 0.30 to 1.00 on the model output parameters. In Chapter 5, we discuss the effects of roughness on microphysical hail parameters. Through simulations of rough, smooth, spherical and oblate hailstones for each of 20 severe hail days, we investigate the relative effects of oblateness and roughness on model hailstone size at ground and total evolution time, in addition to any combined effects of roughness and oblateness. In Chapter 6, we investigate the sensitivity of HC2 to important hail model parameters, as well as cloud model parameters. The forecast skill of HC2 in predicting maximum hail size is determined in Chapter 7. In this chapter, we determine if there are any differences between the forecast skill scores of the spherical and oblate versions of HC2. Finally, in Chapter 8, the major findings of our research are summarised and recommendations for future studies are presented.

2 MODEL DESCRIPTION

2.1 Introduction

We used a time-dependent hail model coupled with a one-dimensional, steady-state cloud model (referred to as HC2) to study the effects of oblateness and roughness on the evolution of hailstones. HC2 is very computationally efficient, with a 60-min simulation taking less than 1s on a 2.53 GHz personal computer. The HAILCAST microphysical hail model developed by Brimelow et al. (2002b) was extended to include the effects of hailstone oblateness. The 1-D steady-state cloud model that we used is essentially identical to the HAILCAST cloud model (Brimelow et al., 2002b). The cloud model is described in detail by Brimelow (1999) and Brimelow et al. (2002b), and a short description is presented in Section 2.3. Preceding the cloud model description, we will introduce HC2's microphysical hail model.

2.2 The Hail Model

2.2.1 Background of the HC2 Microphysical Hail Model

The predecessor of Brimelow's microphysical model, created by Poolman (1992), was based on the work of Musil (1970) and Dennis and Musil (1973). Brimelow (1999) developed HAILCAST by making significant improvements to both the 1-D cloud model and the hail microphysics model. He used the method of Rasmussen and Heymsfield (1987a,b) to model the terminal velocity of the hailstones, the shedding of excess water from hailstones, and the Nusselt and Sherwood numbers in the heat budget scheme. In the HC2 hail model the governing equations of hail growth and hailstone thermal energy budget were modified to allow for oblate hailstones. Furthermore, the terminal velocity of hailstones and the water shedding schemes were replaced in HC2 with the schemes and equations of Böhm (1989), García-García and List (1992), Greenan and List (1995) and Levi and Lubart (1998).

In the original HAILCAST model, the modelled hailstones remain perfectly spherical throughout their lifetime. Observed hailstones, however, are typically oblate spheroids (for example: Knight, 1986; Matson and Huggins, 1980; Barge and Isaac, 1973 and Macklin, 1977). We developed the HC2 microphysical hail model by extending HAILCAST's microphysical model for the purposes of investigating and quantifying the effects of oblateness on the evolution of hailstones. We implemented more recent terminal velocity and shedding schemes, and altered the heat budget calculations and mass growth equations to simulate the evolution of non-spherical hailstones. In HC2, we assumed that hailstones evolve as oblate spheroids and that their degree of oblateness may be described by a single parameter: the aspect ratio.

The majority of natural hailstones have rough surfaces (Böhm, 1989). Surface roughness affects the drag of falling hailstones; according to Lozowski and Strong (1978), even slight roughness can enhance the drag by one third. A rough hailstone surface also increases the efficiency of heat transfer compared to a hailstone with a perfectly smooth surface. HAILCAST modelled spherical hailstones of "realistic" roughness, using the parameterizations of Rasmussen and Heymsfield (1987a). In HC2, we made it possible to simulate the growth of a hailstone with either a realistically rough surface or a smooth surface; that is, roughness can be either "switched on" or "switched off". Being able to run simulations for both rough and smooth hailstones allows us to investigate the importance of surface roughness during their evolution.

2.2.2 Growth Equations

In its most general form, the mass growth equation, which describes the rate of change of the mass, *M*, of a hailstone due to the accretion of supercooled water droplets and ice crystals, is

$$\frac{dM}{dt} = \frac{dM_w}{dt} + \frac{dM_i}{dt} = A_c V_T \left[\chi_w E_{net} + \chi_i E_i \right], \tag{2.1}$$

assuming a continuous collection process (e.g. Dennis and Musil, 1973). dM_w/dt is the rate of change of the hailstone's mass due to the accretion of supercooled water droplets; dM_i/dt is the rate of change of the hailstone's mass due to the accretion of ice crystals; A_c is the average cross-sectional area (perpendicular to the direction of motion) of the hailstone; V_T is the terminal velocity of the hailstone; χ_w is the cloud liquid water content; χ_i is the cloud ice content; E_{net} is the net collection efficiency; and E_i is the collection efficiency of cloud ice. The terminal velocity of the hailstone, V_T, is calculated using the method of Böhm (1989), described in Section 2.2.6. The quantity $A_c V_T$ represents the volume of the cylinder swept out by the hailstone per unit time interval. The only processes that are assumed to contribute to the hailstone's mass growth are the collection of cloud water and the collection of cloud ice. Mass growth due to deposition of water vapour to the hailstone's surface is neglected based on the fact that the growth by deposition for particles with a diameter greater than 0.1 mm is much smaller than their growth due to the accretion of cloud water and ice (Dennis and Musil, 1973).

Note the inclusion of the parameter E_{net} in place of E_w, the collection efficiency of cloud water. E_{net} is the net collection efficiency, and is part of the new shedding scheme used by HC2. The net collection efficiency is a measure of the mass fraction of water droplets, in the geometrically swept out volume of cloud, permanently accreted on the falling hailstone (List et al., 1995; García-García and List, 1992). The exact formulation of E_{net} is given in Section 2.2.4. For now, it is sufficient to note that E_{net} is the same as E_w (the collection efficiency of cloud water) when the hailstone is not shedding, and has a value that is less than E_w when the hailstone is shedding. The collection efficiency of ice, E_i, is assumed to be equal to 1.0 during wet growth and wet shedding growth. This means that during wet growth, all ice crystals that the hailstone encounters are assumed to stick to its surface. During dry growth, E_i is assumed to be 0.2, which is near the upper limit of 0.25 used in modelling studies (Orville, 1977). A value of $E_i = 0.2$ was used by Geresdi (1998) for the collection efficiency between hail and rimed ice particles.

The average cross-sectional area of the hailstone (i.e. the area presented to the flow), A_c, is not an easy quantity to determine. Kry and List (1974a,b) investigated the free-fall behaviour of oblate spheroids. They found that the most common motion undergone by falling spheroids is symmetric gyration, in which the spheroid spins about its minor axis, which in turn precesses and nutates, describing a horizontal (circular) cone with its apex located at the centre of the particle (Figure 2.1). The effects of this tumbling motion should, ideally, be included in the parameter A_c. According to Böhm (1989), however, the cross-sectional area presented to the flow can be assumed to be its (circular) maximum cross section, $\pi D^2/4$, because the effects of irregular falling behaviour are included in the empirically determined drag coefficient (Section 2.2.6).

The rate of change of a hailstone's major diameter with respect to time may be derived from the mass growth equation. If we assume that a hailstone's aspect ratio, α, is a function of its major diameter, D, we may use the following equation to model the evolution of a hailstone's major diameter:

$$\frac{dD}{dt} = \frac{3}{2}\frac{V_T}{\rho_H}\frac{1}{D(d\alpha/dD) + 3\alpha}\left[\chi_w E_{net} + \chi_i E_i\right], \tag{2.2}$$

where ρ_H is the density of the hailstone. Refer to Appendix B for a derivation of (2.2).

2.2.3 The Heat Budget of an Evolving Hailstone

The heat budget of a hailstone is governed by four heat transfer processes: (1) Convection and conduction (Q_k), (2) Sublimation or evaporation (Q_s), (3) Latent heat of freezing due to the accretion of supercooled water (Q_a), and (4) Accretion of cloud ice crystals (Q_c). According to Dennis and Musil (1973), the expression for the total heat, Q_T, gained by the hailstone per unit time is

$$\frac{dQ_T}{dt} = \frac{dQ_k}{dt} + \frac{dQ_s}{dt} + \frac{dQ_a}{dt} + \frac{dQ_c}{dt}. \tag{2.3}$$

The heat budget equations, which can be readily derived from the above expression, are used to calculate the surface temperature of the hailstone, T_s, and its fractional water content, F_w (the amount of liquid water present on the hailstone's surface). The transfer of heat to and from the hailstone's surface controls both the growth phase of the hailstone and the amount of water and ice that can be frozen onto it. We assume that the temperature is uniform throughout the hailstone.

If a hailstone is undergoing dry growth, all collected cloud water is assumed to freeze on its surface, and all collected ice crystals are assumed to stick to its surface. The fractional water content of a hailstone undergoing dry growth is assumed to be zero, and the exchange of heat between the hailstone and its environment determines its surface temperature:

$$\frac{dT_s}{dt} = -\frac{T_s}{M}\frac{dM}{dt} + \frac{1}{MC_i}\frac{dQ_T}{dt}, \tag{2.4}$$

where C_i is the specific heat of ice. During wet growth and wet shedding growth, not all collected cloud water is frozen and the hailstone may carry with it a nonzero fraction of water. A hailstone enters the wet (or wet shedding) growth regime once its surface temperature reaches 0°C. When this occurs, the change of the hailstone's fractional water content with time is determined by the heat budget:

$$\frac{dF_w}{dt} = -\frac{F_w}{M}\frac{dM}{dt} + \frac{1}{ML_f}\frac{dQ_T}{dt}, \tag{2.5}$$

where L_f is the latent heat of freezing.

A model hailstone's surface temperature and fractional water content are evaluated at each time step using either (2.4) or (2.5), depending on the current growth regime. The growth regime at the current time step is determined by examining the hailstone's surface temperature at the previous time step. The type of wet growth (shedding or no shedding) that the hailstone experiences depends on the liquid water content and ambient temperature of the cloud at the hailstone's current location, along with its size (Levi and Lubart, 1998).

Before we discuss the individual terms of the heat budget equation, we will justify two assumptions that were made: the temperature is uniform throughout the hailstone and the transition from dry to wet growth occurs at a hailstone temperature of 0°C. Empirical studies (García-García and List, 1992) indicated that the transition from wet to dry growth does not generally occur at a temperature of exactly $T_{so} = 0°\text{C}$, where T_{so} is the Schuman-Ludlam limit, but at a slightly lower temperature instead: $-1 \leq T_{so} \leq -0.25°\text{C}$. However, Levi and Lubart (1998) showed that it is still a good approximation to use $T_{so} = 0°\text{C}$ for the purposes of modelling the growth of hailstones, so we used that value in HC2. We also assumed that the surface temperature of a hailstone is uniform. List et al. (1995) measured the surface temperature of a growing oblate hailstone at different locations on its surface and documented temperature differences across the stone's surface that were as high as 5.9°C. However, it is not practical to implement a non-homogeneous surface temperature in a microphysical hail model. Levi and Lubart (1998) assumed that their simulated hailstones had uniform surface temperatures. In HC2, we adopt this same assumption.

We now summarize the individual terms of the heat budget equation (2.3). In all cases, the heat transfer terms for oblate hailstones were derived by combining those presented by Dennis and Musil (1973) with those of Lesins and List (1986).

Convection and Conduction

The rate of convection and conduction of heat to and from an oblate hailstone is

$$\frac{dQ_k}{dt} = \frac{A_s}{D/2} \,\mathrm{Nu}\, k \left(T_a - T_s\right), \tag{2.6}$$

where Nu is the Nusselt number, k is the thermal conductivity of air, A_s is the surface area of a smooth oblate hailstone ($\alpha \neq 1$), and T_a is the ambient temperature. According to English (1973), the surface area of a smooth oblate hailstone is

$$A_s = \frac{\pi D^2}{4}\left[2 + \frac{\alpha^2}{\varepsilon}\ln\left(\frac{1+\varepsilon}{1-\varepsilon}\right)\right], \tag{2.7}$$

where $\varepsilon = \left(1-\alpha^2\right)^{1/2}$ is the hailstone's eccentricity. For a sphere ($\alpha = 1$), (2.7) becomes $A_s = \pi D^2$. Roughness effects are not included explicitly in the expression for the surface area of an oblate hailstone (2.7), but are included in the

Nusselt number, Nu, which is a measure of the efficiency of heat transfer by convection and conduction. This parameter depends on the roughness of the hailstone, as well as its shape, and is generally a function of the Prandtl number, Pr, and the Reynolds number, Re. In HC2, we combined the Nusselt number formulations of Macklin (1963), Bailey and Macklin (1968) and Rasmussen and Heymsfield (1987a) to derive a suitable expression for an oblate hailstone (Appendix C).

Equation (2.6) tells us that if the ambient air has a higher temperature than that of the hailstone's surface, then heat is conducted towards the hailstone, resulting in a positive contribution to its heat budget. The opposite is true if the ambient temperature is colder than the hailstone's surface.

Evaporation or Sublimation

The heat exchange due to evaporation or sublimation for an oblate hailstone is

$$\frac{dQ_s}{dt} = \begin{cases} -2\pi(A_s/D)\mathrm{Sh}L_v d_{wa}\Delta\rho & \text{for } T_s \geq 0°\mathrm{C} \\ -2\pi(A_s/D)\mathrm{Sh}L_s d_{wa}\Delta\rho & \text{for } \mathrm{T_s} < 0°\mathrm{C} \end{cases}, \tag{2.8}$$

where Sh is the Sherwood number, L_v is the latent heat of vaporization, L_s is the latent heat of sublimation, d_{wa} is the diffusivity of water vapour in air, and $\Delta\rho$ is the difference between the water vapour density at the hailstone's surface (ρ_s) and that of the environmental air (ρ_e). Following Dennis and Musil (1973), we assumed that the environmental vapour density varies between saturation with respect to water and saturation with respect to ice, depending on the ambient temperature. The vapour density at the hailstone's surface is assumed to be equal to the saturation with respect to water during wet growth (and wet shedding growth) and the saturation with respect to ice during dry growth.

The Sherwood number in (2.8) is similar to the Nusselt number in the convection/conduction expression (2.6). Sh is a measure of the efficiency of heat transfer by evaporation or sublimation. It depends on the surface roughness of the hailstone and its degree of oblateness, and is generally a function of the Schmidt number, Sc, and the Reynolds number. The expression for the Sherwood number of an oblate hailstone in HC2 was obtained in the same manner as the Nusselt number (Appendix C).

Latent Heat of Freezing of Accreted Cloud Water

The heat gained by an oblate hailstone due to the freezing of accreted cloud water is

$$\frac{dQ_a}{dt} = \frac{dM_w}{dt} L_f - \left(A_c V_T \chi_w E_w\right) C_w \left(T_s - T_a\right), \tag{2.9}$$

where C_w is the specific heat of water. All accreted cloud water is assumed to be at ambient temperature T_a. We assumed that any water shed from the hailstone contains no ice and has been warmed, or cooled, to the hailstone surface temperature, T_s, before being shed in the hailstone's wake.

The rate of accretion of cloud water by a hailstone depends on its net collection efficiency. A hailstone in the wet shedding growth regime collects a fraction, E_w, of the mass of water droplets in the geometrically swept out volume of cloud and then sheds a mass of water per unit time interval, equal to $dM_s/dt = \left(E_w - E_{net}\right) A_c V_t \chi_w$, in its wake. Any shed water first comes into contact with the surface of the hailstone and is brought to the temperature T_s before it is shed.

Accretion of Cloud Ice Crystals

The heat exchange due to the accretion of cloud ice for an oblate hailstone is

$$\frac{dQ_c}{dt} = \frac{dM_i}{dt} C_i \left(T_a - T_s\right), \tag{2.10}$$

where T_a, the ambient temperature, is the temperature of the cloud ice crystals.

2.2.4 Shedding Above the Cloud Base

The shedding scheme implemented in HC2 is based on the findings of García-García and List (1992), Greenan and List (1995), and Levi and Lubart (1998). List and his colleagues conducted a series of laboratory experiments that involved empirically determining the liquid water content at the onset of shedding as a function of ambient temperature. This work also yielded expressions for the collection efficiency of water (no shedding) and for the net collection efficiency (shedding). Levi and Lubart (1998) expanded on the work of García-García and List (1992) and Greenan and List (1995). Numerical experiments with the empirical shedding parameters of List and his colleagues resulted in an expression for the liquid water content at the onset of shedding as a function of the major diameter of a hailstone and the ambient temperature.

At each model time step, if the hailstone is in the wet growth regime, the liquid water content of the cloud, χ_w, at the hailstone's height is compared to the liquid water content at the onset of shedding (Levi and Lubart, 1998),

$$\chi^* \left[g \cdot cm^{-3}\right] = \left\{0.928 - 0.059T_a + \left(3.227 - 0.210T_a\right)/D\right\} \times 10^{-6} . \qquad (2.11)$$

If χ_w is less than or equal to χ^*, the hailstone remains in the wet growth regime, and the net collection efficiency is equal to the collection efficiency for water (2.14). On the other hand, if χ_w is greater than χ^*, then the hailstone has entered the shedding growth regime, and its net collection efficiency is reduced accordingly. In mathematical form, this translates to (García-García and List, 1992)

$$E_{net} = \begin{Bmatrix} E_w & \chi_w \le \chi^* \\ \dfrac{E_w}{1 + K_E\left(\chi_w - \chi^*\right)} & \chi_w > \chi^* \end{Bmatrix}, \qquad (2.12)$$

where

$$K_E \left[cm^3 \cdot g^{-1}\right] = \left(0.10 + 0.004T_a\right) \times 10^6 . \qquad (2.13)$$

Note that ambient temperature T_a, is in °C and major diameter, D, is in cm.

According to Greenan and List (1995), the collection efficiency of water for a hailstone is

$$E_w = 0.59K^{0.15} = 0.59\left(\frac{2\rho_d V_T r_d^{\,2}}{9\eta_a r_H}\right)^{0.15}, \qquad (2.14)$$

where K is the Stokes parameter, ρ_d is the density of cloud water droplets (1 g cm^{-3}), η_a is the dynamic viscosity of air, r_H is the semi-major axis of the hailstone ($D/2$), and r_d is the median volume radius of the droplets colliding with the hailstone. Following Greenan and List (1995), we assumed that $r_d = 25.5$ μm in HC2. The collection efficiency of water and the net collection efficiency indirectly depend on the axis ratio of the hailstone through the parameters V_T, r_H, and, in the case of E_{net}, χ^* (through D). The effects of tumbling on the collection process are included implicitly, as the above parameterizations were developed through experiments with gyrating hailstones.

To apply this shedding scheme to HC2, we assumed that the liquid water droplet embryo of a hailstone does not enter into the wet shedding growth regime. This choice was made since the empirical formulae do not apply to water droplets. We also assumed that the liquid fraction of the cloud water content, χ_w, determines the onset of shedding, as opposed to the total water content of the cloud that consists of all water in liquid and ice form. By running HC2 for 20 severe and 42 non-severe hail days within the Alberta Hail Project data set, we determined that, at least for these data, hailstones tend to shed near cloud base, at ambient temperatures greater than - 20°C. The microphysical hail model parameterizes the amount of cloud ice present at a given ambient temperature according to the method of Vali and Stansbury (1965). In this scheme, there is no cloud ice present at ambient temperatures above - 20°C. In our data set, shedding does not occur at such low temperatures, therefore it is reasonable to use cloud liquid water content to determine whether or not a hailstone is shedding.

2.2.5 Shedding Below the Cloud Base

When an evolving hailstone descends below cloud base, it enters a region where the ambient temperature is usually above zero. In this environment, hailstones typically melt partially before they fall to the ground. While below cloud base, a hailstone sheds melted water in its wake and, as there is no "new" supercooled liquid water for the hailstone to collect, this means that its mass growth rate is negative. To use a net collection efficiency parameter to describe the shedding of excess water from a hailstone, the hailstone must be in an environment where the liquid water content is nonzero. It is not possible to have a negative mass growth rate when using HC2's shedding scheme, because if the liquid water content is zero, (2.1) predicts a mass growth rate of zero. Therefore we must use a different approach to describe the melting and shedding processes that a hailstone undergoes when it descends below cloud base and its mass growth rate becomes negative.

To properly simulate the melting of a hailstone below cloud base, we used a modified version of the shedding scheme by Rasmussen and Heymsfield (1987a). Their approach is based on the assumption that a rough-surfaced, spherical hailstone cannot hold any liquid water in excess of a threshold value termed the "critical surface mass of liquid water", M_{crit}. Any mass of water that the hailstone contains in excess of M_{crit} is assumed to be lost through shedding. We assume that the critical surface water mass depends on the surface area of the hailstone, as well as the mass of its ice core. A hailstone with a larger surface area should be able to retain more surface water than one with the same mass but a smaller surface area. Thus, to describe melting below the cloud base, the following modified expression is used for the critical surface water mass of an oblate hailstone:

$$M_{crit}{}^{*} = \frac{A_s}{\pi D_{eq}{}^2} M_{crit} = \frac{A_s}{\pi D_{eq}{}^2}\left(0.268 + 0.1389 M_i\right), \tag{2.15}$$

where M_i is the mass of the ice core of the hailstone, A_s is the actual surface area of the hailstone, and $\pi D_{eq}{}^2$ is the surface area of a spherical hailstone with the same mass as the oblate hailstone. The quantity $A_s / \pi D_{eq}{}^2$ is always positive for an oblate hailstone. This implies that an oblate hailstone is capable of retaining more water on its surface than a spherical hailstone with an ice core of the same mass. As a consequence, the oblate hailstone should lose less mass during the melting process as it falls to the ground.

It is not entirely clear how hailstone oblateness affects the melting process below cloud base. Empirical work, such as that of Rasmussen and Heymsfield (1987a) is needed to determine the effects of oblateness on the melting of hailstones below cloud base. However, we expect the total effect of melting on the growth of hailstones to be fairly small, because it only occurs below cloud base for a few minutes at most.

2.2.6 Terminal Velocity of the Hailstone

We used the formulation of Böhm (1989), to calculate the terminal velocity of an oblate hailstone in the HC2 microphysical hail model. Böhm (1989) developed a general equation for the fall speed of hydrometeors, in which the terminal velocity depended on aspect ratio as well as the degree of surface roughness. He defined a roughness factor, q, to represent the ratio

$$q = A_e / A, \tag{2.16}$$

where A_e is the effective projected cross-sectional area of the particle presented to the flow and A is the area of the smallest circle or ellipse that completely contains A_e. According to Böhm (1989), the actual drag coefficient of the particle, C_{De}, is related to the drag coefficient corresponding to the circumscribed disk, C_D, as follows:

$$\frac{C_D}{C_{De}} = q^{3/4}. \tag{2.17}$$

From the above expression, Böhm (1989) derived a general expression for the Best number, X, that included the roughness factor, q:

$$X = C_D \mathrm{Re}^2 = \frac{8Mg\rho_a}{\pi\eta_a^{\;2} q^{1/4}}, \tag{2.18}$$

where M is the mass of the hailstone, g is the acceleration due to gravity, and η_a is the dynamic viscosity of air. Böhm (1989) also formulated a semi-empirical expression for the drag coefficient of solid precipitation particles, C_{De}, and used it to calculate the Reynolds number for an oblate, rough hailstone:

$$\mathrm{Re} = 8.5\left[\left(1 + 0.1519X^{1/2}\right)^{1/2} - 1\right]^2. \tag{2.19}$$

The effects of hailstone roughness and irregular motions, such as tumbling and gyration, are included implicitly in the above expression. We assume that a hailstone falls with its circular maximum cross-section presented to the flow because tumbling effects are implicitly included in C_{De} and, hence, Re. The inclusion of roughness effects in the drag coefficient also allows us to take $q = 1$ when calculating the Best number.

The terminal velocity of a rough, oblate hailstone is

$$V_T = \frac{\mathrm{Re}\,\eta_a}{\rho_a D}, \tag{2.20}$$

where ρ_a is the density of the ambient air and the characteristic length for the hailstone is assumed to be its major diameter, D. Böhm (1989) calculated the terminal velocity as above for a range of hailstone diameters, assuming $\alpha = 0.77$, and compared the results to data collected by Matson and Huggins (1980) and Roos and Carte (1973), to validate his terminal velocity expressions. He found that his formulae yielded terminal velocities for rough, oblate hailstones that agreed well with observations.

2.2.7 The Evolution of Aspect Ratio

The HC2 model hailstones begin their lives as embryos: droplets of water that are assumed to have shed from previously grown hailstones. In HC2, we assume that hail embryos originate as frozen water drops no larger than 1 mm in size. Water drops of these sizes are almost perfectly spherical (Pruppacher and Klett, 1978) and thus it reasonable to assume that hailstone embryos are also spherical. Yet, at their later growth stage, hailstones tend to become more oblate (e.g. Browning and Beimers, 1967). The aspect ratio, therefore, does not remain constant during the growth of a hailstone. Browning and Beimers (1967), Barge and Isaac (1973), and Knight (1986) independently reported that aspect ratio generally decreases as the major diameter, D, of the hailstone increases.

We have yet to determine exactly how aspect ratio varies with major diameter. Knight (1986) analyzed hailstones from three different regions (Oklahoma, N. E. Colorado and Alberta) and produced a plot of axis ratio vs. hailstone maximum dimension for each region, spanning 1 mm < D < 55 mm. From Knight's data, it can be seen that the aspect ratio is close to 1, and does not change significantly, within error, for major diameters smaller than about 1 cm.

Thus in HC2 we assume that the model aspect ratio is equal to 1 for D less than 1 cm.

Studies focusing on hailstone shape reported the aspect ratio and size of hailstones at the ground. The results reported were for a sample of hailstones, often falling from different storms. Barge and Isaac (1973) reported an average aspect ratio ranging from 0.75 and 0.79, while Matson and Huggins' (1980) average aspect ratio was 0.77. Knight's (1986) data showed that, in all cases, the hailstones reached an aspect ratio that lies between 0.70 and 0.80 at a major diameter of around 2 cm. Beyond 2 cm, especially for the data from Oklahoma and Colorado, aspect ratio did not appear to change overly much. Knight's (1986) data for Alberta hailstones was slightly different: the aspect ratio did not tend to remain constant beyond major diameters of 2 cm, and the absolute values of aspect ratio reached ($\alpha \sim 0.60$) were lower than the other two regions. However, the largest hailstones in Knight's (1986) Alberta data set had major diameters of around 5 cm (as opposed to 5.5 cm for the other two data sets). The error bars for the Alberta data are also large beyond 4 cm.

Based on the evidence, we assume that model hailstones reach a constant aspect ratio of 0.77 once their major diameters exceed 2 cm. In HC2, we have defined a parameter, α_c, which represents the constant aspect ratio attained when the major diameter increases beyond 2 cm; it can be adjusted as necessary to investigate the effects of degree of oblateness on the evolution and final size of a model hailstone.

We now have representative values for the aspect ratio of a hailstone when it has a major diameter less than 1 cm ($\alpha = \alpha_1 = 1$) and greater than 2 cm ($\alpha = \alpha_c = 0.77$). We have yet to specify the aspect ratio for a hailstone with a major diameter between 1 cm and 2 cm. We know that aspect ratio must decrease from $\alpha = 1$ to $\alpha = \alpha_c$ (where $\alpha_c < 1$) in the region 1 cm $\leq D \leq$ 2 cm. The simplest way to specify the aspect ratio as a function of major diameter in this region is to fit a straight line between the points (D = 1 cm, $\alpha = 1$) and (D = 2 cm, $\alpha = \alpha_c$). Browning and Beimers (1967) measured aspect ratio as a function of major diameter for a number of hailstones and calculated the average value of $d\alpha/dr_H$, where r_H is the semi-major axis ($r_H = D/2$). They assumed that $d\alpha/dr_H$ was a constant (i.e. that the relationship between aspect ratio and semi-major axis was linear). Therefore, following Browning and Beimers (1967), we will assume that the relationship between aspect ratio and major diameter is linear in the region 1 cm $\le D \le$ 2 cm.

To summarize, aspect ratio is assumed to depend on the major diameter of the evolving hailstone as follows:

$$\begin{aligned} &\alpha(D) = \alpha_1 = 1 && \text{for } D \le D_1 \\ &\alpha(D) = \alpha_1 + [(\alpha_c - \alpha_1)(D - D_1)]/(D_2 - D_1) && \text{for } D_1 \le D \le D_2\,. \\ &\alpha(D) = \alpha_c && \text{for } D \ge D_2 \end{aligned} \tag{2.21}$$

Recall that we chose $D_1 = 1$ cm and $D_2 = 2$ cm for our control values. Both of these limits can be changed within HC2 to conduct sensitivity studies. The constant α_c has a control value of 0.77.

2.3 The Cloud Model

HC2's one-dimensional steady-state cloud model is the same cloud model that Brimelow et al. (2002a,b) used for his hail prediction model, HAILCAST. It is similar to those developed by Simpson and Wiggert (1969), Chisholm (1973), Sanders and Garett (1975), Matthews and Henz (1975), and Anthes (1977). In this section, we present a short description of the cloud model; a more complete description can be found in Poolman (1992), Brimelow (1999) and Brimelow et al. (2002b).

Modelling and field studies have established that the largest hailstones are formed in the hail growth zone, a region close to the adiabatic core of the thunderstorm updraft (e.g. English, 1973; Browning, 1977; Nelson, 1983; Foote, 1984; Miller et al., 1988). HC2's cloud model mimics the conditions prevalent in the hail growth zone. This cloud model parameterizes the effects of both cloud-top and lateral entrainment using the saturation-point analysis scheme of Betts (1982a,b). Either cloud-top or lateral entrainment is assumed to influence the in-cloud temperature and saturation mixing ratio, depending on the intensity of the storm: cloud-top entrainment is assumed to dominate in large cumulus clouds and lateral entrainment in small cumulus clouds (Blyth et al., 1988). The amount of condensed water that is allowed to evaporate due to entrainment of relatively dry environmental air is not allowed to exceed 10% (Brimelow et al., 2002b). The updraft velocity at each level, $W(z)$, is calculated using the following formula:

$$W^2 = W_0^{\,2} + 2g\int_{z_{lcl}}^{z_{el}}\left(\frac{T^*-T}{T} - \chi\right)dz \qquad (2.22)$$

where W_0 is the updraft velocity at the lifting condensation level, z_{lcl}, g is the gravitational acceleration, z_{el} is the equilibrium level, χ is the water loading term (the amount of condensed cloud water at each level after entrainment) and T^* and T are the virtual in-cloud and ambient temperatures, respectively (Brimelow et al., 2002b). We assume $W_0 = 3$ m s^{-1} consistent with English (1973, p. 56). This is also the value used by Poolman (1992) for hailstorms in southern Africa. Brimelow et al. (2002a,b) used $W_0 = 4$ m s^{-1}, which is appropriate for severe storms, but probably excessive for non-severe convection or for cases without convection. The cloud model input consists of vertical profiles of temperature, dewpoint, and the horizontal wind components (obtained from an upper-air sounding that is representative of the storm environment), along with the observed values for the surface temperature and dewpoint. The lifting condensation level is determined for each sounding by adiabatically lifting a parcel of air from the surface until the saturation point is reached (Brimelow et al., 2002b).

2.4 Coupling the Microphysical Model with the Cloud Model

Our approach to modelling maximum hail size involves coupling a steady-state cloud model with a time-dependent hail model. As HC2's cloud model is steady-state, the cloud conditions remain the same for an infinite amount of time. Updrafts in real hailstorms have a finite lifetime that can be anywhere between 20 minutes (for single cell storms) and several hours (for supercell storms). The residence time of a hailstone within the hail growth zone has a significant effect on its final size at ground (Nelson, 1983; Miller et al., 1988) so it is important to specify an updraft duration in the HC2 model that depends on the type of storm within which the simulated hailstone evolves.

The updraft duration in HC2 is specified according to the criteria outlined by Brimelow et al. (2002b): the updraft duration is assigned based on the product of CAPE × SHEAR, where CAPE represents the observed surface-based convective available potential energy and "SHEAR" represents the magnitude of the mean vertical shear of the observed winds recorded between 1.5 and 6.0 km MSL (Penhold, Alberta, 905 m MSL). This approach accounts for the combined effects of buoyancy and vertical wind shear on the updraft duration, with larger products indicating an increased potential for long-lived updrafts (Brimelow, 1999).

2.5 Choice of Initial Embryo Diameter

The purpose of the HC2 model is to predict maximum hail size, and maximum hail size can be quite sensitive to initial embryo diameter, as we determined through a series of sensitivity experiments (Chapter 6). In the HC2 model, the hailstone embryo is assumed to originate from a water droplet previously shed from other hailstones within the storm. According to Lesins and List (1986), hailstones shed water droplets that can be up to approximately 1 mm in diameter. Given that a droplet embryo of this type can be anywhere between 100 μm and about 1 mm in diameter, and because final hailstone diameter is, in some cases, sensitive to initial diameter, we decided to select an embryo size for each severe hail day, within this interval, that produced the largest final diameter at ground.

For each severe hail day sounding, a number of runs were made by varying the embryo diameter between 100 μm and 800 μm, in 100 μm increments. We selected an upper limit of 800 μm because, for some severe hail days, the updraft at cloud base was unable to support embryos with diameters in excess of 800 μm. From these ensemble runs, we chose an embryo diameter for each day that produced the largest hail in the shortest amount of time. Most of the chosen embryo diameters for the 20 severe hail days were either 400 μm or 700 μm (Table D1, Appendix D). For all non-severe hail days and no hail days, the embryos were assumed to be 400 μm in diameter, as larger embryo diameters tended either to be too large to be supported by the weaker storm updrafts, or they produced hailstones with approximately the same final diameters as the 400 μm embryo.

3 DEPENDENCE OF MICROPHYSICAL PARAMETERS ON DEGREE OF OBLATENESS

3.1 Introduction

The growth of a hailstone is influenced by a number of factors: its mass growth rate, heat transfer rate, the amount of shedding that occurs, and its terminal velocity. However, the individual effects of oblateness on the aforementioned parameters cannot be entirely distinguished from each other by means of a numerical model; the model is most useful for investigating the overall, or bulk, effects of oblateness on hailstone evolution. Here we seek to understand the individual effects of oblateness as well as the overall effects. To gain further insight regarding the effects of oblateness on the evolution of a hailstone, it is useful to examine separately the influence of aspect ratio on each of the factors that affect hail growth. In this chapter, we develop analytical expressions for key parameters that influence the evolution of hailstones as a function of aspect ratio.

The approach will be the same for the analysis of hailstone terminal velocity, instantaneous mass growth rate and the rate of convection and conduction of heat to (or from) a hailstone. In all instances, we assume constant ambient conditions. For each parameter, P, we consider a hailstone of fixed mass and density; aspect ratio is the only hailstone variable that is allowed to change. We then obtain an analytical expression for P as a function of aspect ratio: $P(\alpha)$. For simplicity, we have elected to represent each $P(\alpha)$ as a ratio with respect to the value of the parameter P for a spherical hailstone: $P(\alpha = 1)$. We refer to this ratio as $F(P)$, where

$$F(P) = \frac{P(\alpha)}{P(\alpha = 1)}. \tag{3.1}$$

Using this method, we arrive at a relationship between the parameter P and aspect ratio that represents the instantaneous influence of oblateness on that particular parameter. Note that by expressing each parameter as a ratio, we eliminate all factors that do not depend on aspect ratio, which allows us to isolate the exact dependence on degree of oblateness.

We begin this chapter with a discussion of the geometry of an oblate hailstone. Specifically, we present simple formulae for the dependence of major diameter, D, maximum cross-sectional area, A_c, and surface area, A_s on hailstone aspect ratio. Terminal velocity, mass growth rate, and heat transfer rates of hailstones all depend, to some extent, on one or more of these geometrical parameters.

The maximum dimension of an oblate hailstone is its major diameter (D). The dependence of D on aspect ratio may be isolated by rearranging the equation for equivalent diameter (1.2) to give $F(D) = D/D_{eq} = \alpha^{-1/3}$. An oblate hailstone with an aspect ratio of α will have a larger major diameter than a spherical hailstone of the same mass and density. For example, a hailstone with an aspect ratio of 0.77 will have a major diameter that is 1.09 times that of a spherical hailstone.

The maximum cross-sectional area, hereafter referred to as cross-sectional area (A_c), of an oblate hailstone is a function of its major diameter alone: $A_c = \pi D^2/4$. This geometrical parameter depends on aspect ratio through major diameter: $F(A_c) = A_c(\alpha)/A_c(\alpha = 1) = [F(D)]^2 = \alpha^{-2/3}$. Thus, an oblate hailstone has a larger cross-sectional area than a spherical hailstone of the same mass and density. For example, a hailstone with an aspect ratio of 0.77 has a cross-sectional area that is 1.19 times larger than that of a spherical hailstone. A hailstone's instantaneous mass growth rate is partially influenced by its cross-sectional area (Section 3.3).

The surface area of an oblate hailstone affects its heat budget, because a larger surface area leads to more efficient heat transfer. We may determine the dependence of surface area on the degree of oblateness, by dividing (2.7) by the surface area of a spherical hailstone of the same mass and diameter, $A_s(\alpha = 1) = \pi D_{eq}{}^2$:

$$F(A_s) = \frac{\alpha^{-2/3}}{4}\left[2 + \frac{\alpha^2}{\varepsilon}\ln\left(\frac{1+\varepsilon}{1-\varepsilon}\right)\right], \qquad (3.2)$$

where ε is the eccentricity. Equation (3.2) is valid for $0 < \alpha < 1$. According to (3.2), the surface area of an oblate hailstone is larger than that of a spherical hailstone of the same mass. For example, a hailstone with an aspect ratio of 0.77 has a surface area that is 1.01 times larger than that of a spherical hailstone. Note that surface area does not depend on aspect ratio as strongly as major diameter and cross-sectional area do.

3.2 Terminal Velocity

A hailstone's terminal velocity is the speed at which it falls when its drag force balances the force of gravity acting on it in still air. The terminal velocity has a direct influence on a hailstone's evolution within a storm updraft. A hailstone's terminal velocity affects its mass growth rate (2.1); the larger a hailstone's terminal velocity is, the larger its instantaneous mass growth rate. Perhaps more importantly, terminal velocity determines the maximum size of a hailstone that a given storm updraft is capable of supporting. The largest hailstone that an updraft with a maximum velocity of W_{max} can support is one with a terminal velocity equal to W_{max}. Terminal velocity depends on the drag coefficient of a hailstone through the Reynolds number (2.18, 2.19 and 2.20) and drag coefficient is dependent on hailstone shape. Thus, terminal velocity depends on the degree of oblateness of a hailstone. To determine the exact nature of this dependence, we derived an analytical expression for terminal velocity as a function of aspect ratio, using (2.18), (2.19), and (2.20), for a hailstone with a constant mass M and constant density ρ_H. Assuming constant ambient conditions, we arrived at the following relation:

$$F(V_T) = \alpha^{1/3}. \qquad (3.3)$$

The relationship between terminal velocity and aspect ratio is shown in Figure 3.1. A hailstone with an aspect ratio of 0.77 has a terminal velocity that is 0.92 times that of a spherical hailstone of the same mass. The terminal velocity of a hailstone depends, to some extent, on the cross-sectional area presented to the flow. Given that oblate hailstones have larger cross-sectional areas than spherical hailstones of the same mass, they have lower terminal velocities. In general, increasing hailstone oblateness means decreasing hailstone terminal velocity. Oblate hailstones, with their reduced terminal velocities, can be supported by the updraft for longer periods than spherical hailstones and thus have longer total growth times. We may also conclude that because an oblate hailstone must be larger than a spherical hailstone in order to reach the same terminal velocity, a given updraft should be capable of supporting more massive oblate hailstones.

3.3 Mass Growth Rate

The instantaneous mass growth rate of a hailstone depends on aspect ratio through the hailstone's terminal velocity, its net collection efficiency, and the cross-sectional area presented to the flow (2.1). Mass growth rate is also influenced by the hailstone's current growth regime, whether or not it is shedding, and the relative concentrations of cloud ice and cloud water in the vicinity of the growing hailstone. Growth regime and shedding both influence collection efficiency, which depends, to some extent, on aspect ratio (refer to Appendix E for details). In this section, we determine the functional dependence of mass growth rate on aspect ratio for a hailstone of constant mass and density for each of three cases: 1) The collection efficiencies for cloud ice and cloud water, as well as the ambient liquid water content, are assumed to be constant. This situation may occur, for example, when the hailstone enters a region where all ambient water is in the form of ice; 2) No shedding is taking place, and the collection efficiency is not constant. In this situation, the hailstone may be undergoing either wet growth or dry growth; and 3) The hailstone is in the wet shedding growth regime, where net collection efficiency may depend on aspect ratio. For each calculation, we assumed that all ambient conditions remain constant. The dependence of mass growth rate on aspect ratio for the three cases is shown in Figure 3.2.

3.3.1 Constant Collection Efficiency

In the HC2 model, the collection efficiency is constant when the hailstone is in a region of the cloud where there is no liquid water present and it grows by accreting cloud ice only. In this situation, the hailstone is most likely in the dry growth regime. As there is no liquid water present, the mass growth rate equation (2.1) is simplified. Combining (2.1) and (3.3) yields an analytical expression for mass growth rate as a function of aspect ratio:

$$F(dM/dt) = \alpha^{-1/3}. \tag{3.4}$$

According to (3.4), an oblate hailstone has a larger mass growth rate than a spherical hailstone of the same mass. For example, the mass growth rate of an oblate hailstone of aspect ratio 0.77 is 1.09 times that of a spherical hailstone of the same mass (Figure 3.2). The oblate hailstone has a lower terminal velocity than the spherical one (3.3), and given that terminal velocity is directly proportional to mass growth rate, this, by itself, would lead to a lower mass growth rate. However, the oblate hailstone's cross-sectional area is larger, enabling it to collect more cloud water in a given amount of time. A larger cross-sectional area means a larger mass growth rate, and this effect dominates the dependence on terminal velocity.

3.3.2 Growth without Shedding

For this calculation, we assume that the hailstone is in a region that contains cloud water only, but is not shedding. In this situation, the hailstone may be undergoing either wet or dry growth. The collection efficiency for cloud water was used for this calculation, because we assumed that there was no cloud ice in the vicinity of the growing hailstone. The collection efficiency for cloud water (2.14) depends on aspect ratio in the following manner:

$$F(E_w) = \left[\frac{F(V_T)}{F(D)}\right]^{0.15} = \alpha^{1/10}. \tag{3.5}$$

From (2.1) and (3.5) we obtained the following expression for the dependence of hailstone mass growth rate on aspect ratio:

$$F(dM/dt) = F(A_c)F(V_T)F(E_w) = \alpha^{-7/30}. \quad (3.6)$$

The above expression is partially based on empirical findings by Greenan and List (1995). When the dependence of collection efficiency on aspect ratio is taken into account and no shedding is taking place, the mass growth rate of an oblate hailstone is still larger than that of a spherical hailstone of the same mass. For example, the mass growth rate of a hailstone with an aspect ratio of 0.77 is 1.06 times that of a spherical hailstone of the same mass. The difference between the mass growth rate of a spherical and an oblate hailstone is not at large as it is when collection efficiency is constant, because according to the theory presented by Greenan and List (1995), oblate hailstones collect slightly less cloud water than spherical hailstones (Appendix E).

3.3.3 Growth with Shedding

The final mass growth rate calculation that we present is for a hailstone in the wet shedding growth regime, in a region where there is no cloud ice present. We calculated the dependence of mass growth rate on aspect ratio using the empirical relations for net collection efficiency during shedding (2.11, 2.12, 2.13 and 2.14) that we adopted for the HC2 model. The dependence of E_{net} during shedding on aspect ratio is discussed in Appendix E. Net collection efficiency does not depend directly on aspect ratio, so it was not possible to derive a simple analytical expression for mass growth rate as a function of aspect ratio during wet shedding growth. Instead, we calculated this relationship numerically and the results are shown in Figure 3.2. We selected appropriate values for the ambient temperature (T_a = - 15°C), air density (ρ_a = 0.6 kg m^{-3}) and cloud liquid water content (χ_w = 6 g m^{-3}). The calculation was done for a hailstone with a density of ρ_H = 900 kg m^{-3} and an equivalent diameter of 2 cm (i.e. a mass of 3.77 g).

Even when the hailstone was assumed to be shedding, we found that the mass growth rate of an oblate hailstone was still larger than that of a spherical hailstone. According to Figure 3.2, a shedding hailstone with an aspect ratio of 0.77 has a mass growth rate that is 1.05 times that of a spherical hailstone of the same mass. The difference between the mass growth rate of an oblate hailstone and that of a spherical hailstone is smaller during shedding than it is during non-shedding growth.

In all the cases we examined, oblate hailstones had larger growth rates than spherical hailstones of the same mass. The main contributor to this increase is the difference in cross sectional area; oblate hailstones have a larger cross-sectional area than spherical hailstones of the same mass, and thus are able to sweep out more cloud water per unit time. Spherical hailstones shed less water than oblate hailstones of the same mass, due to the tumbling and irregular motions of the latter, but because oblate hailstones have larger cross-sectional areas, they are able to compensate for this loss (Appendix E). With their higher mass growth rates, oblate hailstones within a storm should usually grow larger than spherical hailstones.

3.4 Heat Transfer

The efficiency of heat transfer between a hailstone's surface and the ambient environment depends on a number of different factors, including the hailstone's surface area, major diameter and its Nusselt and Sherwood numbers, Nu and Sh. As supercooled water droplets freeze on the hailstone's surface, they release latent heat, which is first transferred to the stone and then transferred to the air mainly through conduction and convection. If the rate of release of latent heat is higher than the rate at which it is removed from the surface of the hailstone, then the surface temperature rises. The efficiency of heat transfer at the hailstone's surface controls its growth regime and in turn influences its evolution. In this section, we examine the dependence of one heat transfer term (convection/conduction) on hailstone aspect ratio. All four heat transfer terms (2.6, 2.8, 2.9 and 2.10) depend, to some extent, on the degree of oblateness of a hailstone. We chose to examine the convection/conduction term as an example because we are able to derive a simple analytical expression for $F(dQ_k/dt)$.

From (2.6), we may derive an analytical expression for the dependence of the rate of heat transfer due to convection and conduction on aspect ratio, assuming constant ambient conditions:

$$F\left(\frac{dQ_k}{dt}\right)=\frac{F(A_s)}{F(D)}F(\mathrm{Nu}). \qquad (3.7)$$

where $F(A_s)$ is given by (3.2) and $F(D)$ is given in Section 3.1. For the HC2 model, Nusselt number is calculated using the empirical formulae of Rasmussen and Heymsfield (1987a) and Macklin (1963) (Appendix C). The dependence of Nusselt number on hailstone aspect ratio, according to this formulation, can be calculated by rearranging (C.6) in Appendix C to yield $F(\mathrm{Nu})=\kappa/\kappa(\alpha=1)$, where $\kappa=1.02-0.26\alpha$ and $\kappa(\alpha=1)=0.76$. Equation (3.7) is plotted in Figure 3.3 for $0.30\le\alpha\le1.00$.

The rate of transfer of heat by convection and conduction increases with increasing degree of oblateness, due to the increased surface area of oblate hailstones. This is not a strong effect, however: a hailstone with an aspect ratio of 0.77 has a convection/conduction heat transfer rate that is 1.001 times that of a spherical hailstone of the same mass. The increase in heat transfer is more substantial at lower aspect ratios: a hailstone with an aspect ratio of 0.50 has a convection/conduction heat transfer rate that is 1.02 times that of a spherical hailstone of the same mass.

The rate of heat transfer by evaporation and sublimation (2.8) has the same dependence on aspect ratio as dQ_k/dt, since the expression for Sherwood number is the same as that for Nusselt number but for one constant (Appendix C). The other two heat transfer terms in (2.3) also depend on aspect ratio to a certain degree, but the dependence is not as clear as that for convection and conduction.

Overall, oblate hailstones transfer heat more efficiently than spherical hailstones of the same mass. Heat transfer rate affects the surface temperature of a hailstone at any given time, which in turn determines the hailstone's growth regime. The growth regime in turn affects a hailstone's mass growth rate by influencing the amount of intercepted cloud water that remains with the hailstone.

We expect that the differences in heat transfer between oblate and spherical hailstones may influence their mass growth rates to some extent.

3.5 Summary

Under constant ambient conditions, oblate hailstones have lower terminal velocities than spherical hailstones of the same mass and density. The mass growth rate of an oblate hailstone is larger than that of a spherical hailstone, regardless of growth regime or the amount of cloud ice present. Oblate hailstones also have slightly higher heat transfer rates due to convection and conduction. The effects of oblateness on terminal velocity, instantaneous mass growth rate and heat transfer rate can be traced back to the geometrical differences between spherical and oblate hailstones, for the most part.

4 MODELLING THE EFFECTS OF OBLATENESS

4.1 Introduction

In this chapter, the effects of oblateness on the evolution, maximum final equivalent diameter, and total growth time of hailstones are investigated. Two case studies of severe hail days, both on which golfball-sized hailstones were reported, are discussed in detail: 11 July 1985 and 6 July 1984. The evolution of an oblate hailstone that reaches an aspect ratio of 0.77 is described for each of these case study days, followed by a comparison of the HC2 model output for a spherical model hailstone and "very oblate" model hailstone (that reaches an aspect ratio of 0.50). Differences in the final equivalent diameters and total growth times of an "average oblate" ($\alpha_c = 0.77$) hailstone and a spherical hailstone are also calculated for each of the 20 severe hail days in our AHP data set. Finally, we determine the effects of varying aspect ratio on the HC2 model output. Specifically, for each of the 20 severe hail days the evolution of hailstones with aspect ratios ranging between 0.40 and 1.00 is simulated using the HC2 model.

4.2 11 July 1985

4.2.1 Observed Synoptic Situation and Weather Conditions

Smith and Yau (1993a) conducted a detailed investigation of the events on this day. This case was used by Brimelow et al. (2002b) as a case study day for the HAILCAST model, on which HC2 is based. In the early afternoon on 11 July 1985, towering cumulus clouds developed throughout the western Alberta Hail Project area and, by late afternoon, convective activity was present throughout the project area. The most intense storms were those over the Medicine Lake, Ponoka, Sundre and Rumsey regions. The maximum echoes of these intense storms exceeded 60 dBZ for several hours. In total, 228 hail reports were received in the northern half of the Alberta Hail Project area, and of those, 33 were severe (Brimelow et al., 2002b). The largest hailstones produced by these storms were classified as golfball-sized (3.3 – 5.3 cm in diameter), and the longest observed hailswath was in excess of 200 km long (Brimelow et al., 2002b). The 1715 LT upper-air sounding released from Penhold indicated that these severe storms were associated with relatively high buoyant energy and strong vertical wind shear (Figure 4.1). Specifically, the surface-based CAPE was 760 J kg^{-1} and the vertical wind shear in the lowest 6 km above ground level was 6.5×10^{-3} s^{-1}. This combination of relatively high CAPE and strong wind shear imply the possibility of strong and sustained deep convection (Brimelow et al., 2002b).

4.2.2 Cloud Model Output

The CAPE and vertical wind shear on this day indicate the potential for strong multicell storms. The updraft duration, as calculated using the method of Brimelow et al. (2002b), is 60 minutes. The model-derived profiles of updraft velocity and liquid water content for this date are shown in Figures 4.3 and 4.4. The updraft increases from 3 m s^{-1} at the cloud base, where the temperature is 5.7°C, to a maximum of 27 m s^{-1} near a temperature of - 23°C. The calculated maximum updraft is 69% of the maximum buoyancy-derived value of 39 m s^{-1}, using $W_{\max} = (2 \cdot \mathrm{CAPE})^{1/2}$. The forecast cloud-top temperature is - 46°C, and the cloud top height is 9415 m AGL (above ground level). The maximum value of the liquid water content is 3.5 g m^{-3} at a temperature of - 26.3°C and a height of approximately 7219 m AGL. This closely corresponds to the height of the forecast maximum updraft velocity: 6744 m AGL. Above this maximum at 7219 m AGL, the total cloud water content decreases to 3.0 g m^{-3} at the cloud top, where the cloud consists entirely of ice crystals. Table 4.1 summarises the output on this date from the cloud and hail model, as well as observed cloud parameters and maximum hail sizes.

4.2.3 Hail Model Output for the Control Case

In this section, we describe the evolution of a hailstone in the 11 July 1985 storm environment as determined by the HC2 model. For the control case, the simulated hailstone is assumed to have an aspect ratio of 0.77; hereafter we will refer to such as an "average oblate" hailstone. Figure 4.5 (a-f) displays the hail model output for three hailstones, each with different aspect ratios. The control case output, which we shall focus on in this section, is shown as a thick solid black line. Depicted are the height, surface hailstone temperature, equivalent diameter, mass growth rate, terminal velocity and the growth regime (1 = dry, 2 = wet, 3 = wet shedding) as functions of time, t.

At $t = 0$ min, a 700-μm droplet is introduced into the updraft at cloud base. It is rapidly carried upwards, where it freezes upon passing through the - 8°C level and enters the dry growth regime ($T_S < 0°C$; $F_w = 0$). At this point in its evolution, the hailstone is still perfectly spherical. The hailstone remains in the dry growth regime and continues to rise rapidly through the supercooled region of the cloud. By the time it reaches the - 40°C level, at about $t = 14$ min, the hailstone has grown to a diameter of about 0.4 cm. While above this level, it grows very slowly by accreting ice crystals, as all cloud water is assumed to be frozen at ambient temperatures below - 40°C. When the hailstone reaches a size of 1 cm, at a time of 29 minutes, its aspect ratio begins to decrease as it starts to grow as an oblate spheroid. The hailstone is still above the - 40°C level when it begins to become oblate. At about $t = 36$ min, the hailstone has grown sufficiently to descend below the - 40°C level. When it re-enters the mixed-phase region of the cloud, the hailstone has an equivalent diameter of 1.3 cm and an aspect ratio of 0.92. A period of rapid growth begins at this point, because the hailstone now has a relatively large cross-sectional area and is in a region with high LWC (the hail growth zone). As a result, the stone's mass growth rate increases rapidly between $t = 36$ and 53 min (see Figure 4.5d). During its descent, the hailstone encounters strong updrafts and is prevented from falling prematurely from the cloud. This allows the hailstone to grow substantially from 1.3 to 5.8 cm in equivalent diameter during its 17-minute passage through the supercooled region of the cloud. The hailstone reaches its minimum aspect ratio value of 0.77 and a major diameter is 2 cm at a time of 40 minutes. As the hailstone accretes water during its descent, the latent heat of freezing causes the hailstone's surface temperature to rise steadily. It enters the wet shedding growth regime ($T_s = 0$°C, $F_w > 0$, $\chi_w \geq \chi^*$) at $t = 50$ min at an in-cloud temperature of - 11.4°C. The shedding of excess water from the hailstone's surface slows its rate of growth. The hailstone reaches its maximum equivalent diameter of 5.8 cm at $t = 53$ min. There is a brief period of time (between $t = 52.8$ min and $t = 53.3$ min) when the hailstone stops shedding and enters the wet growth regime ($T_s = 0$°C, $F_w > 0$, $\chi_w < \chi^*$). When the hailstone reaches cloud base at $t = 53.3$ min, it begins to melt (its mass growth rate becomes negative) and thus sheds excess water in its wake. The hailstone spends about one minute below cloud base before reaching the ground at $t = 54.5$ min with a final equivalent diameter of 5.3 cm and a terminal velocity of 28.8 m s^{-1}. The HC2 model produced a hailstone with an equivalent diameter at the upper limit of the observed range of 3.3 to 5.3 cm (Table 4.1). The hailstone's fractional liquid water content at the ground is 0.13 (not shown); which is relatively low and indicative of hard hail.

4.2.4 The Effects of Oblateness

To model the effects of oblateness on the case study day 11 July 1985, we ran HC2 for three hailstones, each having a different degree of oblateness. The control case that we described was for an average oblate hailstone: one with an aspect ratio equal to an observed average value of 0.77 for hailstones in Alberta (Barge and Isaac, 1973). We also ran HC2 for a spherical hailstone ($a_c = 1$) and for a "very oblate" hailstone ($a_c = 0.50$). The growth time histories for the spherical and very oblate hailstones are shown in Figure 4.5. This sub-section summarizes the differences in model output for a spherical, average oblate and very oblate hailstone.

Up to a time of about 29 minutes after the droplet embryo is released near cloud base, the evolution of a hailstone in this storm environment is the same for the spherical hailstone, the average oblate hailstone and the very oblate hailstone, as all are spherical until then. At $t = 29$ min, the hailstone diameter, in all cases, reaches 1 cm. Beyond this time, the aspect ratios of the average oblate hailstone and the very oblate hailstone both begin to decrease as they approach their respective values of α_c. Up to this point, the hailstones have all grown mostly by accreting cloud ice crystals above the - 40°C level (Figure 4.5).

Once the hailstones all exceed 1 cm in major diameter, the spherical hailstone's terminal velocity begins to exceed those of the two oblate hailstones (Figure 4.5e). The spherical hailstone is thus the first to descend below the - 40°C level at t = 35 min ($D = D_{eq}$ = 1.3 cm; V_T = 22.5 m s^{-1}). As it is the first hailstone to re-enter the supercooled region of the cloud, there is a brief period of time, beginning at about 35 minutes, where the mass growth rate of the spherical hailstone exceeds those of the two oblate hailstones, which are still trapped above the - 40°C level.

At t = 40 min, the spherical hailstone has a diameter of 2 cm, the average oblate hailstone has an equivalent diameter of 1.8 cm and the very oblate hailstone has an equivalent diameter of 1.6 cm. The average oblate hailstone has descended below the - 40°C level but the very oblate hailstone is still trapped above the - 40°C level. The very oblate hailstone does not grow large enough to descend below the - 40°C level until t = 45 min.

Between 40 and 46 minutes, the spherical hailstone grows at a higher rate than both of the oblate hailstones. This is because the higher terminal velocity of the spherical hailstone enables it to remain "ahead" of the oblate hailstones as it descends back through the storm updraft and the supercooled region of the cloud, collecting more cloud water per minute than the other two hailstones. At t = 48 min, the spherical hailstone enters the wet shedding growth regime, and its growth rate slows down. The average oblate hailstone is still higher up in the cloud and has not yet encountered the region where wet, or wet shedding, growth begins. The very oblate hailstone is even further behind, but it has now descended to a region where its mass growth rate begins to rise, although at this point its growth rate is well below the growth rates of the other two hailstones.

The average oblate hailstone's mass growth rate exceeds the maximum obtained by the spherical hailstone as it continues its descent back through the storm's updraft. The relatively large cross-sectional area of the average oblate hailstone allows it to collect more water than the spherical hailstone was able to during its descent. We have already established, in Chapter 3, that oblate hailstones have larger instantaneous mass growth rates than spherical hailstones; the HC2 model results are consistent with this fact. Specifically, the maximum mass growth rate obtained by the average oblate hailstone is about 1.5 times larger than the maximum mass growth rate obtained by the spherical hailstone. At t = 50 min, the average oblate hailstone enters the wet shedding growth regime, two minutes after the spherical hailstone enters this growth regime. As a result, the growth rate of the average oblate stone decreases.

At t = 50 min, the very oblate hailstone is still much higher in the storm's updraft than either of the two other hailstones, at an ambient temperature of - 35°C. Its mass growth rate increases at this time as it makes its own descent through the supercooled region of the cloud, but its equivalent diameter and mass growth rate are still considerably smaller than those of the other two hailstones.

The spherical hailstone reaches its maximum diameter of 5.0 cm at a time of 50 minutes. Shortly thereafter, it descends below cloud base and melts slightly, reaching the ground at a time of 52.0 minutes with a final diameter of 4.6 cm. The average oblate hailstone reaches its maximum equivalent diameter of 5.8 cm after 53 minutes. When it reaches the ground after 54.5 minutes, its final equivalent diameter is 5.3 cm, 7 mm larger than that of the spherical hailstone.

Right around the time when the spherical hailstone reaches the ground, the mass growth rate of the very oblate hailstone surpasses the mass growth rate of the average oblate hailstone. The very oblate hailstone's mass growth rate reaches its maximum, which is twice as large as the maximum reached by the average oblate hailstone (3.2 times as large as the spherical hailstone's maximum mass growth rate), at approximately t = 58 min. It enters the wet shedding growth regime at t = 58 min. The cloud's updraft collapses at t = 60 min; when this occurs, the very oblate hailstone is no longer supported within the cloud. The cessation of the cloud's updraft makes little difference in the rest of this hailstone's evolution, however, given that it is very close to cloud base when the updraft ceases to exist. The very oblate hailstone reaches cloud base at t = 61 min, where it attains its maximum equivalent diameter of 7.5 cm. It reaches the ground at $t = 62.1$ min with a final equivalent diameter of 6.9 cm, which is considerably larger than the final equivalent diameters of the average oblate and spherical hailstones.

Oblate hailstones have lower terminal velocities than spherical hailstones, as discussed in Chapter 3, and thus also have longer total growth times (the total time between the release of the embryo at cloud base and the hailstone reaching the ground). As terminal velocity decreases with decreasing hailstone oblateness, the spherical hailstone had the shortest growth time and the very oblate hailstone had the longest for this case study day. The updraft collapsed while the very oblate hailstone was still growing within the storm, but this occurred when the hailstone was near cloud base and thus had little (if any) effect on its evolution. Its final equivalent diameter was significantly larger (about 30% larger) than that of the average oblate hailstone. The comparatively large cross-sectional areas of the oblate hailstones enabled them to collect more cloud water than the spherical one as they descended through the supercooled region of the storm.

For two hailstones of different aspect ratios to have identical terminal velocities, the hailstone with the lower aspect ratio must be larger. This implies that the maximum size of a hailstone that a particular storm updraft is able to support increases with increasing degree of oblateness. The model output for 11 July 1985 was consistent with this theory: the very oblate hailstone was the largest and the spherical hailstone was the smallest of the three hailstones. The effects of oblateness on the heat budget had little impact on the evolution of these hailstones. All hailstones entered into the wet shedding growth regime as they approached cloud base and had similar fractional water contents when they reached the ground.

4.3 6 July 1984

4.3.1 Observed Synoptic Situation and Weather Conditions

The synoptic situation on 6 July 1984 was a typical example of deep convection over central Alberta. The low-level flow advected warm, humid air from the east. The upper level flow indicated a short wave trough contributing to synoptic-scale ascent via vorticity advection. A capping inversion with a deep layer of convectively unstable air aloft resulted in the classical "loaded gun" profile typical for Alberta hailstorms (Smith and Yau, 1993a,b). This capping inversion was removed by surface heating, based on the observed temperature and dewpoint (Figure 4.2).

The first radar echoes detected by the Penhold S-Band radar appeared south of Rocky Mountain House in the late morning. An early afternoon line of cells formed that extended from Edmonton south to Sundre, and the most activity occurred in the Penhold – Big Valley – Three Hills region. The maximum reflectivity observed on this day was 50 dBZ. A total of 127 hail reports were received within the southern half of the Alberta Hail Project area, of which 15 were severe. The largest reported hail was classified as golfball (3.3 - 5.3 cm in diameter).

4.3.2 Cloud Model Output

The CAPE and vertical wind shear on this day indicate the potential for air-mass or weak multi-cell storms, according to the criteria used by Brimelow et al. (2002b). The updraft duration, as calculated by the model-based CAPE and shear, is 46 minutes. The model-derived profiles of updraft velocity and liquid water content for this date are shown in Figures 4.3 and 4.4, respectively. The updraft increases from 3 m s^{-1} at cloud base (at height 1010 m AGL with a temperature of 6°C) to a maximum of 19.7 m s^{-1} at a temperature of approximately - 12°C. The calculated maximum updraft is 65% of the maximum buoyancy-derived value of 30.1 m s^{-1}. The forecast cloud-top temperature is -27.3°C, and the cloud top height is 5719 m AGL. The maximum value of the LWC is 3.8 g m^{-3} at cloud top; here, the cloud consists of a mix of ice crystals and supercooled water droplets. The maximum LWC value is located nearly 2000 m above the height of the maximum forecast updraft velocity. Table 4.1 summarizes the cloud and hail model output for this case study day, along with selected observed quantities.

4.3.3 Hail Model Output for the Control Case

Figure 4.6 (a-f) shows the growth time history of an average oblate hailstone, along with that of a spherical and a very oblate hailstone, simulated by the HC2 model in the storm environment of 6 July 1984. In this section we will concentrate on the evolution of an average oblate hailstone (thick solid black line in Figure 4.6).

At t = 0 min, a 400-μm droplet is introduced into the updraft at the cloud base, which freezes upon passing through the - 8°C level and enters the dry growth regime. The hailstone remains in the dry growth regime and continues to rise rapidly through the supercooled region of the cloud. At t = 11 min, the hailstone reaches the apex of its trajectory at an in-cloud temperature of - 26°C and a height of 5663 m AGL; it now has a diameter of 0.4 cm. In this region, the cloud water is mostly in the form of supercooled droplets, with a mere 3% in the form of ice crystals. Soon after the apex of its trajectory is reached, the hailstone begins its descent back through the cloud. At 15 minutes, it has reached a diameter of 1 cm and its aspect ratio begins to decrease. The hailstone enters into a period of rapid growth between 15 and 25 minutes. The updraft encountered by the descending hailstone is sufficient to keep it from falling prematurely from the cloud, allowing it to grow from 1 cm to an equivalent diameter of 3.9 cm during its 12-minute passage through the supercooled region of the cloud. The hailstone reaches its minimum aspect ratio value of 0.77, when its major diameter is 2 cm, at t = 19 min. The hailstone's surface temperature never drops below - 14.5°C, and reaches a local maximum of - 4.1°C at around t = 14 min, before rapidly decreasing to - 11°C and then rising slowly again. It enters the wet growth regime at t = 22 min at an in-cloud temperature of - 12.5°C. The hailstone begins to shed when it enters the wet shedding growth regime at t = 23 min at an in-cloud temperature of - 9.7°C. For a brief period of time beginning at t = 26 min, the hailstone once again enters the wet growth regime (no shedding) and remains in that growth regime until it reaches cloud base at t = 27 min. The maximum equivalent diameter of 3.9 cm is attained at 27 minutes and decreases thereafter as the hailstone melts below cloud base. The hailstone spends less than one minute below cloud base before reaching the ground at 27.9 minutes with a final equivalent diameter of 3.6 cm. The HC2 model produced golfball-sized hail on this severe storm day, in agreement with observations (Table 4.1). The hailstone's fractional water content at the ground is 0.13, which is indicative of hard hail.

4.3.4 Effects of Oblateness

We now compare the modelled growth of the average oblate hailstone with those of the spherical and very oblate hailstones. The spherical and very oblate hailstones evolve in the same manner as the average oblate hailstone until 15 minutes after their droplet embryos were released near cloud base. At $t = 15$ min, their diameters reach 1 cm and the average and very oblate hailstones' aspect ratios begin to decrease towards their respective minimum values. In this time, all three hailstones were carried by the storm's updraft to a maximum height of 5663 m AGL at an in-cloud temperature of - 26°C and, following that, began their descent back through the supercooled region of the cloud.

As with the previous case study day, the spherical hailstone has the largest terminal velocity of the three, so it falls back through the cloud more quickly than the other two. This particular storm's cloud top is at a temperature of - 27.3°C, so there is no region ($T_a < -40°C$) characterized by a slow hailstone growth process due to accretion of cloud ice crystals only. All three hailstones reach their maximum heights relatively quickly, and then descend back through the cloud. The spherical hailstone falls through the storm faster than the average oblate hailstone, which is in turn faster than the very oblate hailstone, so at any time after $t = 15$ min, the three hailstones are at different heights in the storm. The modelled hailstones never reach the - 40°C level and consequently, there are no instances where the oblate hailstones grow more slowly than the spherical hailstone. At any point in time before the three hailstones reach cloud base, the spherical hailstone has the smallest equivalent diameter and mass growth rate while the very oblate hailstone has the largest equivalent diameter and mass growth rate (Figure 4.6).

The spherical hailstone enters the wet growth regime at t = 22 min, which causes its mass growth rate to decrease shortly thereafter. The spherical hailstone attains its maximum diameter of 3.4 cm when it reaches cloud base at t = 26 min; at this point, it is still in the wet growth regime. When it reaches the ground at 26.8 minutes, its final diameter is 3.2 cm. Both oblate hailstones are still descending through the cloud when the spherical hailstone reaches the ground.

The average oblate hailstone enters the wet growth regime at t = 22 min and then begins to shed about one minute later, remaining in the wet shedding growth regime until it reaches the ground. Its mass growth rate reaches its maximum value at t = 24 min; this hailstone's peak value is 1.5 times larger than the maximum growth rate of the spherical hailstone. The average oblate hailstone reaches its maximum equivalent diameter of 3.9 cm when it reaches cloud base at 27 minutes, and melts to a final equivalent diameter of 3.6 cm by the time it reaches the ground at 27.9 minutes.

The very oblate hailstone goes straight from the dry growth regime to the wet shedding growth regime at t = 23 min. Except for a very brief time around cloud base where it enters the wet growth regime, the very oblate hailstone sheds until it reaches the ground. This hailstone's mass growth rate reaches its maximum value at 26 minutes; its peak value is three times larger than that of the spherical hailstone and twice as large as that of the average oblate hailstone. The very oblate hailstone reaches its maximum equivalent diameter of 5.0 cm at t = 28 min when it reaches cloud base, then melts to a final equivalent diameter of 4.7 cm by the time it reaches ground at 29.7 minutes. The minimum (i.e. most negative) mass growth rate of the three hailstones is achieved by the very oblate one as it is melting below cloud base, but this hailstone still grows significantly larger than the other two hailstones in the 6 July 1984 storm environment.

The updraft duration on this day is 46 minutes and the maximum growth time of all three hailstones is less than 30 minutes, so updraft collapse has no influence on the evolution of the hailstones in this storm environment. The very oblate hailstone grew to the largest equivalent diameter of the three and also had the longest growth time. Its relatively low terminal velocity was responsible for the longer growth time; the very oblate hailstone's terminal velocity was smaller than those of the other two hailstones (Figure 4.6e), even though it was larger than the other two at any point in time.

The instantaneous mass growth rate at any point in time after t = 15 min during these simulations appeared to be proportional to the degree of oblateness of the hailstone. If we examine Figure 4.6, we notice that differences in mass growth rate become apparent as soon as the aspect ratios of the average oblate and very oblate hailstones begin to decrease, at t = 15 minutes. In Chapter 3, we determined that mass growth rate is influenced by the degree of oblateness of a hailstone: an oblate hailstone has a larger mass growth rate than a spherical hailstone of the same mass. As soon as the aspect ratios of the average and very oblate hailstones in this simulation began to decrease, their cross-sectional areas increased, relative to that of a spherical hailstone of the same mass. These initial increases in cross-sectional area caused the mass growth rates of the average and very oblate hailstones to become larger than that of the spherical hailstone (Section 3.3). Until the hailstones in this simulation fell below cloud base, the very oblate hailstone had the largest mass growth rate of the three, due to its larger mass and greater cross-sectional area, while the spherical hailstone had the smallest mass growth rate.

This simulation highlighted the effects of oblateness on the growth regime. The spherical hailstone never shed while it was above cloud base. The shape and size of the average oblate hailstone enabled it to begin shedding before it descended below cloud base, after experiencing a period of wet growth without shedding. The very oblate hailstone went directly from dry to wet shedding growth, with an episode of wet growth around the time it reached cloud base. Despite the increased shedding of the oblate hailstones, they still grew larger than the spherical stone, and, in the end, the growth regime did not have a large effect on the final equivalent diameters of the hailstones relative to one another. We saw in Chapter 3 that aspect ratio has only a small effect on a hailstone's heat budget parameters; the results of this simulation support that conclusion.

4.4 Effects of Oblateness on 20 Severe Hail Days

On both case study days, 6 July 1984 and 11 July 1985, the spherical hailstone had the shortest growth time, while the very oblate hailstone had the longest growth time. The spherical hailstone was the smallest of the three different types while the very oblate hailstone was the largest, all comparisons being done once the hailstones had reached the surface. We now investigate the rest of the 20 severe hail days between 1983 and 1985 to determine the overall effects of oblateness on the final mass and total growth time of hailstones.

For each of these 20 severe hail days, HC2 was run twice: once with a spherical hailstone and once with an average oblate hailstone. For each day, the final equivalent diameters and the total growth times were compared. Table 4.2 shows the absolute difference in equivalent diameter and growth time for oblate hailstones and spherical hailstones ($D_{eq} - D_S$ and $\tau - \tau_S$, respectively). These numbers are also shown in percentages with respect to the values for the spherical hailstone. For 18 out of 20 severe hail days, the average oblate hailstone grew larger than the spherical hailstone. On one day, 23 July 1985, HC2 predicted pea sized hail, with a final equivalent diameter of 1.1 cm for both the spherical and average oblate runs. On 24 June 1983, the spherical hailstone actually grew about 4% larger than the average oblate hailstone. This anomalous result is related to the duration of the storm, specifically, the location of the hailstone within the storm when the updraft collapses. The cloud model assigned an updraft duration of 60 minutes to this particular storm. The total growth time was 63.1 minutes for the spherical hailstone and 63.7 minutes for the oblate hailstone; these values were not much longer than the storm duration. When the updraft collapsed at t = 60 min during the simulation, the hailstones were still located relatively high in the cloud. Their respective passages through the hail growth zone were cut short, as there was no updraft available to slow their descents. Before the updraft collapsed, the oblate hailstone, with its lower terminal velocity, remained suspended in the upper reaches of the cloud for a longer period of time than the spherical hailstone did. As a result, the spherical hailstone entered the supercooled region of the cloud ahead of the oblate hailstone, so the former got a head start on its rapid growth stage. When the updraft collapsed, the oblate hailstone was higher in the storm, and smaller than, the spherical hailstone. The average oblate hailstone did not spend as much time in the region of rapid hail growth and, as a consequence, evolved to have a smaller final equivalent diameter than the spherical hailstone. To ensure that updraft termination was the only factor that allowed the spherical hailstone to grow larger than its oblate counterparts, we changed the updraft duration on 24 June 1983 from 60 to 70 minutes and re-ran the spherical and average oblate hailstone simulations. The extra 10 minutes that were added to updraft duration yielded quite different results: the oblate hailstone grew 18% larger than the spherical hailstone. The effects of updraft duration on final hailstone size are discussed in detail in Chapter 6.

On average, oblate hailstones grew 10.1% larger than spherical ones. If we extend the duration of the 24 June 1983 storm to 70 minutes and use the output data from that run to calculate the average increase in equivalent diameter, this number becomes 11.2% (not shown in Table 4.2). On all 20 severe hail days, the growth time of the average oblate hailstone was longer than that of the spherical hailstone: on average 1.1 minutes or 2.5% longer.

An increase of 10% in equivalent diameter may not seem overly large, but it is still of some significance if we consider the increase in terms of the potential hail damage. If we assume that the terminal velocity of a large hailstone near the ground is proportional to $D_{eq}^{1/2}$ (Rogers and Yau, 1989, p. 125), then the kinetic energy of a hailstone is proportional to D_{eq}^{4}. We calculated the percent increase in kinetic energy of an oblate hailstone compared to a spherical hailstone for each of the 20 severe hail days, using their final maximum equivalent diameters (Table 4.2). The average increase in kinetic energy for all severe hail days is 49.9% (55.3% if we use the 70-minute duration output for 24 June 1983). As the kinetic energy of a hailstone is directly related to the amount of damage that it may cause, a 10% increase in equivalent diameter translates to about one-and-a-half times the amount of damage that may occur during a hailstorm (assuming that there are no strong winds present).

For most of the severe hail days that were examined, model oblate hailstones grew larger than the modelled spherical hailstones. Oblate hailstones remained within the storm longer than spherical stones, as reflected in their increased growth time. Updraft duration plays a significant role in determining the final size of a given hailstone. If the updraft collapses before, or soon after, the hailstone descends below the - 40°C level, then that hailstone's residence time in the rapid growth region of the cloud is cut short, resulting in a reduced final equivalent diameter.

4.5 Effects of Aspect Ratio on Model Output

Field experiments have shown that hailstones have aspect ratios that lie within the range 0.30 - 1.00 (Barge and Isaac, 1973). We already determined that the degree of oblateness of a hailstone influences model output parameters such as final maximum equivalent diameter and total growth time. However, up to now we have only run simulations on severe hail days for hailstone with three different aspect ratios: 1.00, 0.77 and 0.50. In this section, we determine how final maximum equivalent diameter, D_{eq}, and total growth time, τ, vary with aspect ratio, α_c.

For each severe hail day in our data set, we ran HC2 for hailstones with aspect ratios within the range 0.40 and 1.00. The maximum final equivalent diameters and total growth times are listed in Tables 4.3 (case study days) and 4.4 (average for all severe hail days). Absolute values as well as percent differences (compared to a model spherical hailstone produced by the same storm) are shown.

The maximum growth time of 30 minutes for the $\alpha_c = 0.40$ hailstone on 6 July 1984 was much less than the updraft duration of 46 minutes, so we may assume that the updraft duration parameter had no effect on these results. As Table 4.3 (b) indicates, final equivalent diameter and total growth time both increase steadily as aspect ratio decreases. The $\alpha_c = 0.40$ hailstone had a final equivalent diameter of 5.4 cm, which is 68.8% larger than that of a spherical hailstone produced by the same storm. This extremely oblate hailstone had 711% (or about 8 times) more kinetic energy than the spherical hailstone.

Updraft duration had only a small influence on final equivalent diameter as a function of aspect ratio on 11 July 1985. Hailstones with final aspect ratios less than 0.50 were suspended within the storm long enough for the collapse of the updraft to cut short their growth times, leading to relatively smaller hailstones than would be produced in the same storm with an increased duration. On 11 July 1985, the $a_c = 0.40$ hailstone had a final equivalent diameter of 7.3 cm, which is 60.7% larger than the spherical hailstone produced by the same storm. The total growth time for this extremely oblate hailstone was 63 minutes, and the storm's updraft duration was 60 minutes; the updraft collapsed before this hailstone had a chance to grow to its full potential. The hailstone with a final aspect ratio of 0.40 had 566% (or about 6.7 times) more kinetic energy than a spherical hailstone produced on 11 July 1985.

The average final equivalent diameter for all severe days increases monotonically with decreasing aspect ratio (Table 4.4). Average growth time also increases monotonically with decreasing aspect ratio. The most oblate hailstone ($a_c = 0.40$) produced an average final equivalent diameter increase of about 44% which caused an increase in kinetic energy of 412% (Table 4.4). Therefore, on average, extremely oblate hailstones grew large enough to quite a bit more damage than spherical hailstones.

The results in Tables 4.3 and 4.4 are shown in graphical form in Figure 4.7. The curve representing the results for 11 July 1985 follows the same general shape as the other two curves down to an aspect ratio of 0.50. For 11 July 1985 hailstones with aspect ratios less than 0.50, updraft duration effects begin to become apparent, leading to a less rapid increase in final equivalent diameter as a function of aspect ratio. The relationship between total growth time and aspect ratio is also slightly different for extremely oblate hailstones on 11 July 1985: growth time does not increase as rapidly with decreasing aspect ratio. This is due to the fact that a portion of these hailstones' lifetimes is spent in free-fall, shortening their residence times in the cloud and thus their total growth times.

4.6 Summary

We investigated in detail the evolution of three hailstones (spherical, average oblate and very oblate) on each of two case study days: 11 July 1985 and 6 July 1984. In both cases, golfball-sized hailstones were reported. The HC2 model predicted golfball-sized hailstones on both of these days for the control case (average oblate hailstone). In each case, the spherical hailstone had the smallest equivalent diameter at ground and the very oblate hailstone had the largest.

Simulations were run for two types of model hailstones for each of 20 severe hail days: an average oblate hailstone with an aspect ratio of 0.77 and a spherical hailstone. On average, oblate hailstones were about 10% larger (at ground) than spherical hailstones and had 1.5 times more kinetic energy. The average oblate hailstones had growth times that were, on average, 2.5% longer than those of the spherical hailstones. On average, for the 20 severe hail days in our data set, growth time and final equivalent diameter both increase with decreasing aspect ratio. The size that a hailstone attains before it falls to the ground depends on the amount of time it resides in the hail growth zone. If the storm updraft collapses prematurely, the hailstone's residence time in the hail growth zone is cut short and thus it does not grow as large. Updraft collapse sometimes enabled spherical model hailstones to grow larger than oblate model hailstones. As oblate hailstones have longer total growth times, and lower terminal velocities, than their spherical counterparts, they have less residence time in the hail growth zone if the updraft collapses before the hailstones hit the ground.

5 EFFECTS OF ROUGHNESS AND FACTOR SEPARATION ANALYSIS

5.1 Introduction

In the previous chapters, we estimated and modelled the effects of oblateness on the evolution of hailstones and the parameters that govern their growth. The focus of this chapter shifts to the role of the roughness of the hailstone surface and, in particular, the relative importance of roughness compared to oblateness.

Field observations of hailstones (e.g. Barge and Isaac, 1973; Knight and Knight, 1970b) indicate that hailstones collected at ground typically have rough surfaces with numerous "bumpy" irregularities (e.g. Figure 1.2). For a given mass, a rough hailstone has a larger surface area compared to a smooth hailstone. This increased surface area changes the terminal velocity because it affects the balance between the gravitational force and the drag force. The roughness of the hailstone surface also affects the heat exchange properties as quantified by the Nusselt and Sherwood numbers. Carefully analysed measurements of the heat exchange for rough hailstones and perfectly smooth hailstones in ice chambers have yielded expressions for Nusselt and Sherwood numbers (e.g. Bailey and Macklin, 1968; Greenan and List, 1995). However, the scientific literature does not contain documentation of experimental or theoretical studies that directly quantify the impact of surface roughness on the heat budget of an evolving hailstone.

All results presented in the previous chapters are based on empirical data obtained for typically rough-surfaced hailstones. For example, the terminal fall speed formulae (Böhm, 1989) include all roughness effects in an empirical drag coefficient. To model the "artificially" smooth-surfaced hailstones, we will alter the aforementioned expressions accordingly.

To quantify the relative contributions of roughness and oblateness to the final size of a hailstone, we will use the Factor Separation Method of Stein and

Alpert (1993). This is a powerful tool that we use to separate the contributions of the various factors (hailstone roughness and shape) and also to quantify the simultaneous interaction of these factors in regards to the final size of hailstones. The Factor Separation Method has been used widely in atmospheric sciences: for example, see Alpert and Tsidulko (1994), Alpert et al. (1995a,b), Alpert et al. (1996a,b), Deng and Lilly (1992), Eastman et al. (2001), Guan and Reuter (1996), Khain et al. (1993), Krichak et al. (1997a,b), Ramis and Romero (1995), Romero et al. (1997, 1998), and Reuter and Guan (1995).

5.2 Simulating the Evolution of a Smooth-Surfaced Hailstone

To simulate the evolution of a smooth-surfaced hailstone, we must know how the microphysical parameters that govern hail growth change when the hailstone's surface is smooth rather than rough. We have already indicated that surface roughness influences the heat budget parameters Nu and Sh along with the hailstone's terminal velocity. In this section we obtain expressions for these parameters for smooth-surfaced hailstones.

5.2.1 Terminal Velocity of a Smooth-Surfaced Hailstone

According to Böhm (1989), a hailstone's drag coefficient is influenced by its surface roughness. The enhancement to the drag coefficient for a hailstone with a roughness factor of *q* compared to a perfectly smooth-surfaced hailstone of the same mass and shape is

$$\frac{C_{De}}{C_D} = q^{-3/4} = \left(\frac{A_e}{A}\right)^{-3/4} , \qquad (5.1)$$

where C_D is the drag coefficient of a smooth-surfaced hailstone, C_{De} is the drag coefficient of a rough-surfaced hailstone, A_e is the effective projected cross-sectional area of the hailstone presented to the flow and A is the area of the smallest circle or ellipse that completely contains A_e.

Castellano and Nasello (1997) reported that natural hailstones have roughness factors that are between 0.7 and 1. According to Lozowski and Strong

(1978), surface roughness can enhance the drag of a realistically rough hailstone by one third. For a hailstone with a roughness factor of 0.7, the enhancement to the drag coefficient is (from 5.1)

$$\frac{C_{De}}{C_D} = q^{-3/4} = (0.7)^{-3/4} = 1.31,$$

or about one third. Based on the work by Lozowski and Strong (1978) and Castellano and Nasello (1997), we decided that an appropriate value for the roughness factor of a realistically rough hailstone is 0.7.

For a hailstone in free-fall, there exists a critical Reynolds number (Re*) at which it experiences an abrupt decrease in its drag coefficient, which in turn causes an increase in terminal velocity (Prandtl, 1923). This drop is followed by a slow, steady increase in drag coefficient for Re > Re*, due to increasing friction drag (Eng Young and Browning, 1967). Equation (5.1) is valid for hailstones that are in the super-critical regime, according to Böhm (1989). That is, a rough hailstone has a higher drag coefficient, and thus a lower terminal velocity, compared to a smooth hailstone of the same mass, as long as both the smooth and rough-surfaced hailstones are in the supercritical regime.

Experimental work with model hailstones in wind tunnels, as well as in free-fall, has yielded values for the critical Reynolds number for hailstones of different degrees of roughness. The critical Reynolds number for a smooth sphere is about 200 000 (this corresponds to a hailstone diameter of approximately 8 cm), according to Hoerner (1958). Experimental work by Bicknell (1962), Willis et al. (1964), Eng Young and Browning (1967), and Roos and Carte (1973) indicate that a rough surface can trigger the transition from sub-critical to super-critical flow at a lower Reynolds number than is required for smooth hailstones. According to Willis et al. (1964), rough-surfaced hailstones have critical Reynolds numbers as low as about 40 000 (diameters as small as 2 cm). These observations imply that, for hailstones with Reynolds numbers between 40 000 and 200 000, it is likely that a rough-surfaced hailstone will be in the super-critical flow regime while a smooth-surfaced hailstone will be in the sub-critical flow regime. The rough-surfaced hailstone will thus have a lower drag coefficient (and a higher terminal velocity) than the smooth-surfaced hailstone, provided that they are of equal mass. To simulate a smooth-surfaced hailstone using the HC2 model, we assume that, on average, its terminal velocity is lower than that of a rough hailstone of the same mass and shape.

We can use Böhm's (1989) equations for the terminal velocity of an oblate hailstone to estimate the reduction of the terminal velocity of a smooth-surfaced hailstone compared to that of a rough-surfaced hailstone (with a roughness factor of 0.7) of the same mass and shape:

$$V_{T(smooth)} = 0.95V_T, \tag{5.2}$$

where V_T is the terminal velocity of a realistically rough hailstone, calculated using the semi-empirical formulae of Böhm (1989) (2.18, 2.19 and 2.20). This reduction in terminal velocity has an effect on the evolution of smooth hailstones. In HC2, the terminal velocity is calculated at each time step using Böhm's method. The terminal velocity of smooth hailstones is computed using (5.2).

The instantaneous mass growth rate of a hailstone is directly proportional to its terminal velocity (2.1). Based on this fact, we expect smooth-surfaced hailstones to have lower instantaneous mass growth rates compared to rough-surfaced hailstones; they will grow more slowly in an identical storm environment and will thus have longer growth times. Also, due to this difference in terminal velocities, we expect that a storm updraft of a given strength will be able to support larger smooth hailstones than rough hailstones. Smooth hailstones thus have the potential to grow larger than rough hailstones, but only if the growth time is not limited by updraft duration.

5.2.2 Heat Budget Parameters for a Smooth-Surfaced Hailstone and Effects of Roughness on Nu and Sh

When modelling a hailstone with a smooth surface, we must alter its heat budget parameters accordingly, in addition to its terminal velocity. A rough hailstone has a larger surface area than a smooth hailstone of the same mass and shape. This increased surface area in turn causes an increase in the efficiency of heat transfer to and from a hailstone. However, as it is difficult to calculate the exact surface area of a rough hailstone, the effects of roughness are usually included within the Nusselt and Sherwood numbers (Appendix C). These heat budget parameters must be altered accordingly when simulating the growth of a smooth-surfaced hailstone. For the HC2 model, we have derived expressions for Nu and Sh of a smooth-surfaced hailstone by removing all roughness effects (Appendix C; C.8).

Nusselt number and Sherwood number depend on roughness as well as the degree of oblateness of a hailstone. To determine the relative importance of each of these factors to a hailstone's heat budget, we calculated Nu for four different types of hailstones with Reynolds numbers between Re = 0 ($D_{eq} = 0$) and Re = 60000 ($D_{eq} = 3.7$ cm for $T_a = -15$°C). Nusselt number as a function of Reynolds number for each of four types of hailstones is shown in Figure 5.1: a rough, oblate hailstone with $\alpha = 0.77$; a smooth, oblate hailstone with $\alpha = 0.77$; a rough, spherical hailstone; and a smooth, spherical hailstone. When the hailstone is rough and oblate, Nu is highest, and therefore heat transfer is most efficient. The heat transfer is least efficient when the hailstone is smooth and spherical. Heat transfer to and from a hailstone of constant roughness is increased slightly when it is flattened into an oblate spheroid, due to the increase in surface area. The heat transfer to and from a hailstone with a rough surface is much more efficient than that of a hailstone of identical mass and shape with a smooth surface. For example, for a Reynolds number of 40 000 ($D_{eq} = 2.9$ cm for $T_a = -15$°C), Nu of a rough, oblate hailstone is about 3 times larger than that of a smooth, oblate hailstone.

Given that heat transfer is more efficient for rough hailstones than for smooth ones, smooth hailstones will more readily enter the wet growth regime than rough hailstones of the same mass, under identical ambient conditions. This difference in heat transfer efficiency can influence the growth of smooth hailstones. The influences on hailstone growth are likely to be most apparent near the end of a smooth-surfaced hailstone's evolutionary path, when the release of latent heat due to freezing of cloud water droplets warms the hailstone enough to bring its surface temperature to 0°C, allowing it to enter the wet growth regime (or the wet shedding growth regime, depending on the ambient liquid water content).

5.3 The Factor Separation Method

The HC2 model was developed so that hailstone oblateness can be either "switched on" or "switched off". A model run with oblateness switched off is a simulation of the growth of a spherical hailstone. There is also an option for the simulated hailstone to evolve with either a smooth surface (roughness switched off) or a rough surface (roughness switched on). The effects of turning off roughness are included in the terminal velocity calculations and in the heat budget (i.e. Nusselt and Sherwood number) calculations. In the remainder of this chapter, we analyze the relative effects of roughness and oblateness on the evolution of a hailstone. The analysis is based on four model runs for each of the 20 severe hail days, where roughness and oblateness were either switched on or switched off. Hereafter we will refer to these runs as *RO* (roughness and oblateness both switched on), *SO* (roughness switched off and oblateness switched on), *RS* (roughness switched on and oblateness switched off) and *SS* (roughness and oblateness both switched off).

A common interpretation of an individual effect, such as hailstone roughness, on a certain variable, *f*, is *f(RO) - f(SO)*. Similarly, the effect of oblateness on *f* is given by the expression *f(RO) - f(RS)*. According to Stein and Alpert (1993), this interpretation of an individual effect may not be entirely correct. The value *f(RO) - f(SO)* not only includes the individual effects of hailstone roughness but also mutual effects that arise from the interaction of the roughness effects with the oblateness effects. This fact is also true for the expression *f(RO) - f(RS)*. If the mutual interaction effect happens to be significant, then the above simple interpretation of comparing the *SO* or *RS* run with the *RO* run is misleading. Stein and Alpert described an alternative technique based on factor separation that avoids the ambiguity related to the mutual interaction technique (refer to Stein and Alpert, 1993, for details). We used their Factor Separation Method to analyse the effects of roughness and oblateness to determine the specific effects of surface roughness on the evolution of a hailstone, and also to validate our findings on the effects of oblateness (Chapter 4). The following expressions were used to analyse the effects of roughness and oblateness on final equivalent diameter, D_{eq}, and total growth time, τ, for each of the 20 severe hail days:

$$f_T = \frac{f(RO) - f(SS)}{f(SS)}, \tag{5.3}$$

$$f_R = \frac{f(RS) - f(SS)}{f(SS)}, \tag{5.4}$$

$$f_O = \frac{f(SO) - f(SS)}{f(SS)}, \text{ and} \tag{5.5}$$

$$f_M = \frac{f(RO) - f(RS) + f(SS) - f(SO)}{f(SS)}, \tag{5.6}$$

where f_T is the total effect, f_R is the pure roughness effect, f_O is the pure oblateness effect, and f_M is the mutual interaction effect. The total effect is the sum of both the individual effects and the mutual interaction effect: $f_T = f_R + f_O + f_M$.

Table 5.2 lists the total, individual and mutual effects, in percentages, on the final equivalent diameter of a hailstone for each of 20 severe hail days. The average of each effect for the severe hail days is also listed in the last row. Table 5.3 gives the same information but for total growth time. We will discuss in turn the factor separation analysis for both of the case study days, and then concentrate on the general trends displayed for all the severe hail days. Total growth times and final equivalent diameters for each Factor Separation Method experiment are summarised in Table 5.1 for the case study days 11 July 1985 and 6 July 1984.

5.4 Factor Separation Analysis for the Case Study Days

5.4.1 11 July 1985

The growth time histories for four different model hailstones (*RO*, *RS*, *SO* and *SS*) on 11 July 1985 are shown in Figure 5.2 (a-f). The pure roughness effect is a reduction of 7% in the final size of the hailstone (Table 5.2). The pure oblateness effect on this case study day is a 16.4% increase in final equivalent diameter, compared to the value of 17.1% that we attained earlier for rough hailstones. There is a small mutual interaction effect of - 0.4% which implies that, for the most part, the effects of roughness and oblateness are independent of each other on this day. The total effect is a 9% increase in final equivalent diameter.

The pure roughness effect reduces the total growth time by 9%. This effect stems from the increase in terminal velocity of a rough hailstone, which reduces the stone's residence time in the updraft and ultimately reduces its size. Oblateness alone causes a 5.5% increase in total growth time (Table 5.3), which is fairly consistent with our previous observations (Table 4.3a). Oblate hailstones have lower terminal velocities than spherical hailstones of the same mass; this accounts for the increased growth time. The total effect of roughness and oblateness is to reduce the growth time by 4.9%, while the mutual interaction effect is a decrease of 1%. Given that the total effect, and the mutual interaction effect, are both negative, we may conclude that roughness dominates total growth time with respect to oblateness. In other words, the decrease in growth time on account of roughness is greater than the increase in growth time on account of oblateness.

Terminal velocity differences between smooth and rough hailstones account for the 7% reduction in final equivalent diameter of rough hailstones. The effects of hailstone terminal velocity pertaining to roughness and oblateness are visible in the growth time history shown in Figure 5.3. The rough spherical hailstone (highest terminal velocity) grows to the smallest final diameter and has the shortest growth time, while the smooth oblate hailstone (lowest terminal velocity) grows to the largest final equivalent diameter and has the longest growth time (Table 5.1).

There are some differences in growth regime as a function of time between the four experiments (Figure 5.2f), but these differences are apparent only during the last few minutes of each hailstone's trajectory. Final equivalent diameter differences and growth time differences appear to be dominated by the effects of roughness and oblateness on terminal velocity.

5.4.2 6 July 1984

The growth time histories for four different model hailstones (*RO*, *RS*, *SO* and *SS*) on 6 July 1984 are shown in Figure 5.3 (a-f). The pure roughness effect reduces the final equivalent diameter by 4.5% (Table 5.2), while pure oblateness causes an increase in final hailstone size of 13.9%. The explanation for these effects is much the same as for the previous case study day: they are, for the most part, related to the effects of roughness and oblateness on terminal velocity. On 6 July 1984 there is no mutual interaction effect; roughness and oblateness independently influence the final equivalent diameter of the hailstone. The total effect of an increase in final equivalent diameter of 9.3% is dominated by the effects of oblateness on the evolution of a hailstone. Table 5.1 summarises the final equivalent diameters and total growth times for the model hailstones in each of the four factor separation experiments.

Pure roughness decreases the total growth time of a hailstone by 5.1%, while oblateness alone increases the growth time by 4.2%. Once again, the influences of roughness and oblateness on hailstone growth time are caused mostly by their effects on hailstone terminal velocity. The mutual interaction effect is relatively small and leads to a decrease of 0.3% in total growth time. The total effect of roughness and oblateness on total growth time is a decrease of 1.2%. As this number is negative, total growth time is dominated by the effects of surface roughness.

5.5 Factor Separation Analysis for 20 Severe Hail Days

For the majority of the severe hail days (12 out of 20), roughness increased the final equivalent diameter. On the other 8 days, including the two case study days, roughness had a negative effect. The average effect of roughness on final hailstone size was 5.4%, with numbers ranging from - 7% up to 52%. We can see the influences of updraft duration in the large range of numbers for the pure roughness effect on final hailstone size. Rough hailstones have higher terminal velocities than smooth hailstones, and thus shorter evolution times. Consequently, when both rough and smooth hailstones (within an identical storm updraft) are able to reach the ground well before the updraft collapses, a rough hailstone should grow to have a smaller equivalent diameter than a smooth hailstone. This accounts for any negative pure roughness effects. However, if the updraft duration is close to the hailstones' total growth times, rough hailstones may grow larger than smooth hailstones. In this situation, the rough hailstone's total growth time is short enough so that it is able to reach the ground without updraft collapse reducing its final size. On the contrary, the smooth hailstone has a longer total growth time and falls prematurely from the cloud, which reduces its final size. This accounts for any positive pure roughness effects, and appears to dominate the results for the 20 severe hail days.

For the majority of the 20 severe hail days, oblateness led to an increase in final equivalent diameter, with two exceptions. On 23 July 1985, the pure oblateness effect was zero. As we noted in Chapter 4, our model only predicted pea-sized hail (slightly larger than 1 cm) on this day. The oblate hailstones did not grow large enough for any differences with spherical hailstones to become apparent in their evolution (aspect ratio only begins to decrease once the hailstone reaches a diameter of 1 cm). Oblateness had a negative effect on final equivalent diameter on 12 July 1984 (- 9.8%). When we analysed the effects of oblateness on rough hailstones in Chapter 4, we found that oblate hailstones grew larger on this day, yet when we calculated the pure oblateness effects using the Factor Separation Method we arrived at the opposite conclusion. The mutual interaction effect on this day was relatively large: 27.4%. The reason for the negative oblateness effects has to do with storm duration and hailstone growth time. According to the method of Brimelow (1999) and Brimelow et al. (2002b), the updraft was estimated to last 60 minutes. The growth time for a rough oblate hailstone in this storm was comparable to the updraft duration (almost 62 minutes). Given that smooth hailstones require a longer time to evolve than rough hailstones, comparing two smooth hailstones may allow for updraft duration to interfere with the hailstone's growth. On 12 July 1984, the smooth spherical hailstone grew larger than the smooth oblate hailstone. This occurred because the oblate hailstone was much further behind in its evolution when the storm updraft was terminated than the spherical stone, and as a result it did not have as much opportunity to grow rapidly during its descent back through the storm's updraft. On this day, the limited updraft duration led to the negative pure oblateness effect and a large mutual interaction effect. On average for all severe hail days, oblateness on its own caused an 8.1% increase in final equivalent diameter. This value is slightly less than our previous value of around 10%, most likely due to some updraft duration effects that may have appeared due to the longer evolution times associated with smooth-surfaced hailstones.

The mutual interaction effect was relatively small in magnitude for most of the severe hail days, and was also predominantly positive. There were a few cases where the mutual interaction of roughness and oblateness led to a relatively large positive number, and other cases where the effect was negative and relatively large in magnitude compared to the pure and total effects. On average, the mutual interaction effect led to a 2.3% increase in final equivalent diameter. Updraft duration had a large influence on this combined effect on some days. For the 20 severe hail days, the total effect of roughness and oblateness was positive; rough, oblate hailstones were on average 15.8% larger than smooth spherical hailstones.

Roughness always had a negative effect on total growth time for the days studied; the average effect of roughness was to decrease the final diameter by 7.6%. Oblateness had a positive effect on total growth time for all the severe hail days; on average, oblate hailstones had growth times that were enhanced by 2%. Roughness had a more significant effect than oblateness did on growth time. The mutual interaction effect was, for the majority of cases, relatively small and negative. On a few days the mutual interaction of roughness and oblateness was relatively large and positive; these were mostly the days when storm duration was comparable to total growth time. The total effect of roughness and oblateness was always negative (on average, - 5.3%): roughness dominated in terms of total growth time. From these results, it is clear that the effects of roughness and oblateness on growth time were dominated by the differences in terminal velocity between rough, smooth, oblate and spherical hailstones.

5.6 Summary

Surface roughness may result in either smaller or larger hail at ground, depending on the duration of the updraft in which the hailstone is growing. For the two case study days, the effect of roughness on final equivalent diameter was negative; storm duration did not influence the evolution of these hailstones because they, for the most part, were able to reach the ground before the updraft was terminated. Roughness and oblateness did not have a large mutual interaction effect on final equivalent diameter for the majority of the 20 severe hail days, but there were storm days where the two effects interacted strongly. Overall, rough, oblate hailstones grew 15.8% larger than smooth spherical hailstones. Also, oblateness is of comparable importance to roughness when modelling the evolution of hailstones. Terminal velocity is the dominant factor in determining the final size of hail; this parameter directly influences growth time, the maximum hailstone mass a storm may support, and growth rate.

6 MODEL SENSITIVITY AND OTHER CONSIDERATIONS

6.1 Hail Model Sensitivity Tests

In this section, we discuss sensitivity experiments that show the effect on the final equivalent diameter of a modelled hailstone (D_{eq}) and its total growth time (τ) when the following microphysical parameters are varied: D_1 and D_2, the major diameters at which the hailstone's aspect ratio begins to decrease and then remain constant, respectively; E_i, the collection efficiency for cloud ice; r_d, the median volume cloud droplet radius (required in order to calculate collection efficiency for cloud water and net collection efficiency); ρ_H, the density of accreted ice; and D_0, the initial hail embryo diameter. The sensitivity experiments were conducted for the two case study days, 11 July 1985 and 6 July 1984, and for 20 severe hail days. We also investigate the differences in the evolution of hailstones that result from the use of different model shedding and terminal velocity schemes. HC2's shedding and terminal velocity schemes, based on the work by Levi and Lubart (1998), Greenan and List (1995), García-García and List (1992), and Böhm (1989), will be compared with those of Brimelow et al.'s (2002b) HAILCAST model, which are based on the work by Rasmussen and Heymsfield (1987a).

6.1.1 D_1 and D_2

With HC2, we attempted to simulate the natural decrease of a hailstone's aspect ratio as it increases in size. Attempts were made to measure the exact rate of decrease of aspect ratio with respect to major diameter (e.g. Knight, 1986; Browning and Beimers, 1967) with varying results. These experiments suggested that hailstones, in particular those that evolved from frozen droplet embryos, began their lives as nearly spherical objects, and their aspect ratios decreased as they increased in mass. Figure 6.1 depicts aspect ratio as a function of major diameter in HC2: the hailstone began its life as a spherical object, then, between $D_1 = 1$ cm and $D_2 = 2$ cm its aspect ratio decreased until it reached the constant value of $\alpha_c = 0.77$. We chose D_1 and D_2 in an attempt to be consistent with the measured data on hailstone aspect ratio in relation to size. To estimate the impact that the choice of these parameters has on the evolution of a hailstone in the HC2 model, we conducted extensive sensitivity tests. We ran simulations, for each of the 20 severe hail days, with D_1 varying from D_f (the diameter of the hailstone when it freezes at an in-cloud temperature of - 8°C) to 2.0 cm and with D_2 varying from 1.5 to 3.5 cm (Table 6.1).

Varying D_1 and D_2 had marginal effect on the final equivalent diameter of a hailstone produced by the storm on 11 July 1985. The percent difference between the maximum final equivalent diameter and the minimum final equivalent diameter produced by these tests was 2.3%. This is a small effect compared to that which results from changing a hailstone from spherical to oblate; oblate hailstones with an aspect ratio of 0.77 grew about 17% larger than spherical ones in this storm (Chapter 4). Changing D_1 and D_2 had a comparable effect on total growth time, however: the percent difference between the maximum growth time and the minimum growth time for these runs was almost 5%, which is about the same difference between the growth times of a spherical and an average oblate hailstone. The growth time of hailstones is of little interest compared to the information about maximum size. However, if the chosen D_1 and D_2 values produce a growth time that is comparable to the updraft duration, the final size of the hailstone may be reduced.

The choice of D_1 and D_2 had a larger impact on the final equivalent diameters of the modelled hailstones for 6 July 1984. The percent difference between the two most extreme values in this series of experiments was 9.4%. This difference is still smaller than the difference between the final equivalent diameters of spherical and average oblate hailstones of 14.5%. In this case, the effect of D_1 and D_2 on growth time was relatively small, about 1% compared to the 4% difference between the growth times of spherical vs. average oblate hailstones. The model hailstone spent most of its lifetime in the supercooled region of the cloud where it was able to grow rapidly. It is in this region that differences in aspect ratio produce maximum differences in hailstone evolution, so changing D_1 and D_2 had a relatively large impact on final hailstone size.

On average, for all 20 severe hail days, the choice of D_1 and D_2 had only a moderate effect on the final equivalent diameter. The difference between the two extreme average equivalent diameters was 4.3%, compared to the average 10% difference between the final sizes of spherical and average oblate hailstones. The effect on growth time was, on average, relatively large: 6% compared to the 2.5% difference between spherical and average oblate hailstones.

While the choice of D_1 and D_2 had, in general, a considerably smaller impact on final hailstone diameter than oblateness did, it still introduced some uncertainties in the model output. As, to our knowledge, these parameters are not very well known, the best approach to treat this uncertainty in final hailstone equivalent diameter would be to run this model as an ensemble with D_1 and D_2 varying within reasonable values, and then take an average, or use the maximum value, because the purpose of the HC2 model is to predict the largest possible hail that may be produced by a given sounding.

6.1.2 Collection Efficiency of Ice, E_i

We varied the collection efficiency for cloud ice (during dry growth) within the range 0.10 – 0.25. All other parameters were set to their control values. Changing E_i had no effect on 6 July 1984. The hailstone grew mainly by accretion of supercooled water droplets in this particular storm environment; the highest percentage of ice in this cloud that the hailstone encountered was 3%, near the apex of its trajectory.

Changing E_i had a noticeable effect on both final equivalent diameter and total growth time of the 11 July 1985 hailstone, because, for a significant period of time, this hailstone remained above the - 40°C level and thus grew by collection of ice crystals only. The total growth time decreased from 67 minutes for $E_i = 0.10$ down to 50 minutes for $E_i = 0.25$, as lower ice collection efficiencies led to slower growth in the glaciated region of the cloud. The final equivalent diameter was 1.9 cm for $E_i = 0.10$. Growth above the - 40°C level was comparatively slow at this collection efficiency, and thus the hailstone was still within this region at the time when the updraft collapsed. When the relatively small hailstone was no longer supported by the cloud updraft, it descended rapidly through the cloud and fell to the ground. The final equivalent diameter increased to 5.4 cm when E_i was increased to 0.16, with a total growth time of 60 minutes. For collection efficiencies larger than 0.16, the final equivalent diameter of the hailstone remained constant at 5.3 cm. On average, for 20 severe hail days, final equivalent diameter increases with increasing E_i, and growth time decreases with increasing E_i (Table 6.2).

6.1.3 Median Volume Cloud Droplet Radius, r_d

Following Greenan and List (1995), we used a median volume cloud droplet radius (r_d) of 25.5 μm for the model control value. To investigate the sensitivity of the hail model to this parameter, r_d was varied from 20.4 μm – 30.6 μm (± 20%). In general, changing r_d had little effect on final equivalent hailstone diameter. For 11 July 1985, the final equivalent diameter for $r_d = 20.4$ μm was 5.2 cm and for $r_d = 30.6$ μm it was 5.4 cm. Total growth time, τ, decreased from 55 minutes ($r_d = 20.4$ μm) to 54 minutes ($r_d = 30.6$ μm). The effects of varying r_d on final equivalent diameter and total growth time for 6 July 1984 hailstones were relatively small, as were the corresponding effects on the averages for 20 severe hail days (Table 6.3). We conclude, therefore, that the modelled hail growth in HC2 is relatively insensitive to changes in r_d.

6.1.4 Hailstone Density, ρ_H

We varied the density of accreted ice between 0.8 and 0.9 g cm^{-3}, based on the range of observed densities of natural hailstones (English, 1973). The results are summarized in Table 6.4. On 11 July 1985, reducing ρ_H from 0.9 to 0.8 g cm^{-3} increased final equivalent diameter from 5.3 to 6.0 cm and increased total growth time from 55 to 56 minutes. Changing the density of accreted ice had a comparable effect on the final equivalent diameter of a hailstone produced on 6 July 1984: reducing ρ_H from 0.9 to 0.8 g cm^{-3} increased D_{eq} from 3.6 to 4.1 cm. Growth time on 6 July 1984 was affected very little by changing ρ_H, while the average growth time for 20 severe hail days was increased from $\tau = 49$ min for $\rho_H = 0.9$ g cm^{-3} to $\tau = 51$ min for $\rho_H = 0.8$ g cm^{-3}. The average final equivalent diameter for 20 severe hail days was 5.1 cm for $\rho_H = 0.8$ g cm^{-3} and 4.7 cm for $\rho_H = 0.9$ g cm^{-3}.

6.1.5 Initial Embryo Diameter, D_0

The purpose of the HC2 model is to predict the maximum possible hailstone size that may be produced by a given storm, so for each of the 20 days we chose the D_0 that produced the largest hail size in the shortest time (Chapter 2). The choice of D_0 for each severe hail day was based on a series of sensitivity experiments, which we will outline in this section. Typically, we should expect that for storms with strong updrafts (> 25 m s^{-1}), larger embryos of about 700 or 800 μm in diameter produce the largest hailstones in the least amount of time (English, 1973). For storms with weaker updrafts, final equivalent diameter should not be very sensitive to D_0 (English 1973; Brimelow et al., 2002b).

The results of sensitivity experiments in which D_0 was varied between 100 and 800 μm are shown in Table 6.5 for the two case study days (11 July 1985 and 6 July 1984) and for another severe hail day: 28 July 1984. The pre-storm environment of 28 July 1984 was characterized by large CAPE (2580 J kg^{-1}) and a high maximum updraft velocity (44 m s^{-1}). The largest observed hailstones on this day were classified as greater than golfball-sized.

For 6 July 1984, final equivalent diameter was not sensitive to initial embryo diameter. This result is consistent with the findings of Brimelow et al. (2002b) and English (1973); the maximum updraft on this day was 19.7 m s^{-1} (less than 25 m s^{-1}), so initial embryo diameter should not influence final hailstone size overly much. Total growth time decreased from 30 minutes for $D_0 = 100$ μm to a minimum of 28 minutes for $D_0 = 400$ μm, and then increased to 31 minutes for D_0

= 800 μm. The control value for D_0 on this day was chosen to be 400 μm because this was the embryo diameter that minimized growth time.

On 11 July 1985, the equivalent diameter of the modelled hailstones was not sensitive to initial embryo diameter so long as D_0 was greater than 300 microns. Total growth time decreased from 67 minutes to a minimum of 55 minutes as D_0 increased from 100 μm to 700 μm. Again, for $D_0 = 800$ μm, growth time increased slightly. The optimum D_0 value for this severe hail day was 700 μm. A 300 μm initial embryo diameter produced slightly larger hail (5.4 as opposed to 5.3 cm in equivalent diameter), but the shortest growth time was for an embryo of 700 μm diameter.

Final equivalent diameter was sensitive to D_0 on 28 July 1984. A 100-μm diameter embryo produced a hailstone with an equivalent diameter of 4.3 cm while a 700-μm diameter embryo produced a hailstone with an equivalent diameter of 10.9 cm. Growth time changed from 63 minutes to 32 minutes when initial embryo diameter was increased from 600 to 700 μm. A 600-μm diameter embryo was light enough to be rapidly carried above the - 40°C level, where it then grew slowly by accreting cloud ice until it became large enough to descend back through the supercooled region of the cloud. When the initial embryo diameter was 700 μm, however, it took longer for the evolving hailstone to reach the - 40°C level (Figure 6.2 a-f; solid line). It was almost 1 cm in diameter when it entered this region of the cloud, and only remained there for about 15 minutes. While the hailstone was above the - 40°C level, it remained in the wet growth regime and thus all accreted cloud ice was assumed to stick to it surface. Given that dry growth was not encountered above the - 40°C level, the hailstone grew rapidly in this region.

Figure 6.2 (dotted line) depicts the evolution of a 400-μm hailstone on this same severe hail day. The hailstone was advected above the - 40°C level about 4 or 5 minutes earlier than the 700-μm hailstone was, at a diameter of half a centimetre. The hailstone that started with $D_0 = 400$ μm was in the dry growth regime the entire time that it was above the - 40°C level and so it took about 47 minutes to grow large enough to descend back into the supercooled region of the cloud.

6.1.6 Effects of Model Shedding Scheme on Final Hailstone Size

The main differences between Brimelow et al.'s (2002b) HAILCAST model and the HC2 hail model, besides the inclusion of an aspect ratio that evolves with time, are the shedding scheme and the terminal velocity scheme. HAILCAST's shedding scheme and terminal velocity scheme are based on those of Rasmussen and Heymsfield (1987a,b). HC2 uses the method of Böhm (1989) to calculate the hailstone's terminal velocity at each time step; Böhm's formulae are semi-empirical and are functions of the hailstone's aspect ratio. The shedding scheme that we used in HC2 is the one proposed by Levi and Lubart (1998), which is a modified version of the shedding scheme presented in a series of papers by List and colleagues (Greenan and List, 1995; García-García and List, 1992).

We conducted a series of experiments, using 62 Albert Hail Project soundings collected in the summers of 1983 – 1985, to determine how the evolution of a hailstone governed by the HC2 shedding and terminal velocity schemes differs from that governed by the HAILCAST shedding scheme. HAILCAST was run for all 20 severe hail days and all 42 non-severe hail days using Brimelow et al.'s (2002b) control parameter values (initial embryo diameter of 300 µm, ice collection efficiency of 0.21, cloud base velocity of 4 m s^{-1}). The original 1-D, steady-state cloud model had a small error when station (surface) pressure was assigned; this was corrected before the runs were made using HAILCAST. The corrected version of the cloud model was also used in HC2. The original, uncorrected cloud model assigned a station pressure of 910 mb for every run; we changed the model so that station pressure is obtained from the sounding for which the model is currently being run. All statistics for the original HAILCAST model in this chapter were obtained using the corrected cloud model.

To directly compare the shedding and terminal velocity schemes of the two hail models, we ran HC2 assuming the model hailstone has a rough surface and remains spherical throughout its evolution. As we used the same control parameter values that were used in HAILCAST, the only differences between these two sets of data may be attributed to the shedding and terminal velocity schemes. Table 6.6 shows the final diameter, hail size category and total growth time predicted for each of 20 severe hail days by HAILCAST and HC2. Table 6.7 shows the absolute and percent changes in final diameter at ground and total growth time when the HC2 model is used compared to HAILCAST.

Hailstones grown using the HC2 shedding and terminal velocity schemes were consistently larger than those grown using the corresponding HAILCAST schemes; on average, they were 26.2% (or almost 1 cm) larger. The HC2 model produced larger hailstones in less time than HAILCAST: the growth times were on average 1.3 minutes or 2.6% less. On 6 July 1984, HC2 predicted a hailstone that was 11.5% larger and a growth time that was almost 2% less than the hailstone predicted by HAILCAST. On 11 July 1985, the HC2 model hailstone was 16% larger and had a growth time that was 6.8% less than the stone modelled by HAILCAST.

We also compared the output from the two different models for the 42 non-severe hail days between 1983 and 1985. On average, the HC2 spherical model predicted (non-severe) hail that was 14.3% larger in final diameter than that predicted by HAILCAST, and the HC2 growth times were 6.5% less.

The HC2 shedding and terminal velocity schemes are typically more efficient than the HAILCAST schemes at producing large hail in shorter periods of time. In some cases, the model shedding scheme had an impact on the final hailstone diameter that was comparable to that of hailstone oblateness. The efficiency of hailstone growth is improved because the HC2 shedding scheme allows for more water to accumulate on the hailstone's surface before it begins shedding. The onset of shedding in HC2 depends on a variety of factors (Greenan and List 1995, García-García and List 1992): liquid water content, air temperature, size of the hailstone, and its aspect ratio. Shedding is assumed to occur during a HAILCAST simulation when the amount of water on the surface exceeds a critical mass, based on the current mass of the hailstone's ice core.

Both schemes are based on experimental evidence and produce different results when incorporated into a hail model.

6.2 Cloud Model Sensitivities and Considerations

In this section, we discuss the importance of the updraft duration parameter in relation to total growth times and final sizes of oblate and spherical hailstones. This discussion centres on a specific example: we examine the evolution of a hailstone with an initial embryo diameter (D_0) of 400 μm in the environment characterized by the 28 July 1984 sounding. The total growth time of an average oblate hailstone ($\alpha_c = 0.77$) with $D_0 = 400$ μm on this day is 63.9 minutes, while the updraft duration is 60 minutes, so updraft duration may play an important part in the evolution of hailstones in this environment. As mentioned previously, the pre-storm environment was characterised by very high CAPE (2580 J kg^{-1}) and a high maximum updraft velocity (44 m s^{-1}). We first discuss the evolution of three hailstones of different degrees of oblateness in this storm environment, focussing on the effects of updraft termination. Next, we examine the differences in the evolution of the same three hailstones when the updraft duration is increased by 10 minutes.

6.2.1 The Evolution of Hailstones on 28 July 1984, $D_0 = 400$ μm

In this section, we discuss the influences of updraft duration on three different types of model hailstones in the storm environment of 28 July 1984: a spherical hailstone ($\alpha_c = 1.00$), an average oblate hailstone ($\alpha_c = 0.77$) and a very oblate hailstone ($\alpha_c = 0.50$). Each of these hailstones has an embryo diameter of 400 μm. The growth histories of these three hailstones are shown in Figure 6.3.

The evolution of hailstones on 28 July 1984 was drastically influenced by the termination of the updraft: the spherical hailstone grew larger than the average oblate hailstone. As its terminal velocity was the largest, the spherical hailstone was the first to descend from the - 40°C level into the supercooled region of the cloud, where it was supported by the cloud updraft for about 5 minutes. In this time, it was able to grow substantially (its diameter exceeded the average oblate hailstone's equivalent diameter at about t = 58 min). The average oblate hailstone was only supported in this region for 2 minutes before the updraft collapsed; its mass growth rate never reached that of the spherical hailstone. When the updraft ceased to exist, all hailstones fell freely to the ground. Despite its enhanced cross-sectional area, the average oblate hailstone was not able to grow larger than the spherical hailstone as it fell through the supercooled region of the cloud.

The very oblate hailstone was able to grow to a larger equivalent diameter than either of the two other hailstones before it reached the ground, despite the fact that it was still above the - 40°C level when the updraft collapsed. Even though it was not ever supported by the updraft in the supercooled region, its relatively large cross-sectional area enabled it to collect enough water to exceed the masses of the other two hailstones while it passed through this region.

If the updraft had not collapsed at t = 60 min, the spherical hailstone would have been the smallest produced by this storm, followed by the average oblate hailstone and then the very oblate hailstone. On 28 July 1984, the final hail size of each hailstone was primarily determined by its position with respect to the - 40°C level when the updraft collapsed.

6.2.2 Extending the Storm Duration by 10 Minutes

To verify that updraft duration led to spherical hail growing larger than oblate hail on 28 July 1984, we repeated the experimental run discussed in the previous section with the updraft duration extended by 10 minutes (i.e. an updraft duration of 70 minutes). When the updraft duration was set to 70 minutes, the spherical hailstone had the smallest equivalent diameter of the three model hailstones when it reached the ground (D_{eq} = 8.7 cm, τ = 66.1 minutes), followed by the average oblate hailstone (D_{eq} = 10.3 cm, τ = 69 minutes) and then the very oblate hailstone (D_{eq} = 13.6 cm, τ = 72.1 minutes).

6.2.3 Discussion

The role of the updraft duration should not be neglected when evaluating the effects of oblateness on the final sizes of hailstones, especially when modelling hail in very severe storms (those with large CAPE and high updraft velocities). Given sufficient time, oblate hailstones will grow larger than spherical hailstones. However, if the updraft collapses before the hailstones hit the ground, the opposite may occur.

There were a few cases in our data set where updraft duration influenced the evolution of hailstones by allowing spherical hail to grow larger than oblate hail. Estimating realistic updraft duration is difficult, because it is estimated roughly in the model based on the CAPE and shear calculated from the proximity sounding. Hence, we could not justify adding an extra 10 minutes to the duration of severe storm runs to allow oblate hailstones sufficient time to surpass spherical hailstones in mass. Our main focus in this work is the microphysical hail model; we made no major improvements to the cloud model. We wished to reduce the effects of updraft duration as much as possible for this analysis so that the effects of oblateness (and roughness) could be determined. This was achieved by selecting an embryo diameter that both maximized the size of hail produced by a particular storm and minimized the growth time (Chapter 2). Figure 6.4 illustrates the evolutionary history of a spherical hailstone, an average oblate hailstone and a very oblate hailstone on 28 July 1984 for an initial embryo diameter of 700 μm and the model-derived storm duration of 60 minutes. Increasing the hailstone diameter from 400 to 700 μm results in similar final hailstone equivalent diameters as increasing the duration by 10 minutes on a D_0 = 400 μm run: the spherical hailstone has a final equivalent diameter of 9.2 cm, the average oblate hailstone has a final equivalent diameter of 10.9 cm, and the very oblate hailstone has a final equivalent diameter of 14.3 cm. The main difference between these model runs and the ones discussed in Section 6.2.2 is the average growth time of the hailstones; increasing the initial embryo diameter from 400 to 700 μm reduces growth times by about half.

Given that the steady-state cloud model used in HC2 only gives a rough estimate of the updraft duration based on the CAPE and shear, a different technique should be used to estimate this parameter for forecasting purposes. One possibility would be to use the hail model in conjunction with real-time radar data: the storm duration could be estimated from the radar data. Once an estimate for updraft duration has been determined in this way, the model could then be run numerous times using different D_0 values in order to predict the maximum possible hail size that can be produced by a particular storm. This proposed technique, however, is not ideal because the storms would already be active and possibly producing hail before one could determine a representative updraft duration. Consequently, one would not necessarily have a lead time that is less than using certain radar-based parameters to infer the hail size present in the storms. Alternatively, one could estimate the updraft duration for a large sample of storms using radar and compare these values to those of the CAPE*SHEAR calculation from a proximity sounding. This would be an improvement over the current technique.

6.3 Summary and Discussion

We conducted sensitivity experiments to determine the effects of key microphysical parameters, shedding and terminal velocity schemes, and updraft duration on the growth of hailstones. Hail growth was found to be most sensitive to the following microphysical parameters, when varied over the range of typical values used in other hail modelling studies:

(1) **D_1 and D_2**: Varying the major diameters at which the hailstone's aspect ratio begins to decrease (D_1) and remains constant (D_2), can in turn cause variations in the final equivalent hailstone diameter of up to 10%. The magnitude of this effect depends on the amount of time a hailstone is trapped in the glaciated portion of the cloud (i.e. above the - 40°C level). If the hailstone never reaches the glaciated region of the cloud, varying D_1 and D_2 has a relatively large effect on the final

equivalent diameter. The effect of varying D_1 and D_2 is much less pronounced for hailstones that spend a large amount of time above the - 40°C level, such as the modelled hailstones for 11 July 1985.

(2) **Collection Efficiency of Ice, E_i:** The effects of varying E_i (during dry growth) on hailstone growth also depend on whether or not the hailstone enters the glaciated portion of the cloud. On days when the hailstone is advected above the - 40°C level, lowering E_i too much causes the hailstone to become trapped there until the cloud updraft collapses, resulting in a smaller equivalent diameter at ground. If, on the other hand, there is very little cloud ice present in the hailstone's environment (for example 6 July 1984), changing E_i has no effect on the final equivalent hailstone diameter.

(3) **Hailstone Density, ρ_H:** Decreasing the hailstone ice density results in longer total growth times and larger final equivalent diameters. A cloud updraft of a given strength can support a hailstone of a given mass. If a hailstone of a given mass has a lower density, then its equivalent diameter is proportionally larger.

(4) **Initial Embryo Diameter, D_0:** If this parameter is too small in storms with maximum updraft velocities greater than 25 m s^{-1}, the hail embryo is rapidly transported to the glaciated region of the cloud, where it remains trapped until the updraft collapses. Insufficiently large hailstone embryo diameters thus lead to smaller final equivalent hailstone diameters on days with strong updrafts. Increasing D_0 results in larger final equivalent diameters and shorter growth times. Varying D_0 has little effect on hailstones evolving in storm environments with maximum updraft velocities less than 25 m s^{-1}; increasing D_0 has next to no effect on final equivalent diameter and a relatively small effect on total growth time.

The model shedding and terminal velocity schemes influence the evolution of hailstones on severe hail days. The HC2 shedding and terminal velocity schemes are more efficient at producing hail than those of Brimelow et al.'s (2002b) HAILCAST model. Specifically, in the HC2 model the simulated hailstones reach larger final diameters in shorter periods of time.

The evolution of a hailstone is very sensitive to its location within the cloud when the updraft collapses. This factor influences the relative sizes of oblate and spherical model hailstones, and is most common in storms characterized by large CAPE. If the updraft collapses when the oblate and spherical hailstones are still relatively high within the cloud, the spherical hailstone may grow larger than the oblate hailstone. Thus, updraft duration should not be neglected when evaluating the influence of oblateness on the final size of a modelled hailstone. We reduced the interference of the updraft duration parameter with the model results by selecting an initial embryo diameter for each severe hail day that produces the maximum equivalent diameter in the shortest amount of time.

In these sensitivity experiments, the focus was mainly on microphysical hail growth parameters, as opposed to cloud model parameters such as surface temperature and dewpoint. Naturally, the final equivalent hailstone diameter and total growth time are quite sensitive to certain cloud model parameters. The reader is referred to the works of Brimelow et al. (2002b) and Brimelow (1999) for a discussion of the sensitivity of hailstone growth to key cloud model parameters.

7 EVALUATION OF THE MODEL PREDICTED MAXIMUM HAIL SIZE

7.1 Introduction

In this chapter, we compare HC2 hail size predictions with maximum hail sizes observed on 20 severe hail days, 42 non-severe hail days, and 98 no-hail days between 1983 and 1985 to determine whether HC2 can realistically simulate the growth of hailstones in Alberta hailstorms. We begin with a discussion about the uncertainties associated with classifying oblate hailstones under different size categories. Specifically, we estimate the difference in size category classification that may result if an oblate hailstone's major diameter is rather than its equivalent diameter to determine its size category. Following that discussion, forecasts of maximum hail size determined using the spherical and oblate versions of HC2 are evaluated against observations of maximum hail size within the Alberta Hail Project area.

7.2 Assigning Size Categories to Oblate Hailstones

To evaluate the skill of HC2 at forecasting the maximum hail size at ground, we compare the model hailstones with the observed hailstone sizes for each hail day between 1983 and 1985. In the AHP data set, hailstones are classified as one of seven size categories, according to their diameters at ground, as follows: shot, diameter < 0.4 cm; pea, $0.4 \leq D_{eq} < 1.3$ cm; grape, $1.3 \leq D_{eq} < 2.1$ cm; walnut, $2.1 \leq D_{eq} < 3.3$ cm; golfball, $3.3 \leq D_{eq} < 5.3$ cm; and larger than golfball, ≥ 5.3 cm (Strong, 1974). A spherical model hailstone may be directly assigned to the appropriate hailstone size category based on its final diameter at ground, but an oblate hailstone could be assigned to a size category based on one of three different dimensions: its final major diameter, its final minor diameter, or its final equivalent diameter. We decided to assign size categories to oblate hailstones based on the final equivalent diameter, because this parameter is directly related to a hailstone's mass ($M \propto D_{eq}^{3}$).

We are not certain how an untrained observer, such as those who were recruited to assist in collecting the AHP hail data, would classify an oblate hailstone. Such an observer may be inclined to use the maximum hailstone dimension to estimate the size of each hailstone. To take any hailstone classification uncertainties into account, we estimated the difference in size category assigned to an oblate hailstone if its major diameter were used instead of its equivalent diameter.

The major diameter, D_M, of an oblate hailstone with an aspect ratio of α is related to its equivalent diameter, D_{eq}, by the following formula:

$$D_{eq}^{3} = \alpha D_{M}^{3} . \qquad (7.1)$$

The fractional difference (f_D) between the major diameter and equivalent diameter is

$$f_D = \frac{D_M - D_{eq}}{D_{eq}} . \qquad (7.2)$$

Combining (7.1) and (7.2) yields an expression for f_D that is a function of axis ratio alone:

$$f_D = \alpha^{-1/3} - 1 . \qquad (7.3)$$

The fractional difference between a hailstone's major diameter and equivalent diameter is shown for a range of aspect ratios in Table 7.1. The major diameter of an oblate hailstone with an aspect ratio of 0.77 is about 9% larger than its equivalent diameter. For an oblate hailstone with an aspect ratio of 0.50, f_D is 26%. We will use f_D to estimate the difference in size category that results when a hailstone's major diameter is used to classify the stone in place of its equivalent diameter.

To determine if an oblate hailstone would be classified under a different size category if its major diameter were used in place of its equivalent diameter, we proceeded as follows. First, for each size category, we selected an equivalent diameter in the middle of the category's diameter range and an equivalent diameter equal to the upper limit of the size category's diameter range (Table 7.2). For both an average oblate hailstone ($\alpha = 0.77$) and a very oblate hailstone ($\alpha = 0.50$), the major diameter was calculated from the equivalent diameter. Next, the major diameter was used to assign a new size category to each oblate hailstone. In all cases that were examined (Table 7.2), using major diameter in place of equivalent diameter to classify the size of a hailstone increased the size category by no more than one. For hailstones with equivalent diameters in the middle of the range of diameters for each size category, using major diameter as the basis for size classification resulted in the same size category for all average oblate hailstones and for the shot and pea-sized very oblate hailstones. The major diameters of the very oblate grape, walnut and golfball-sized hailstones were equal to the lower diameter limits of the next largest size categories (e.g. a very oblate grape-sized hailstone with $D_{eq} = 1.7$ cm had a major diameter of $D_M = 2.1$ cm, which is the lower limit for a walnut-sized hailstone). When major diameter was used to reclassify hailstones with equivalent diameters equal to the upper limits of each defined size category, the new size category was always one higher.

The differences in size category that resulted when average oblate hailstones were classified by major diameter instead of equivalent diameter were not very large. Admirat et al. (1985) found that the observed hail sizes of the AHP hailstones had an error margin of about 10%, compared to a 9% difference between an average oblate hailstone's equivalent diameter and major diameter. Thus, we do not need to take errors related to classifying the size of model average oblate hailstones into account when evaluating the forecast skill of the HC2 model. The corresponding errors for very oblate hailstones should not be ignored ($f_D = 26\%$), but this fact will not influence the following HC2 forecast skill analysis, as only average oblate hailstones are considered.

7.3 Forecast Skill Scores

In this section, forecasts of maximum hail size using HC2 are evaluated against observations of maximum hail size within the Alberta Hail Project area.

Both the spherical and the oblate versions of the model were run for all 160 days between 1983 and 1985 (20 severe hail days, 42 non-severe hail days and 98 no hail days). The hailstones produced by the average oblate and spherical versions of the HC2 model were assigned size categories based on their equivalent diameters at ground. Hereafter, whenever the oblate version of HC2 (or an oblate hailstone) is mentioned, we refer to the average oblate version of the model.

Table 7.3 shows the maximum final equivalent diameter predicted by both the spherical ($\alpha_c = 1$) and oblate ($\alpha_c = 0.77$) versions of HC2 for 20 severe hail days. For all HC2 model runs, the following parameters were used: $E_i = 0.20$ (for dry growth), $D_1 = 1$ cm, $D_2 = 2$ cm, $W_0 = 3$ m s^{-1}. The embryo diameter, D_0, was chosen according to the criteria outlined in Section 2.5. The size categories of the largest hailstones observed on each of those days in the Alberta Hail Project area are also shown in Table 7.3. Size categories (not shown) were assigned to each model hailstone using the criteria outlined in Section 7.1.

To assess and compare the forecasting skills of the oblate and spherical versions of the HC2 model, we calculated several skill scores based on 2 × 2 contingency tables. Contingency tables for the two versions of the HC2 model are shown in Table 7.4. When hail was both observed and forecast, a hit (H) was noted. A miss (M) occurred when hail was observed but not forecast, while a false alarm (FA) occurred when hail was forecast but none was observed. A null was recorded when no hail was observed and no hail was forecast. We calculated and compared four different skill scores: the probability of detection (POD), the false-alarm ratio (FAR), the Heidke skill score (HSS), and the critical success index (CSI) (Appendix F). Marzban and Stumpf (1998) provide details and equations for the various skill scores that may be derived from contingency tables.

Both the spherical and oblate models showed reasonable skill at forecasting the occurrence of hail: the spherical model had a POD of 0.82 and the oblate model had a POD of 0.81; in other words, the spherical model had one less miss than the oblate model did. Overall, the forecast skills of these two models were quite similar. Both had a FAR of 0.23, which, as discussed and explained by Brimelow et al. (2002b) when he evaluated the scores of HAILCAST, represents a relatively large number of false alarms. The HSS and CSI for both the spherical and oblate models showed good overall skill when forecasting the occurrence of hail: the spherical model had a HSS and CSI of 0.66 while the oblate model had a HSS and CSI of 0.65. HC2's forecast skill scores are summarised in Table 7.5 and depicted graphically in Figure 7.1.

For both the spherical and oblate models, 63% of the forecasts were within one size category of the observed hail sizes, based on 62 hail days (Table 7.6). The spherical model was slightly more accurate at forecasting exact hail size; it correctly forecast hail size category on 34% of all hail days, compared with 31% for the oblate model. The oblate model had a slight tendency to overestimate hail size by one or more categories: 39% of the 62 hail days were forecast to be one or more categories too large (18% two or more too large) while 30% were forecast to be one or more categories too small (19% two or more too small). The spherical model did not show a strong tendency to either over- or underestimate the hail size: 34% of forecasts were one or more too small (19% two or more too small) while 33% or forecasts were one or more too large (18% two or more too large).

To gain further insight about HC2's performance, we evaluated the skill of the spherical and oblate models at forecasting severe hail. Following the approach of Brimelow et al. (2002b), each hail day between 1983 and 1985 was classified as either severe (walnut-sized or greater) or non-severe (grape-sized or smaller). 2 × 2 contingency tables were then constructed in order to calculate the skill scores for the model forecasts on severe hail days. A hit was noted when severe hail was both forecast and observed; a miss was noted when severe hail was observed but non-severe hail was forecast; a false alarm was noted when severe hail was forecast but non-severe hail was observed, and a null forecast was noted when non-severe hail was both observed and forecast. The skill scores for forecasting severe hail (POD, FAR, HSS and CSI) are summarised in Table 7.5. Figure 7.1 shows these same skill scores graphically, compared to the corresponding scores for 62 hail days.

Both the spherical and oblate versions of the HC2 model performed well at predicting the occurrence of severe hail; each version scored a POD of 0.95

(both model versions correctly forecast 19 out of 20 severe hail days). On the one day when severe hail was observed but not forecast (23 July 1985), pea-sized hail was forecast by both versions of HC2.

Both the spherical and oblate versions of HC2 had relatively high false-alarm ratios when compared with those for forecasting the occurrence of hail: 0.47 (17 false alarms) and 0.50 (19 false alarms), respectively. The oblate model overestimated maximum hail size on non-severe hail days slightly more often than the spherical model. The spherical model displayed slightly better overall skill, with a HSS of 0.62 and a CSI of 0.51, compared to the oblate model, which scored a HSS of 0.59 and a CSI of 0.49. The slightly poorer skill of the oblate model when forecasting severe hail can be attributed to the fact that it had a slightly higher FAR, because it tended to overestimate maximum hail size more than the spherical model.

Both the spherical and oblate models were reasonably accurate at forecasting the hail size categories for the severe hail days (Table 7.6). Forty-five percent of the oblate model forecasts on severe hail days were correct; while 50% of the spherical model forecasts were correct (this difference corresponded to one severe hail day). The oblate model forecast hail that was within one size category 80% of the time, compared to 75% for the spherical model. The oblate model had a tendency to over-predict the hail size category, with 40% of forecasts being one or more categories too large (15% two or more too large). The spherical model under-predicted hail size as often as it over-predicted hail size: 35% of forecasts were one or more categories too small, and 35% of forecasts were one or more categories too large.

Overall, the performances of the oblate and spherical versions of the model were similar. The oblate model had a tendency to over-predict hail size on both severe and non-severe hail days, which led to slightly lower skill scores than the spherical model. The advantage to using the oblate version is that it is more accurate and realistic than the spherical model, as most observed hailstones are not spherical.

7.4 Summary

When forecasting the occurrence of hail, the spherical and oblate versions of HC2 displayed similar overall skill, with HSS scores of 0.66 and 0.65, respectively. Both versions of the HC2 model performed relatively well on severe hail days, with HSS scores of 0.62 and 0.59, respectively. Almost 65% of the model hail forecasts were within one size category for both the spherical and oblate versions of HC2. On severe hail days, 80% and 75% of the oblate and spherical HC2 model hail forecasts, respectively, were correct to within one size category.

The oblate HC2 model displayed relatively good skill at forecasting the occurrence of hail and, in particular, severe hail. The main weakness of the oblate version of the HC2 model is its tendency to overestimate the size category of hailstones, especially on non-severe days. This behaviour is, in part, related to the model's shedding and terminal velocity schemes (Chapter 6), which promote the development of relatively large hailstones in relatively short periods of time when compared to Brimelow et al.'s (2002b) HAILCAST model. From a forecasting standpoint, we do not improve the model performance significantly by simulating oblate, realistically rough hailstones. However, the physics behind the HC2 microphysical model is more realistic than that of a microphysical model that only simulates spherical hailstones (such as HAILCAST).

8 CONCLUSIONS AND SUGGESTIONS FOR FUTURE WORK

8.1 Conclusions

In this thesis we have extended the hail growth model of Brimelow et al. (2002b) by allowing for more realistic hailstone shape. Specifically, we modelled the hailstone to reach a constant degree of oblateness ($\alpha = \alpha_c$) once it size exceeds a major diameter of 2 cm (rather than remaining spherical). The aspect ratio can be prescribed based on climatology of hailstone shapes. For example, a typical value for the aspect ratio of Alberta hailstones is $\alpha = 0.77$. We found that aspect ratio, the parameter that represents the degree of oblateness of a hailstone, can be included in the model code (in the collection process, hailstone heat budget, shedding process, and terminal velocity calculations) without adding much computational time. A microphysical hail model that includes the effects of hailstone oblateness was found to be equally efficient computationally when compared to its spherical counterpart.

Including the effects of oblateness in a numerical hail model influences the hail growth. Typically, modelling an oblate hailstone (an aspect ratio of 0.77) increases the final equivalent diameter by 10% and increases the growth time by 2.5% when compared with spherical model simulations. Final equivalent diameter generally increases with increasing model hailstone oblateness (i.e. decreasing aspect ratio). A 10% increase in final equivalent diameter corresponds to an increase in hailstone kinetic energy of 50%, which means that oblate hailstones could potentially cause more damage than spherical hailstones.

The main differences in the evolution of a spherical hailstone and an oblate hailstone were found to arise due to differences in their cross-sectional areas and terminal fall speeds. Given that oblate hailstones have lower terminal velocities than spherical hailstones of the same mass, a storm with a given maximum updraft strength can support larger oblate hailstones compared to spherical hailstones, which usually translates into larger hailstones at ground. The reduced terminal velocity of an oblate hailstone also allows it to spend more time in the hail growth zone than a spherical hailstone, where its relatively larger cross-sectional area leads to a larger mass growth rate and ultimately a larger hailstone at ground. The differences in the heat budget of an oblate hailstone compared to a spherical hailstone have very little influence on the hailstone's final mass when it reaches the ground.

Overall, the performances of the oblate and spherical versions of the model were similar in regards to predicting the occurrence of hail and its maximum size at the ground. The oblate model had a tendency to over-predict hail size on both severe and non-severe hail days for the 62 hail days in our dataset, which led to slightly lower forecast skill scores than the spherical model. Oblate hailstones tended to grow larger than spherical hailstones, but other parameters, such as updraft duration, collection efficiency of ice, surface temperature and dewpoint (Brimelow et al., 2002b) had a much larger impact on final hailstone size, under certain circumstances.

The size of a hailstone at the ground is influenced significantly by the duration of the storm's updraft. If the storm updraft collapses before the model hailstone has passed through the HGZ, then its time in this region of maximum growth is cut short, leading to relatively smaller hail at the ground. As oblate hailstones have longer total growth times than spherical hailstones, terminating the updraft prematurely may cause spherical hailstones to grow larger than oblate hailstones. Changing parameters such as the embryo diameter and the collection efficiency of ice can, under certain circumstances, have a comparable effect on final hail size at ground to that of oblateness.

Observations indicate (Barge and Isaac, 1973; Matson and Huggins, 1980) that very few real hailstones are actually spherical. A hail model is therefore more physically correct if it includes the microphysics for oblate hailstones. It does not cost much, in terms of computational time, to allow hailstones to evolve as oblate spheroids in a microphysical model. It is worthwhile to include the assumption of oblate hail in numerical hail models for this reason; even if simulating an oblate hailstone does not improve the overall forecast skill scores of the model.

The effects of hailstone roughness on the final equivalent diameter of a model hailstone were comparable to the effects of oblateness. On average, rough model hailstones had final equivalent diameters that were about 5% larger, and growth times that were about 8% smaller, than those of their smooth counterparts. The average mutual interaction effect of roughness and oblateness was an increase in final equivalent diameter of around 2%. The total effect of roughness and oblateness, averaged over 20 severe hail days, was an increase of about 16% in final equivalent diameter, and a 5% decrease in total growth time.

Terminal velocity is the dominant factor in determining the final size of hail; this parameter directly influences evolution time, the maximum hailstone mass a storm may support, and mass growth rate. Smooth hailstones had lower terminal velocities than rough hailstones of the same shape and mass, which means they had longer total growth times. Smooth hailstones thus tended to grow larger in situations where the updraft did not collapse before the hailstone had passed through the hail growth zone. However, since smooth hailstones tended to have longer growth times, they were more likely than their rough counterparts to have their time in the HGZ cut short when the cloud updraft collapsed.

8.2 Suggestions for Future Work

The HC2 model consists of three complementary components: the microphysical hail model (which was the main focus of this study); the cloud model, which was based on Brimelow et al.'s (2002b) one-dimensional steady-state cloud model; and the coupling of the two models (the updraft duration parameter). There is room for improvements in each of the three parts of the HC2 model.

HC2's microphysical model includes the assumption that the simulated hailstone's density is constant and uniform. Hailstones generally exhibit a layered structure, the different layers representing different growth regimes that it entered during its evolution (Macklin, 1977). Investigations have shown that different hailstone layers have different densities that generally fall within the range 0.82 g cm^{-3} and 0.917 g cm^{-3} (List et al., 1970; Prodi, 1970). If these density variations are incorporated into the HC2 microphysical hail model, the effects of a varying hailstone density on model output parameters can be investigated.

There are even more opportunities for improvement in HC2's cloud model compared to its microphysical hail model. One disadvantage of a steady-state cloud model is that it does not realistically simulate the evolution of a cloud's liquid water content profile with time. As a storm matures, cloud droplets grow by collision and coalescence, eventually leading to the formation of raindrops. These falling cloud droplets and raindrops change the distribution of the cloud's LWC with height as time progresses; the peak of the LWC distribution shifts to lower heights (e.g. Srivastava, 1967). This effect could be parameterized and incorporated into the HC2 model to produce a more realistic representation of a cloud's liquid water content distribution.

Even a one-dimensional cloud model with the above improvements does not approach the level of detail in a three-dimensional, time-dependent cloud model. HC2's microphysical hail model could be run, coupled with a 3-D, time-dependent cloud model, to simulate the growth of hail on particular case study days. Such an investigation may allow for a more accurate evaluation of the microphysical model's skill at forecasting maximum hail size at ground. Multidimensional time-dependent hail models have been developed to simulate hailstorms; these have yielded information on likely hailstone trajectories within storms. Using the information on cloud parameters such as liquid water content, updraft velocity and in-cloud temperature along these trajectories, the growth of an oblate hailstone along such a trajectory could be simulated using HC2's microphysical hail model for a few select cases. Such a simulation would be much less computationally expensive than one involving a 3-D, time-dependent hail model, and would produce similar results.

The cloud model and the hail model are coupled by means of the updraft duration parameter. Updraft duration is estimated by considering a storm's CAPE and wind shear; the updraft duration assigned is between 20 and 60 minutes. We showed that a hailstone's evolution is sensitive to the amount of time it spends in the hail growth zone, and this amount of time in turn depends on the duration of the storm. If the updraft collapses before the hailstone has spent much time in the HGZ, the hailstone is significantly smaller when it reaches the ground. Given that the final size of a hailstone is quite sensitive to the updraft duration, we recommend using a more realistic method to determine that parameter. One possibility would be to use the hail model in conjunction with real-time radar data: the storm duration could be estimated from the radar data. Once an estimate for updraft duration has been maintained in this way, the model could then be run for an ensemble of different initial embryo diameter values to predict the maximum possible hail size that can be produced by a particular storm. HC2 does not take much time to run (less than 1 s on a 2.53 GHz personal computer), so such a nowcasting approach is certainly feasible even with limited computational resources. Alternatively, one could estimate the updraft duration for a large sample of storms using radar and compare these values to those of the CAPE*SHEAR calculation from a proximity sounding. This would also be an improvement over the current technique.

REFERENCES

Admirat, P., G. G. Goyer, L. Wojtiw, E. A. Carte, D. Roos, and E. P. Lozowski, 1985: A comparative study of hail in Switzerland, Canada and South Africa. *J. Climatol.*, **5**, 35-51.

Al-Jumily, K. J., R. C. Charlton, and R. G. Humphries, 1991: Identification of rain and hail with circular polarization radar. *J. Appl. Meteor.*, **30**, 1075-1087.

Alpert, P., and M. Tsidulko, 1994: Project WIND – Numerical simulations with Tel-Aviv PSU/NCAR model at Tel-Aviv University 1994. *Meteor. Monogr.*, No. 25, Amer. Meteor. Soc., 81-95.

Alpert, P., U. Stein, and M. Tsidulko, 1995a: Role of sea fluxes and topography in eastern Mediterranean cyclogenesis. *The Global Atmosphere Ocean System*, Vol. 3, 55-79.

Alpert, P., U. Stein, and M. Tsidulko, 1995b: Can sensitivity studies yield absolute comparisons for the effects of several processes. *J. Atmos. Sci.*, **52**, 597-601.

Alpert, P., S. O. Krichak, T. N. Krishnamurti, U. Stein, and M. Tsidulko, 1996a: The relative roles of lateral boundaries, initial conditions, and topography in mesoscale simulations of lee cyclogenesis. *J. Appl. Meteor.*, **35**, 1091-1099.

Alpert, P., M. Tsidulko, S. O. Krichak, and U. Stein, 1996b: A multi-stage evolution of an ALPEX cyclone. *Tellus*, **48A**, 209-220.

Anthes, R. A., 1977: A cumulus parameterization scheme utilizing a one-dimensional cloud model. *Mon. Wea. Rev.*, **105**, 270-286.

Bailey, I. H., and W. C. Macklin, 1968: Heat transfer from artificial hailstones. *Quart. J. Roy. Meteor. Soc.*, **94**, 93-98.

Barge, B. L., and G. A. Isaac, 1973: The shape of Alberta hailstones. *J. Rech. Atmos.*, **7**, 11-20.

Betts, A. K., 1982a: Cloud thermodynamics models in saturation point coordinates. *J. Atmos. Sci.*, **39**, 2182-2191.

Betts, A. K., 1982b: Saturation point analysis of moist convective overturning. *J. Atmos. Sci.*, **39**, 1484-1505.

Bluestein, H. B., E. W. McCaul Jr., G. P. Byrd, and G. R. Woodall, 1988: Mobile sounding observations of a tornado storm near the dryline: The Canadian, Texas storm of 7 May 1986. *Mon. Wea. Rev.*, **116**, 1790-1804.

Blyth, A. M., M. Alan, W. A. Cooper, and J. B. Jensen, 1988: A study of the source of entrained air in Montana cumuli. *J. Atmos. Sci.*, **45**, 3944-3964.

Bicknell, J., 1962: Report of wind tunnel tests on the aerodynamic drag of spheres with roughness and distortion. pp. 41-47 of *Balloon, high-altitude, fast-rising*, Final report of the U. S. Army Signal Research and Development Laboratory, Fort Monmouth, N. J., Contract No. DA36-039Sc84944.

Boatman, J. F., and A. H. Auer Jr., 1983: The role of cloud top entrainment in cumulus clouds. *J. Atmos. Sci.*, **40**, 1517-1534.

Böhm, J. P., 1989: A general equation for the terminal fall speed of solid hydrometeors. *J. Atmos. Sci.*, **46**, 2419-2427.

Brandes, E. A., J. Vivekanandan, J. D. Tuttle, and C. J. Kessinger, 1995: A study of thunderstorm microphysics with multiparameter radar and aircraft observations. *Mon. Wea. Rev.*, **118**, 1640-1644.

Brimelow, J. C., 1999: Numerical modelling of hailstone growth in Alberta storms. M. Sc. Thesis, University of Alberta, 153 pp.

Brimelow, J. C., T. W. Krauss, and G. W. Reuter, 2002a: Operational forecasts of maximum hailstone diameter in Mendoza, Argentina. *J. Wea. Mod.*, **34**, 8-17.

Brimelow, J. C., G. W. Reuter, and E. R. Poolman, 2002b: Modeling maximum hail size in Alberta thunderstorms. *Wea. Forecasting*, **17**, 1048-1061.

Brooks, H. E., C. A. Doswell III, and R. A. Maddox, 1992: On the use of mesoscale and cloud-scale models in operational forecasting. *Wea. Forecasting*, **7**, 120-132.

Brooks, H. E., C. A. Doswell III, and L. J. Wicker, 1993: STORMTIPE: A forecasting experiment using a three-dimensional cloud model. *Wea. Forecasting*, **8**, 352-363.

Browning, K. A., and J. G. D. Beimers, 1967: The oblateness of large hailstones. *J. Appl. Meteorol.*, **6**, 1075-1081.

Browning, K. A., and G. B. Foote, 1976: Airflow and hail growth in supercell storms and some implications for hail suppression. *Quart. J. Roy. Met. Soc.*, **102**, 499-533.

Browning, K. A., 1977: The Structure and Mechanisms of Hailstorms. *Meteor. Monogr.*, No. 38, Amer. Meteor. Soc., 1-43.

Castellano, N. E., and O. B. Nasello, 1997: Comments about the drag laws used in hail growth simulations. *Atmos. Res.*, **43**, 315-323.

Cheng, L., and D. C. Rogers, 1988: Hailfalls and hailstorm feeder clouds – an Alberta case study. *J. Atmos. Sci.*, **45**, 3533-3545.

Chisholm, A. J., 1973: Alberta Hailstorms. Part I: Radar case studies and airflow models. *Meteor. Monogr.*, No. 36, Amer. Meteor. Soc., 1-36.

Clark, T. L., 1982: Cloud modeling in three spatial dimensions. Hailstorms of the High Plains, Vol. II: Case studies of the National Hail Research Experiment, C. A. Knight and P. Squires, Eds., Colorado Assoc. Universities Press, Boulder, 225-247.

Deibert, R. J., 1984: An overview of weather modification activities in Alberta. *J. Wea. Mod.*, **16**, 66-72.

Deng, L., and D. K. Lilly, 1992: Helicity effect on turbulent decay in a rotating frame. *Preprints, 10th Symp. On Turbulence and Diffusion*, Portland, OR, Amer. Meteor. Soc., 338-341.

Dennis, A. S., and D. J. Musil, 1973: Calculations of hailstone growth and trajectories in a simple cloud model. *J. Atmos. Sci.*, **30**, 278-288.

Eastman, J. L., M. B. Coughenour, and R. A. Pilke, 2001: The effects of CO_2 and landscape changes using a coupled plant and meteorological model. *Global Change Biol.*, **7**, 797-815.

Edwards, R. and R. L. Thompson, 1998: Nationwide comparisons of hail size with WSR-88D vertically integrated liquid water and derived thermodynamic sounding data. *Wea. Forecasting*, **13**, 277-285.

English, M., 1973: Alberta Hailstorms. Part II: Growth of large hail in the storm. *Meteor. Monogr.*, No. 36, Amer. Meteor. Soc., 37-98.

Eng Young, R. G., and K. A. Browning, 1967: Wind tunnel tests of simulated spherical hailstones with variable roughness. *J. Atmos. Sci.*, **24**, 58-62.

Farley, R. D., 1987: Numerical modeling and hailstone growth. Part III: Simulation of an Alberta hailstorm – natural and seeded cases. *J. of Clim. And Appl. Meteor.*, **26**, 789-812.

Foote, G. B., 1984: A study of hail growth utilizing observed storm conditions. *J. Climate and Appl. Meteor.*, **23**, 84-101.

García-García, F., and R. List, 1992: Laboratory measurements and parameterizations of supercooled water skin temperatures and bulk properties of gyrating hailstones. *J. Atmos. Sci.*, **49**, 2058-2073.

Geresdi, I., 1998: Idealised simulation of the Colorado hailstorm: Comparison of bulk and detailed microphysics. *Atmos. Res.*, **45**, 237-252.

Greenan, B. J., and R. List, 1995: Experimental closure of the heat and mass transfer theory of spheroidal hailstones. *J. Atmos. Sci.*, **52**, 3797-3815.

Guan, S., and G. W. Reuter, 1996: Numerical simulation of an industrial cumulus affected by heat, moisture and CCN released from an oil refinery. *J. Appl. Meteor.*, **35**, 1257-1264.

Heymsfield, A. J., A. R. Jameson, and H. W. Frank, 1980: Hail growth mechanisms in a Colorado storm. Part III: Hail formation processes. *J. Atmos. Sci.*, **37**, 1789-1807.

Hoerner, S., 1958: *Fluid dynamic drag.* New York, published by the author, 203 pp.

Khain, A. P., D. Rosenfeld, and I. Sednev, 1993: Coastal effects in the E. Mediterranean as seen from experiments using a cloud ensemble model with detailed description of warm and ice microphysical processes. *Atmos. Res.*, **30**, 295-319.

Knight, C. A., and N. C. Knight, 1970a: Hailstone Embryos. *J. Atmos. Sci.*, **27**, 659-666.

Knight, C. A., and N. C. Knight, 1970b: Lobe Structures of Hailstones. *J. Atmos. Sci.*, **27**, 667-671.

Knight, C. A., and N. C. Knight, 1978: Cylindrical ice accretions as simulations of hail growth: II. The structure of fresh and annealed accretions. *J. Atmos. Sci.*, **35**, 1997-2009.

Knight, N. C., 1981: Climatology of hailstone embryos. *J. Appl. Meteor.*, **20**, 750-755.

Knight, C. A., and P. Squires (Eds.), 1982a: *Hailstorms of the High Plains. Vol. 1: Case Studies of the National Hail Research Experiment.* Colorado Assoc. Universities Press, Boulder, 282 pp.

Knight, C. A., and P. Squires (Eds.), 1982b: *Hailstorms of the High Plains. Vol. 2: Case Studies of the National Hail Research Experiment*. Colorado Assoc. Universities Press, Boulder, 245 pp.

Knight, N. C., 1986: Hailstone shape factor and its relation to radar interpretation of hail. *J. Clim. Appl. Meteorol.*, **25**, 1956-1958.

Krauss, T. W., and J. D. Marwitz, 1984: Precipitation processes within an Alberta supercell hailstorm. *J. Atmos. Sci.*, **41**, 1025-1033.

Kritchak, S. O., P. Alpert, and T. N. Krishnamurti, 1997a: Interaction of topography and tropospheric flow – A possible generator for the Red Sea trough? *Meteor. Atmos. Phys.*, **63**, 149-158.

Kritchak, S. O., P. Alpert, and T. N. Krishnamurti, 1997b: Red Sea trough/cyclone development numerical investigation. *Meteor. Atmos. Phys.*, **63**, 159-170.

Kry, P. R., and R. List, 1974a: Aerodynamic torques on rotating oblate spheroids. *Phys. Fluids*, **17**, 1087-1092.

Kry, P. R., and R. List, 1974b: Angular motions of freely falling spheroidal hailstone models. *Phys. Fluids*, **19**, 1093-1102.

Kubesh, R. J., D. J. Musil, R. D. Farley, and H. D. Orville, 1988: The 1 August CCOPE Storm: Observations and modeling results. *J. Appl. Meteor.*, **27**, 216-243.

Lesins, G. B., and R. List, 1986: Sponginess and drop shedding of gyrating hailstones in a pressure-controlled icing wind tunnel. *J. Atmos. Sci.*, **43**, 2813-2825.

Levi, L., and L. Lubart, 1998: Modelled spongy growth and shedding process for spheroidal hailstones. *Atmos. Res.*, **48**, 59-68.

List, R., J.-G. Cantin, and M. G. Ferland, 1970: Structural Properties of Two Hailstone Samples. *J. Atmos. Sci.*, **27**, 1080-1090.

List, R., B. J. W. Greenan, and F. García-García, 1995: Surface temperature variations of gyrating hailstones and effects of pressure-temperature coupling on growth. *Atmos. Res.*, **38**, 161-175.

Lozowski, E. P., and G. S. Strong, 1978: Further reflections of the calibration of hailpads. *Atmos. Ocean*, **16**, 69-80.

Macklin, W. C., 1963: Heat transfer from hailstones. *Quart. J. Roy. Meteor. Soc.*, **89**, 360-369.

Macklin, W. C., 1977: The characteristics of natural hailstones and their interpretation. *Hail: A Review of Hail Science and Hail Suppression. Meteor. Monogr., No. 38*, Amer. Meteor. Soc., **16**, 65-88.

Matson, R. J., and A. W. Huggins, 1980: The direct measurement of the sizes, shapes and kinematics of falling hailstones. *J. Atmos. Sci.*, **37**, 1107-1125.

Matthews, D. A., and J. F. Henz, 1975: Verification of numerical model simulations of cumulus-environmental interaction in the High Plains. *Pure Appl. Geophys.*, **113**, 803-823.

Marzban, C., and G. J. Stumpf, 1998: A neural network for damaging wind prediction. *Wea. Forecasting*, **13**, 151-163.

Miller, L. J., J. D. Tuttle, and C. A. Knight, 1988: Airflow and hail growth in a severe northern high plains supercell. *J. Atmos., Sci.*, **45**, 736-762.

Miller, L. J., J. D. Tuttle, and G. B. Foote, 1990: Precipitation production in a large Montana hailstorm: Airflow and particle growth. *J. Atmos. Sci.*, **57**, 1619-1646.

Musil, D. J., 1970: Computer modeling of hailstone growth in feeder clouds. *J. Atmos. Sci.*, **26**, 474-482.

Nelson, S. P., 1983: The influence of storm flow structure on hail growth. *J. Atmos. Sci.*, **40**, 1965-1983.

Orville, H. D., 1977: A review of hailstone-hailstorm numerical simulations. *Meteor. Monogr.*, No. 38, Amer. Meteor. Soc., 49-61.

Orville, H. D., and F. J. Kopp, 1977: Numerical simulation of the life history of a hailstorm. *J. Atmos. Sci.*, **34**, 1596-1618.

Paluch, I. R., 1979: The entrainment mechanism in Colorado cumuli. *J. Atmos. Sci.*, **36**, 1596-1618.

Poolman, E. R., 1992: Die voorspelling van haelkorrelgroei in Suid-Afrika. M. Sc. Thesis, Faculty of Engineering, University of Pretoria, 113 pp.

Prandtl, L., 1923: *Ergebnisse der Aerodynamischen Verschsanstalt zu Göttingen.* Munich and Berlin, R. Oldenbourg, 29 pp.

Prodi, F., 1970: Measurements of local density in artificial and natural hailstones. *J. Appl. Meteorol.*, **9**, 903-910

Pruppacher, H. R., and J. D. Klett, 1978: Microphysics of Clouds and Precipitation. Reidel Publishing Company, 714 pp.

Ramis, C., and R. Romero, 1995: A first numerical simulation of the development and structure of the sea breeze in the Island of Mallorca. *Ann. Geophys.*, **13**, 981-994.

Rasmussen, R. M., and A. J. Heymsfield, 1987a: Melting and shedding of graupel and hail. Part I: Model physics. *J. Atmos. Sci.*, **44**, 2754-2763.

Rasmussen, R. M., and A. J. Heymsfield, 1987b: Melting and shedding of graupel and hail. Part II: Sensitivity study. *J. Atmos. Sci.*, **44**, 2764-2782.

Rasmussen, R. M., and A. J. Heymsfield, 1987c: Melting and shedding of graupel and hail. Part III: Investigation of the role of shed drops as hail embryos in the 1 August CCOPE severe storm. *J. Atmos. Sci.*, **44**, 2783-2803.

Reuter, G. W. and S. Guan, 1995: Effects of industrial pollution on cumulus convection rain showers: a numerical study. *Atmospheric Environment*, **29**, 2467-2474.

Rogers, R. R. and M. K. Yau, 1989: A Short Course in Cloud Physics, 3rd Ed. Butterworth-Heinemann, 290 pp.

Romero, R., C. Ramis, and S. Alonso, 1997: Numerical simulation of an extreme rainfall event in Catalonia: Role of orography and evaporation from the sea. *Quart. J. Roy. Meteor. Soc.*, **123**, 537–559.

Romero, R., C. A. Doswell III, and D. J. Stensrud, 1998: Mesoscale model simulations of three heavy precipitation events in the western Mediterranean region. *Mon. Wea. Rev.*, **126**, 1859–1881.

Roos, D. v.d. S., and A. E. Carte, 1973: The falling behaviour of oblate and spiky hailstones. *J. Rech. Atmos.*, **7**, 39-52.

Sanders, F., and A. J. Garrett, 1975: Application of a convective plume model to prediction of thunderstorms. *Mon. Wea. Rev.*, **103**, 874-877.

Simpson, J., and V. Wiggert, 1969: Models of precipitating cumulus towers. *Mon. Wea. Rev.*, **97**, 471-489.

Smith, S. B. and M. K. Yau, 1993a: The causes of severe convective outbreaks in Alberta. Part I. A comparison of a severe outbreak with two nonsevere events. *Mon. Wea. Rev.*, **121**, 1099-1125.

Smith, S. B. and M. K. Yau, 1993b: The causes of severe convective outbreaks in Alberta. Part II: Conceptual model and statistical analysis. *Mon. Wea. Rev.*, **121**, 1126-1134.

Smith, S. B., G. W. Reuter, and M. K. Yau, 1998: The episodic occurrence of hail in central Alberta and the Highveld of South Africa. *Atmos.-Ocean*, **36**, 169-178.

Srivastava, R. C., 1967: A study of the effect of precipitation on cumulus dynamics. *J. Atmos. Sci.*, **24**, 36-45.

Stein, U. and P. Alpert, 1993: Factor separation in numerical solutions. *J. Atmos. Sci.*, **50**, 2107-2115.

Strong, G. S., 1974: Objective measurement of Alberta hailfall. M. S. thesis, Dept. of Earth and Atmospheric Sciences, University of Alberta, 182 pp.

Strong, G. S., and E. P. Lozowski, 1977: An Alberta study to objectively measure hailfall intensity. *Atmos. Ocean*, **15**, 33-53.

Vali, G., and E. J. Stansbury, 1965: Time-dependant characteristics of the heterogeneous nucleation of ice. Sci. Rept., MW-41, Montreal, McGill University, 31 pp.

Willis, J. T., K. A. Browning, and D. Atlas: Radar observations of ice spheres in free fall. *J. Atmos. Sci.*, **21**, 103-108.

Wisner, C., H. D. Orville, and C. Meyers, 1972: A numerical model of a hail-bearing cloud. *J. Atmos. Sci.*, **29**, 1160-1181.

Witt, A., M. D. Eilts, G. J. Stumpf, J. T. Johnson, E. D. Mitchell, and K. W. Thomas, 1998: An enhanced hail detection algorithm for the WSR-88D. *Wea. Forecasting*, **13**, 286-303

Xu, J. L., 1983: Hail growth in a three-dimensional cloud model. *J. Atmos. Sci.*, **40**, 185-203.

APPENDIX A: List of Symbols

A	Area of the smallest circle or ellipse that completely contains A_e (cm^2)
A_c	Average cross-sectional area (perpendicular to the direction of motion) of the hailstone; assumed to be equal to $\pi D^2/4$ (cm^2)
A_e	Effective projected area presented to the flow (cm^2)
A_s	Surface area of an oblate spheroid (cm^2)
C_D	Drag coefficient for the circumscribed disk (with area A) of the hailstone
C_{De}	Actual drag coefficient of the hailstone
C_i	Specific heat of ice (cal g^{-1} K^{-1})
C_w	Specific heat of water (cal g^{-1} K^{-1})
d	Characteristic length; $d = 2(A/\pi)^{1/2} = D$ (cm)
d_a	Thermal diffusivity of air (cm^2 s^{-1})
d_{wa}	Thermal diffusivity of water vapour in air (cm^2 s^{-1})
D	Major diameter (i.e. major axis) of the hailstone (cm)
D_{eq}	Equivalent diameter of the hailstone; $D_{eq} = D\alpha^{1/3}$ (cm)
D_f	Diameter of a model hailstone when it freezes at an in-cloud temperature of - 8°C
$D_{\min}$	Minor diameter (i.e. minor axis) of the hailstone (cm)
D_0	Initial hailstone embryo diameter (μm)
D_1	Maximum major diameter of the hailstone with an aspect ratio of $\alpha = \alpha_1$; control value is D_1 = 1 cm
D_2	Minimum major diameter of the hailstone with an aspect ratio of $\alpha = \alpha_c$; control value is D_2 = 2 cm
dD/dt	Rate of change of major diameter of the hailstone with time (cm s^{-1})
E_i	Collection efficiency of cloud ice
E_{net}	Net collection efficiency of cloud water
E_w	Collection efficiency of cloud water (not including shedding effects)
f_M	Mutual interaction of roughness and oblateness effect on variable f
f_O	Pure oblateness effect on variable f
f_R	Pure roughness effect on variable f
f_T	Total effect of roughness and oblateness on variable f
F_w	Fractional water content of the hailstone
g	Acceleration due to gravity; assumed to be constant (cm s^{-2})
k	Thermal conductivity of air (cal cm^{-1} s^{-1} K^{-1})
K	Stokes parameter
K_E	Curvature parameter used to calculate net collection efficiency (cm^3 g^{-1})

L_f	Latent heat of freezing (cal g^{-1})
L_s	Latent heat of sublimation (cal g^{-1})
L_v	Latent heat of vaporization (cal g^{-1})
M	Total mass of the hailstone at a given time (g)
M_{crit}	Critical surface water mass that a spherical hailstone may retain below cloud base (g)
$M_{crit}*$	Critical surface water mass that an oblate hailstone may retain below cloud base (g)
dM_s/dt	Mass of water shed by the hailstone per unit time (g s^{-1})
M_i	Mass of the hailstone's ice core (g)
dM/dt	Rate of change of hailstone mass due to the accretion of both supercooled water droplets and ice crystals (g s^{-1})
dM_i/dt	Rate of change of hailstone mass due to the accretion of ice crystals (g s^{-1})
dM_w/dt	Rate of change of hailstone mass due to the accretion of supercooled water droplets (g s^{-1})
Nu	Nusselt number: $\mathrm{Nu} = f(\mathrm{Re}, \mathrm{Pr})$
Pr	Prandtl number: $\mathrm{Pr} = \eta_a / \rho_a d_a = 0.71$
q	Roughness factor; $q = A_e / A$
Q_a	Heat gained by the hailstone due to accretion of supercooled cloud water (cal)
Q_c	Heat gained by the hailstone due to accretion of cloud ice (cal)
Q_k	Heat gained by the hailstone due to convection and conduction (cal)
Q_s	Heat gained by the hailstone due to sublimation/evaporation (cal)
dQ_T/dt	Total heat exchange per unit time between the hailstone and its environment (cal s^{-1})
r_d	Median droplet volume radius (cm)
Re	Reynolds number: $\mathrm{Re} = DV_T \rho_a / \eta_a$
r_H	Semi-major axis of hailstone (i.e. $r_H = D/2$) (cm)
Sc	Schmidt number: $Sc = \eta_a / \rho_a d_{wa} = 0.60$
Sh	Sherwood number: $Sh = f(\mathrm{Re}, Sc)$
t	time (s)
T_a	Ambient (in-cloud) temperature (°C)
T_s	Surface temperature of the hailstone (°C)
T_{so}	Schuman-Ludlam limit ($T_{so} = 0°C$)
Vol	Volume of the hailstone (cm^3)
V_T	Terminal velocity of a hailstone with a rough surface (cm s^{-1})
$V_{T(smooth)}$	Velocity of a hailstone with a smooth surface (cm s^{-1})
W	Updraft velocity (m s^{-1})
W_0	Updraft velocity at lifted condensation level (cloud base) (m s^{-1})
X	Best number

z_{lcl}	Lifted condensation level (m)
z_{el}	Equilibrium level (m)
$\alpha(D)$	Aspect ratio of the hailstone, as a function of major diameter
α_1	Constant value of aspect ratio for $D \le D_1$; control value is $\alpha_1 = 1$
α_c	Final (constant) value of the aspect ratio of the evolving hailstone, reached when $D \ge D_2$; control value is $\alpha_c = 0.77$
$d\alpha/dD$	Rate of change of aspect ratio with major diameter (cm^{-1})
$d\alpha/dt$	Rate of change of aspect ratio of the hailstone with time (s^{-1})
ε	Eccentricity of an oblate spheroid: $\varepsilon = \left(1 - \alpha^2\right)^{1/2}$
η_a	Dynamic viscosity of air (g cm^{-1} s^{-1})
ρ_a	Density of the ambient air (g cm^{-3})
ρ_d	Density of cloud water droplets (ρ_d = 1 g cm^{-3})
ρ_e	Vapour density of the environmental air (g cm^{-3})
ρ_H	Density of the hailstone (g cm^{-3})
ρ_s	Vapour density at the hailstone's surface (g cm^{-3})
$\Delta\rho$	Vapour density difference between the hailstone's surface and the environmental air: $\Delta\rho = \rho_s - \rho_e$ (g cm^{-3})
τ	Total hailstone growth time (min)
χ	Mixing ratio of condensed water substance present at each level within the cloud after entrainment
χ^*	Cloud liquid water content at the onset of shedding (g cm^{-3})
χ_i	Cloud ice content (g cm^{-3})
χ_w	Cloud liquid water content (g cm^{-3})

APPENDIX B: Deriving the Rate of Change of the Major Diameter of a Growing Hailstone

The rate of change of a hailstone's major diameter with time (dD/dt) can be derived from the mass growth equation with little effort. To do so, we start with the expression for the mass of a hailstone with major diameter D and aspect ratio $\alpha(D)$:

$$M = \frac{\pi}{6}\alpha(D)D^3\rho_H, \tag{B.1}$$

where it is assumed that aspect ratio is a function of the hailstone's major diameter. The volume of an oblate spheroid of major diameter D and aspect ratio α is

$$Vol = \frac{\pi}{6}\alpha D^3. \tag{B.2}$$

Taking the derivative with respect to time of (B.1) yields

$$\frac{dM}{dt} = \frac{d}{dt}\left(\frac{\pi}{6}\alpha(D)D^3\rho_H\right) = \frac{\pi}{6}\rho_H\frac{d}{dt}\left(\alpha(D)D^3\right). \tag{B.3}$$

Before we proceed further, we must note that major diameter is a function of time and, therefore, aspect ratio is also a function of time, because it is assumed to depend on D. Expanding (B.3) yields

$$\frac{dM}{dt} = \frac{\pi}{6}\rho_H\left[D^3\frac{d\alpha}{dt} + 3\alpha D^2\frac{dD}{dt}\right]. \tag{B.4}$$

We do not know explicitly what $d\alpha/dt$ is, but we may express this time derivative in terms of $d\alpha/dD$, a quantity that is known:

$$\frac{d\alpha}{dt} = \frac{d\alpha}{dD}\frac{dD}{dt}. \tag{B.5}$$

In our case, the rate of change of aspect ratio with major diameter can be calculated using the defined formulae for aspect ratio as a function of major diameter (2.21):

$$
\begin{aligned}
& d\alpha/dD = 0 && \text{for} \quad D < D_1 \\
& d\alpha/dD = (\alpha_c - \alpha_1)/(D_2 - D_1) && \text{for} \quad D_1 \le D \le D_2\,. \\
& d\alpha/dD = 0 && \text{for} \quad D > D_2
\end{aligned}
\qquad (B.6)
$$

Next, we combine (B.5) and (B.4) to yield

$$\frac{dM}{dt} = \frac{\pi}{6}\rho_H D^2 \frac{dD}{dt}\left[D(d\alpha/dD) + 3\alpha\right]. \qquad (B.7)$$

The mass growth equation for a hailstone undergoing the process of continuous collection is

$$\frac{dM}{dt} = \frac{dM_w}{dt} + \frac{dM_i}{dt} = A_c V_t \left[\chi_w E_{net} + \chi_i E_i\right]. \qquad (B.8)$$

As all effects of tumbling and other irregular motions of falling oblate hailstones are included empirically in Böhm's (1989) terminal velocity formulation, we may use the following expression for the average cross-sectional area of the hailstone presented to the flow:

$$A_c = \frac{\pi D^2}{4}. \qquad (B.9)$$

To arrive at an expression for the rate of change of a hailstone's major diameter with respect to time, equate (B.7) with the mass growth equation, use (B.9) to eliminate the variable A_c, then solve for dD/dt:

$$\frac{dD}{dt} = \frac{3}{2}\frac{V_t}{\rho_H}\frac{1}{D(d\alpha/dD) + 3\alpha}\left[\chi_w E_{net} + \chi_i E_i\right]. \qquad (B.10)$$

Note that if we set α to 1 and $d\alpha/dD$ to zero, (B.10) is reduced to the expression for the growth rate of the diameter of a spherical hailstone.

APPENDIX C: Deriving the Nusselt and Sherwood Numbers

C-1: Nu and Sh for Rough, Oblate Hailstones

Rasmussen and Heymsfields' (1987a) parameterizations for the Nusselt number and Sherwood number are based on experimental work done by Macklin (1963) and Bailey and Macklin (1968). In their scheme, Nu and Sh are assigned values depending on the current Reynolds number of the spherical hailstone. For $\mathrm{Re} > 20000$, the spherical hailstones in Brimelow et al.'s (2002b) HAILCAST model were assumed to have rough surfaces, and thus the Nu and Sh expressions presented by Bailey and Macklin (1968) were used. According to these authors, Nu and Sh increase rapidly with increasing Reynolds number when the surface of the hailstone is rough. For $6000 \le \mathrm{Re} \le 20000$, the hailstone was assumed to have a relatively smooth surface, and Nu and Sh were calculated using the expression given by Macklin (1963) for spherical hailstones. For a realistically rough spherical hailstone, Rasmussen and Heymsfield (hereafter referred to as RH87a) used the following expressions for Nu:

$$\begin{array}{ll} \mathrm{Re} < 6000: & \mathrm{Nu} = 0.78 + 0.308\,\mathrm{Pr}^{1/3}\,\mathrm{Re}^{1/2} \\ 6000 \le \mathrm{Re} \le 20000: & \mathrm{Nu} = 0.76\,\mathrm{Pr}^{1/3}\,\mathrm{Re}^{1/2} \\ \mathrm{Re} \ge 20000: & \mathrm{Nu} = \chi\,\mathrm{Pr}^{1/3}\,\mathrm{Re}^{1/2} \end{array} \quad , \qquad \text{(C.1)}$$

where:

$$\chi = 0.57 + 9 \times 10^{-6}\,\mathrm{Re}. \qquad \text{(C.2)}$$

The expressions for the Sherwood number are identical to (C.1) with the Schmidt number, Sc, substituted for the Prandtl number, Pr.

We used the expressions given by Macklin (1963) for Nu and Sh to include the effects of an aspect ratio that is less than one in (C.1). Macklin (1963) conducted a series of experiments with hailstones of varying degrees of oblateness to determine how Nu and Sh varied with aspect ratio. From these experiments, he derived the following expressions:

$$\begin{aligned} \mathrm{Nu} &= \kappa\,\mathrm{Re}^{1/2}\,\mathrm{Pr}^{1/3} \\ \mathrm{Sh} &= \kappa\,\mathrm{Re}^{1/2}\,\mathrm{Sc}^{1/3} \end{aligned}, \tag{C.3}$$

where

$$\kappa = 1.02 - 0.26\alpha \tag{C.4}$$

and

$$\kappa_{sphere} = 0.76\,. \tag{C.5}$$

The Nusselt number for an oblate hailstone may be expressed in terms of the Nusselt number for a spherical hailstone:

$$\mathrm{Nu} = \frac{\kappa}{\kappa_{sphere}}\,\mathrm{Nu}_{sphere}\,, \tag{C.6}$$

with a similar expression for the Sherwood number.

If we combine Macklin's (1963) formulation with that of RH87a, we can derive an appropriate Nusselt number for realistically rough, oblate hailstones:

$$\begin{aligned} &\mathrm{Re} < 6000: && \mathrm{Nu} = \left(\kappa/\kappa_{sphere}\right)\left(0.78 + 0.308\,\mathrm{Pr}^{1/3}\,\mathrm{Re}^{1/2}\right) \\ &6000 \le \mathrm{Re} \le 20000: && \mathrm{Nu} = \left(\kappa/\kappa_{sphere}\right)0.76\,\mathrm{Pr}^{1/3}\,\mathrm{Re}^{1/2} \\ &\mathrm{Re} \ge 20000: && \mathrm{Nu} = \left(\kappa\chi/\kappa_{sphere}^{2}\right)0.76\,\mathrm{Pr}^{1/3}\,\mathrm{Re}^{1/2} \end{aligned}\,, \tag{C.7}$$

with similar expressions for Sh. Note that if the hailstone is spherical, (C.7) reduces to the original expression given by Rasmussen and Heymsfield (1987a).

C-2: Nu and Sh for Smooth, Oblate Hailstones

We have designed the HC2 model so that it is possible to simulate smooth-surfaced hailstones in addition to rough-surfaced hailstones; the model may be run with roughness either "switched on" or "switched off". As Nusselt number and Sherwood number both depend on the surface roughness of a hailstone, we must take surface roughness into account when calculating these important heat budget parameters. The Nusselt number expression (C.7) is valid for oblate hailstones with reasonably rough surfaces, but we must use a slightly different expression for smooth-surfaced hailstones.

Smooth hailstones have lower Nusselt and Sherwood numbers than rough hailstones. The efficiency of heat transfer for smooth hailstones is decreased compared to hailstones with rough surfaces, due to the fact that smooth hailstones have smaller overall surface areas than rough hailstones of the same mass and size. Therefore, the following expressions for Nusselt number (similarly, for Sherwood number) are used when simulating the growth of a hailstone with a smooth surface:

$$\begin{array}{ll} \mathrm{Re} < 6000: & \mathrm{Nu} = \left(\kappa/\kappa_{sphere}\right)\left(0.78 + 0.308\,\mathrm{Pr}^{1/3}\,\mathrm{Re}^{1/2}\right) \\ 6000 \le \mathrm{Re} \le 20000: & \mathrm{Nu} = \left(\kappa/\kappa_{sphere}\right)0.76\,\mathrm{Pr}^{1/3}\,\mathrm{Re}^{1/2} \\ \mathrm{Re} \ge 20000: & \mathrm{Nu} = \left(\kappa/\kappa_{sphere}\right)0.76\,\mathrm{Pr}^{1/3}\,\mathrm{Re}^{1/2} \end{array} . \tag{C.8}$$

APPENDIX D: Selection of Embryo Diameter for Severe Hail Days

Table D1: Observed surface temperature (*T*), dewpoint (T_d), and maximum hail size category for each severe hail day, along with the model embryo diameter (D_0) that yields the largest hail.

Date (dd/mm/yyyy)	T (°C)	T_d (°C)	Size Category	D_0 (μm)
6/22/1983	17	9	WALNUT	700
6/24/1983	23	16	WALNUT	700
7/6/1983	22	15	GOLF	400
7/13/1983	25	13	WALNUT	400
7/21/1983	23	11	WALNUT	700
7/24/1983	25	14	GOLF	700
8/3/1983	27	13	GOLF	700
8/15/1983	26	10	GOLF	700
6/25/1984	20	8	WALNUT	400
7/6/1984	16	8	GOLF	400
7/12/1984	23	12	WALNUT	700
7/28/1984	28	17	>GOLF	700
8/6/1984	26	11	GOLF	700
8/24/1984	25	9	WALNUT	700
6/23/1985	16	7	GOLF	700
7/11/1985	28	10	GOLF	700
7/12/1985	16	11	WALNUT	400
7/23/1985	19	7	WALNUT	400
8/4/1985	28	11	>GOLF	700
8/30/1985	16	9	WALNUT	400

APPENDIX E: Dependence of Collection Efficiency and the Onset of Shedding on Aspect Ratio

E-1: Shedding and Collection Efficiency above Cloud Base

Through carefully controlled experiments, it was observed that not all water that collects on the surface of a hailstone remains with that hailstone (Lesins and List, 1986; García-García and List, 1992). Given appropriate conditions, hailstones may shed water as millimetre-sized drops. Shedding is one of the processes that influence the evolution of a hailstone; a shedding hailstone has a reduced mass growth rate, as not all of the water it collects on its surface remains with it. The point at which the hailstone begins to shed and the fraction of water that it does shed during this stage of growth both depend, to some extent, on the degree of oblateness of that hailstone. Even when the growing hailstone is not shedding, the collection efficiency of cloud water depends on its shape.

Since the collection efficiency of cloud water during non-shedding growth, E_w, the net collection efficiency, E_{net}, and the threshold liquid water content for the onset of shedding, χ^*, all depend to some extent on the degree of oblateness of a hailstone, we endeavoured to calculate their functional dependencies on aspect ratio. For the purpose of these calculations, it was necessary to choose some numbers for the ambient conditions and the hailstone mass and density. The ambient conditions are assumed to remain constant: $T_a = -15°\mathrm{C}$, $\rho_a = 0.6$ kg m^{-3} and $\chi_w = 6$g m^{-3}. To calculate χ^* and E_{net} as functions of aspect ratio, we assumed a hailstone density of 900 kg m^{-3} and an equivalent diameter of 2 cm or, in other words, a constant mass of 3.77 g. All of the calculations that are presented in this appendix are based on the empirically-derived formulae of García-García and List (1992), Greenan and List (1995) and Levi and Lubart (1998). The dependencies on aspect ratio are thus not general; they are based in part on the results of a set of experiments. Still, it is a useful exercise to examine the effects of aspect ratio on collection efficiency and shedding parameters. The following discussion applies to the empirically-derived formulae used in the HC2 model.

When a hailstone is not shedding, its collection efficiency for cloud water depends only on the Stokes parameter, and, through that, on its major diameter. As major diameter is a function of a hailstone's aspect ratio, this implies a dependence on degree of oblateness. E_w is always less than 1 using this formulation, due to the fact that a portion of the smaller cloud droplets are carried around the hailstone and thus never come in contact with its surface (Greenan and List, 1995). The turbulence around the hailstone that causes this to occur is related to its constant tumbling motions. The amount of turbulence around a hailstone is influenced in part by its shape; an oblate hailstone will cause a larger "disturbance" in the air around it as it gyrates than a spherical hailstone will, and, as a result, will collect fewer droplets. From (2.14) we derive an expression for the dependence of E_w on aspect ratio for a hailstone of constant mass:

$$F(E_w) = E_w / E_{w(sph.)} = \alpha^{1/10}, \tag{E.1}$$

where the notation $F(E_w)$ is the same one used in Chapter 3. Oblate hailstones tend to collect slightly less water than spherical hailstones. For example, an oblate hailstone with an aspect ratio of 0.77 has a collection efficiency (when there is no shedding) that is 0.97 times that of a spherical hailstone of the same mass. (E.1) is plotted for a range of aspect ratios in Figure E1.

A growing hailstone is assumed to begin to shed if the ambient liquid water content exceeds the experimentally derived parameter χ* (Levi and Lubart, 1998). The ambient liquid water content at the onset of shedding, χ*, depends on ambient temperature, as well as the major diameter, and hence the aspect ratio, of the hailstone (2.11). For the parameter χ*, it is not possible to derive a simple analytical expression like those presented in Chapter 3. Instead, we determined the relationship between χ* and aspect ratio numerically, assuming constant ambient conditions, for a hailstone of constant mass and density. The results are plotted in Figure E2. The onset of shedding occurs at a lower liquid water content for oblate hailstones than it does for spherical hailstones, which implies that oblate hailstones shed more readily than their spherical counterparts. Oblate hailstones undergo motions that are more erratic than those that spherical hailstones experience, since they are less symmetrical. These erratic motions cause oblate stones to shed more readily.

The net collection efficiency affects a hailstone's mass growth rate (2.1). During dry or wet growth, the net collection efficiency is equal to the collection efficiency for cloud water and when the hailstone is shedding, the net collection efficiency is lower. The rate at which water is shed from a hailstone is controlled by this parameter, which depends on ambient conditions along with the size and aspect ratio of the hailstone in question. As with χ^*, it is not possible to derive a simple analytical expression like those in Chapter 3 for net collection efficiency as a function of aspect ratio. We thus used the same method to calculate the dependence of E_{net} on aspect ratio as we used for χ^*. From (2.12), we calculated E_{net} as a function of aspect ratio for a hailstone that is actively shedding. The dependence of net collection efficiency during shedding on aspect ratio is shown in Figure E1. E_{net} is lower during shedding for an oblate hailstone than it is for a spherical hailstone. The difference between the net collection efficiency of an oblate hailstone and that of a spherical hailstone is larger during shedding than it is when there is no shedding. For example, an oblate hailstone with an aspect ratio of 0.77 has a net collection efficiency that is 0.96 times that of a spherical hailstone of the same mass; this same ratio for a hailstone that is not shedding is 0.97.

Above cloud base, oblate hailstones collect slightly less water during wet and dry growth, begin to shed earlier, and shed more water than spherical hailstones. These factors reduce the mass growth rate of an oblate hailstone when compared to that of a spherical hailstone of the same mass.

E-2: Shedding and Melting Below Cloud Base

Below cloud base, there is no ambient water available to collect on the surface of a hailstone. The temperatures are usually warm enough to cause the hailstone to experience some melting, and some of the melted water is shed as it falls to the ground. When this happens, the rate of melting and shedding is controlled by the parameter M_{crit}, the maximum amount of water that a hailstone may retain on its surface. For a hailstone of a given mass, the amount of water that can accumulate on its surface is assumed to depend on its surface area and, through that, its aspect ratio (2.15). We calculated the relationship between surface area and aspect ratio for a hailstone of constant mass and density (Chapter 3); the results are shown in Figure E3. The amount of water that a hailstone is able to accumulate on its surface during melting has the exact same functional relationship as $F(A_s)$ (3.2). The surface area of an oblate hailstone with an aspect ratio of 0.77 is only 1% larger than that of a spherical hailstone of the same mass, so the amount of water that the hailstone can accumulate on its surface while melting is about 1% larger than that of a spherical hailstone. For an oblate hailstone with an aspect ratio of 0.30, this number changes to 30%.

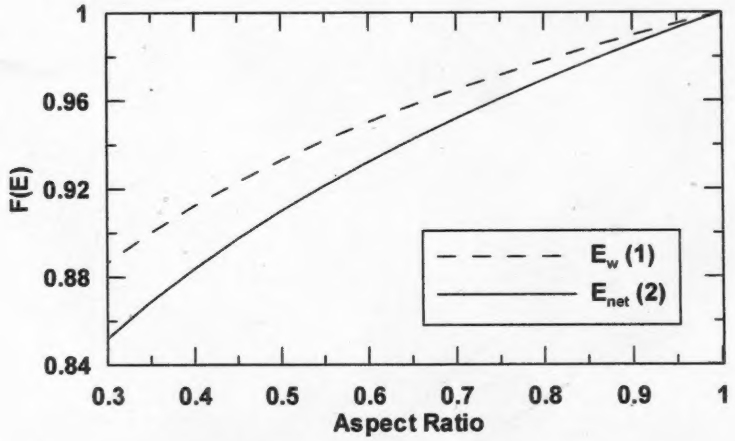

Figure E1: Ratio of the collection efficiency of cloud water of an oblate hailstone to that of a spherical hailstone of the same mass (D_{eq} = 2 cm with a density of ρ_H = 0.9 g cm^{-3}). Calculations are done for two cases: 1) No shedding; 2) Shedding. The following ambient conditions were used for this calculation: T_a = - 15°C, ρ_a = 0.6 kg m^{-3}, χ_w = 6 g m^{-3}, ρ_d = 1 g cm^{-3}, r_d = 25.5 μm.

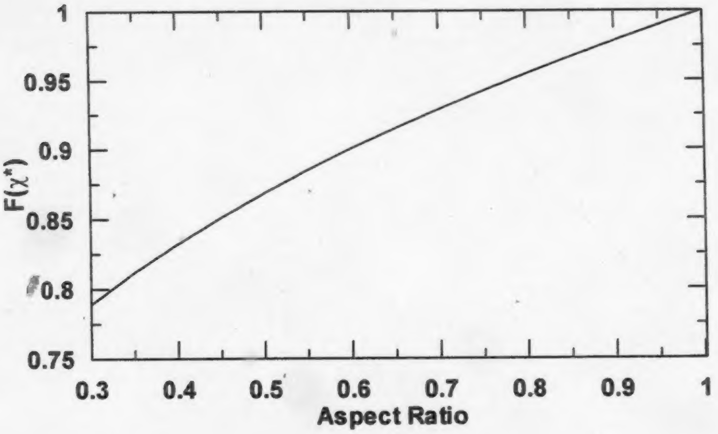

Figure E2: Ratio of the liquid water content at the onset of shedding of an oblate hailstone to that of a spherical hailstone.

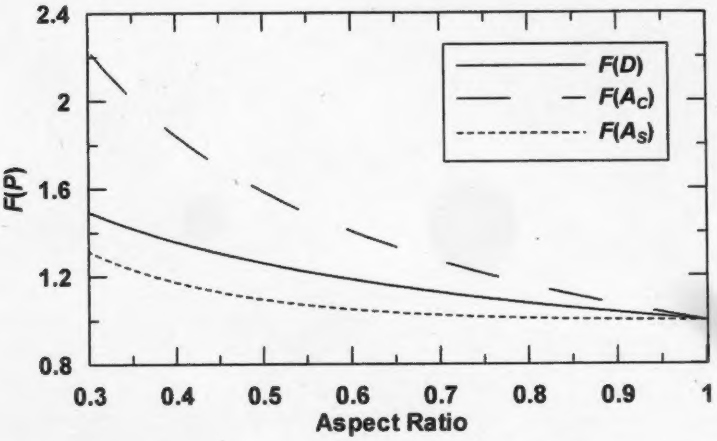

Figure E3: Ratio of the surface area of an oblate hailstone to that of a spherical hailstone of the same mass and density.

APPENDIX F: Forecast Skill Scores

This appendix contains a summary of skill scores used to evaluate hail forecasts. These are all derived from 2 × 2 contingency tables. In all equations, H denotes a hit, M denotes a miss, FA denotes a false alarm and N denotes a null forecast.

Probability of Detection (POD): Measures the ability to detect an event. This forecast skill score varies between 0 and 1, with higher POD scores indicating increased forecast skill.

$$\mathrm{POD} = \frac{\mathrm{H}}{\mathrm{H} + \mathrm{M}} \tag{F.1}$$

False Alarm Ratio (FAR): Measures the number of false alarms. The FAR varies between 0 and 1, with lower FAR scores indicating increased forecast skill.

$$\mathrm{FAR} = \frac{\mathrm{FA}}{\mathrm{FA} + \mathrm{H}} \tag{F.2}$$

Heidke Skill Score (HSS): Measures the true skill of a forecast. HSS varies between -1 for absolutely no forecast skill and 1 for a perfect forecast.

$$\mathrm{HSS} = \frac{2 * (\mathrm{H} * \mathrm{N} - \mathrm{M} * \mathrm{FA})}{\mathrm{M}^2 + \mathrm{FA}^2 + 2 * \mathrm{H} * \mathrm{N} + (\mathrm{M} + \mathrm{FA}) * (\mathrm{H} + \mathrm{N})} \tag{F.3}$$

Critical Success Index: Another way of measuring the true skill of a forecast. CSI varies between 0 for absolutely no forecast skill and 1 for a perfect forecast.

$$\mathrm{CSI} = \frac{\mathrm{H}}{\mathrm{H} + \mathrm{FA} + \mathrm{M}} \tag{F.4}$$

FIGURES

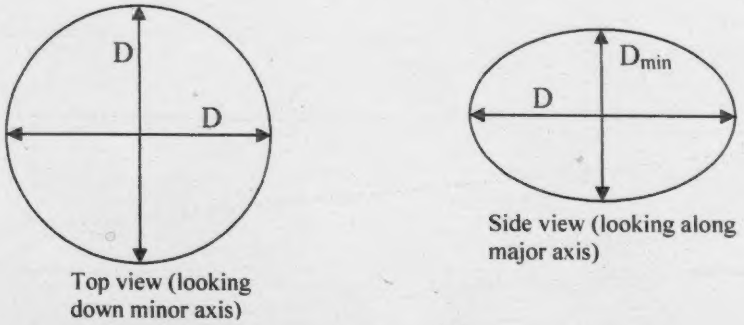
D
D
Top view (looking down minor axis)
Dmin
D
Side view (looking along major axis)

Figure 1.1: Schematic diagram of a smooth, oblate hailstone, presented from two different views: looking down its minor axis (left) and looking along its major axis (right). The length of its minor axis is its minor diameter, D_{min}, and the length of its major axis is its major diameter, D.

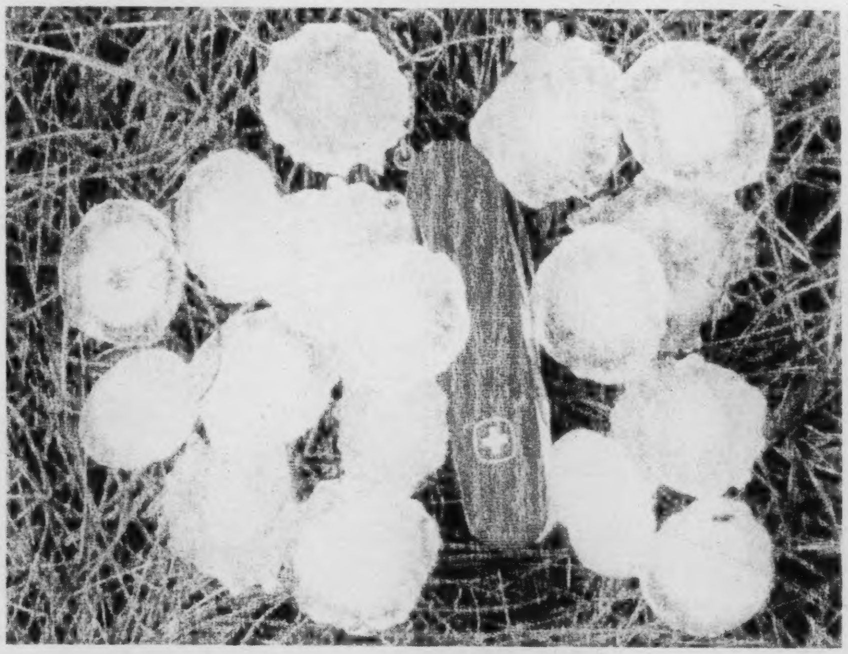

Figure 1.2: Sample of walnut-sized hailstones from a storm on 19 July 2002 near Eckville, AB (courtesy of J. Brimelow). Notice the oblate hailstone next to the bottom right of the knife (this hailstone is viewed looking along its major diameter).

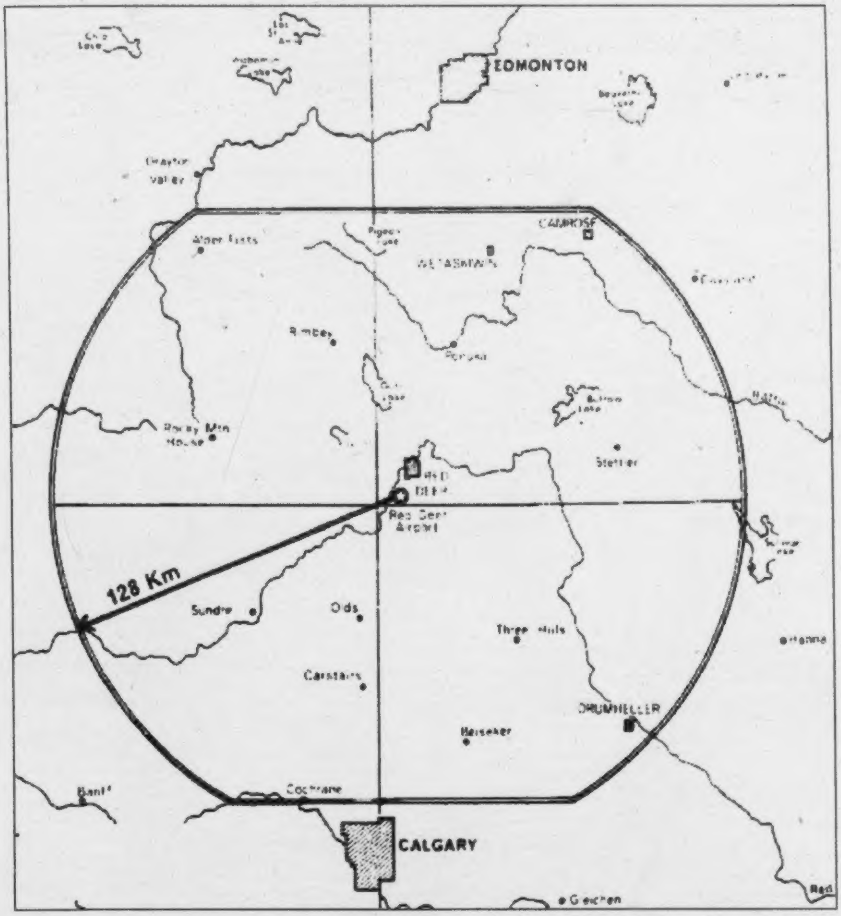
EDMONTON
Drayton Valley
Alder Flats
CAMROSE
WETASKIWIN
Rimbey
Ponoka
Buffalo Lake
Rocky Mtn House
Stettler
RED DEER
Red Deer Airport
128 Km
Sundre
Olds
Three Hills
Hanna
Carstairs
DRUMHELLER
Beiseker
Banff
Cochrane
CALGARY
Gleichen
Red

Figure 1.3: The Alberta Hail Project's principal target area between Edmonton and Calgary and centred on the radar site located at the Red Deer Industrial Airport.

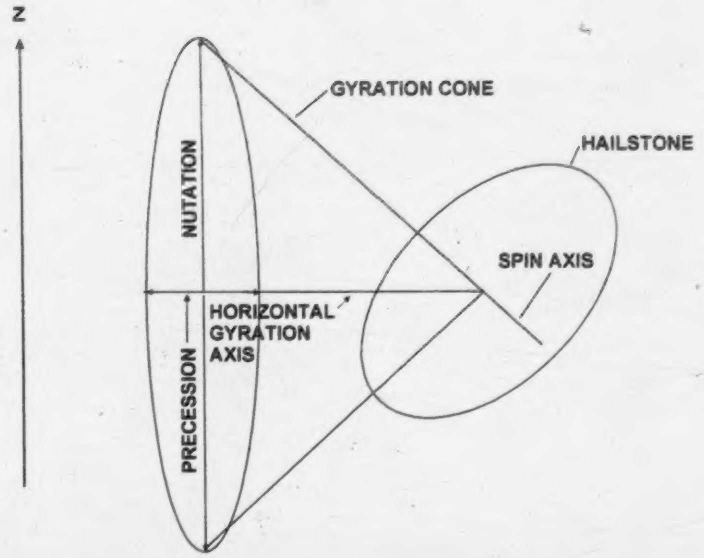
Z
GYRATION CONE
HAILSTONE
NUTATION
SPIN AXIS
HORIZONTAL GYRATION AXIS
PRECESSION

Figure 2.1: Schematic diagram of the tumbling motions of an oblate hailstone. The view of the hailstone is looking down its major axis (i.e. a "side view"), and is falling in the negative Z direction. The oblate hailstone spins about its minor axis (labelled "spin axis"), which in turn precesses/nutates, describing a horizontal (circular) cone ("gyration cone") with its apex located at the centre of the particle. Adapted from García-García and List (1992).

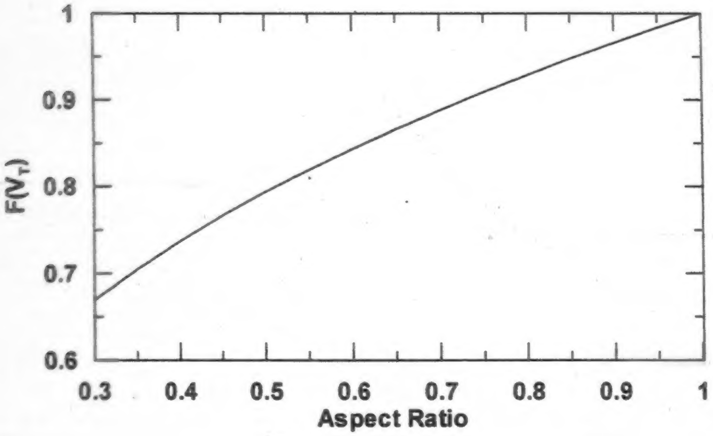

Figure 3.1: Ratio of terminal velocity of an oblate hailstone to that of a spherical hailstone of the same mass.

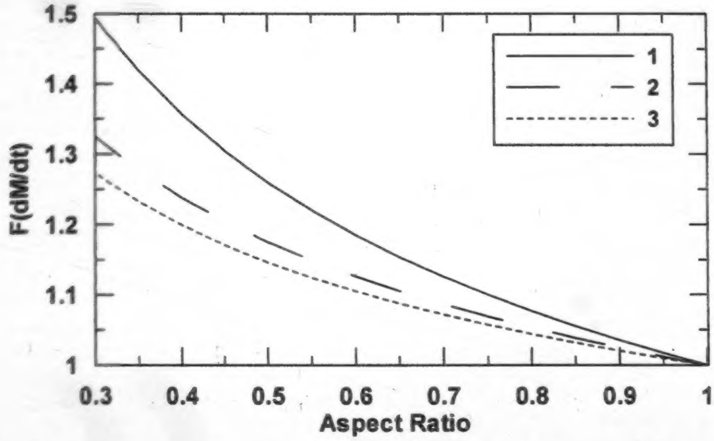

Figure 3.2: Ratio of the mass growth rate of an oblate hailstone to that of a spherical hailstone. Calculations are done for 3 cases: 1) Collection efficiency is constant (this case occurs when the hailstone is in a region where all cloud water is in the form of ice); 2) The hailstone is in a region where there is no cloud ice present and is not shedding (it may be undergoing either wet or dry growth); 3) The hailstone is assumed to be in the wet shedding growth regime, and there is no cloud ice present. In case 3, the following ambient conditions are assumed: $T_a = -15°C$, $\rho_a = 0.6$ kg m^{-3}, $\chi_w = 6$ g m^{-3}. The hailstone for which this calculation is done (case 3) is assumed to have a density of 900 kg m^{-3} and a mass of 3.77 g.

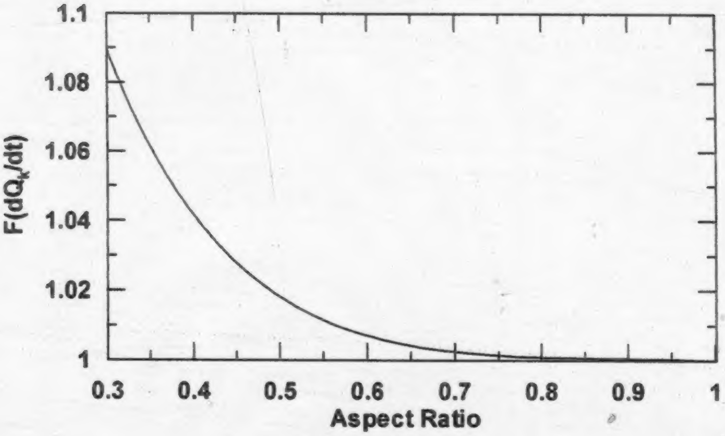

Figure 3.3: Ratio of rate of heat transfer by convection/conduction of an oblate hailstone to that of a spherical hailstone of the same mass.

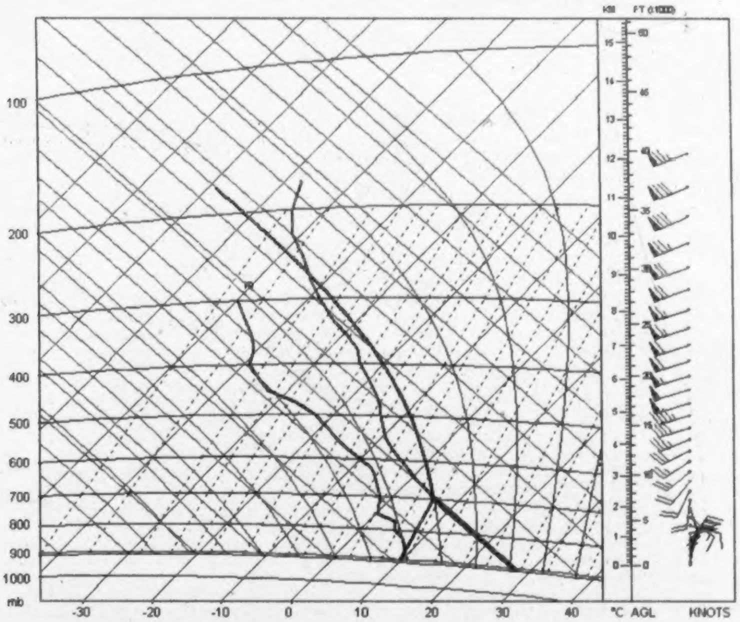

Figure 4.1: Upper-air sounding released from Penhold at 1715 LT on 11 July 1985 plotted on a tephigram. The dashed line represents the dewpoint profile, the solid line is the environmental temperature, and the curved solid line is the pseudoadiabat (based on the observed surface temperature and dewpoint).

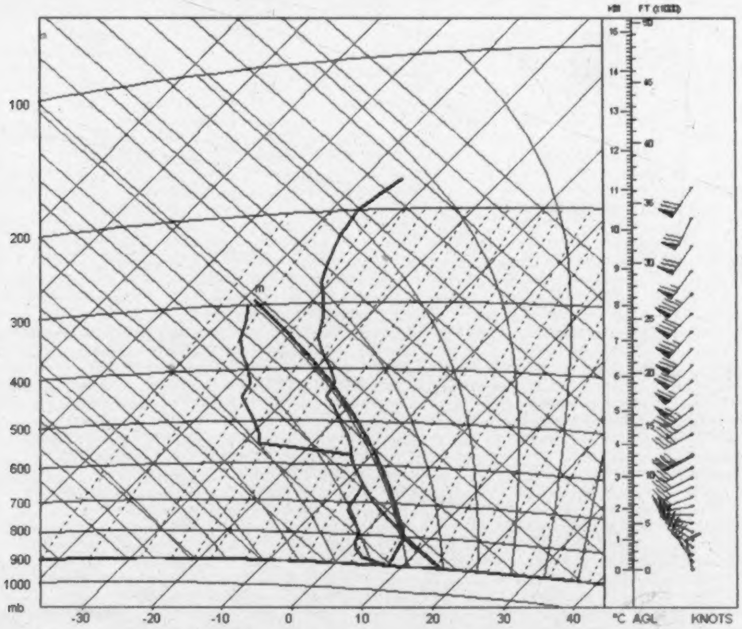

Figure 4.2: Upper-air sounding released from Penhold at 1715 LT on 6 July 1984 plotted on a tephigram. The dashed line represents the dewpoint profile, the solid line is the environmental temperature, and the curved solid line is the pseudoadiabat (based on the observed surface temperature and dewpoint).

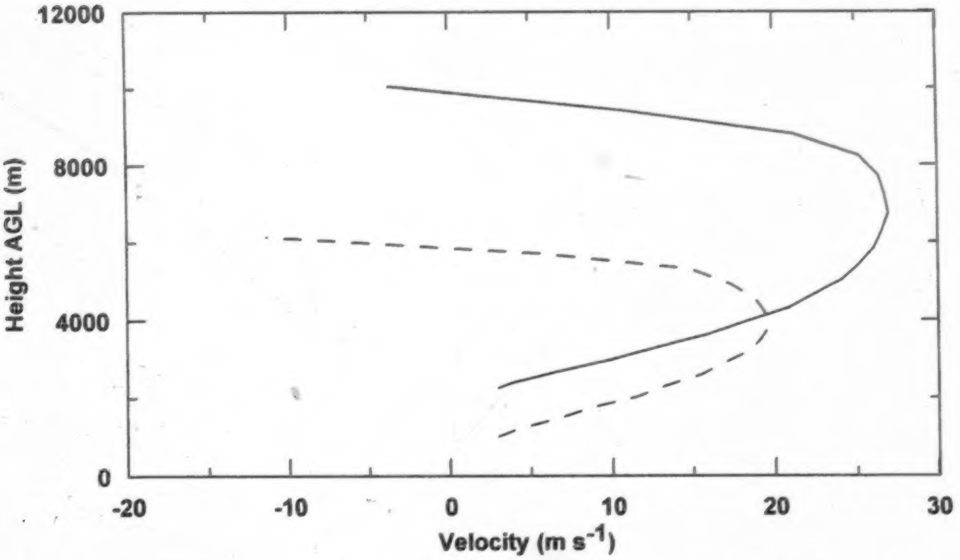

Figure 4.3: Model derived profiles of updraft velocity for 11 July 1985 (solid line) and 6 July 1984 (dashed line).

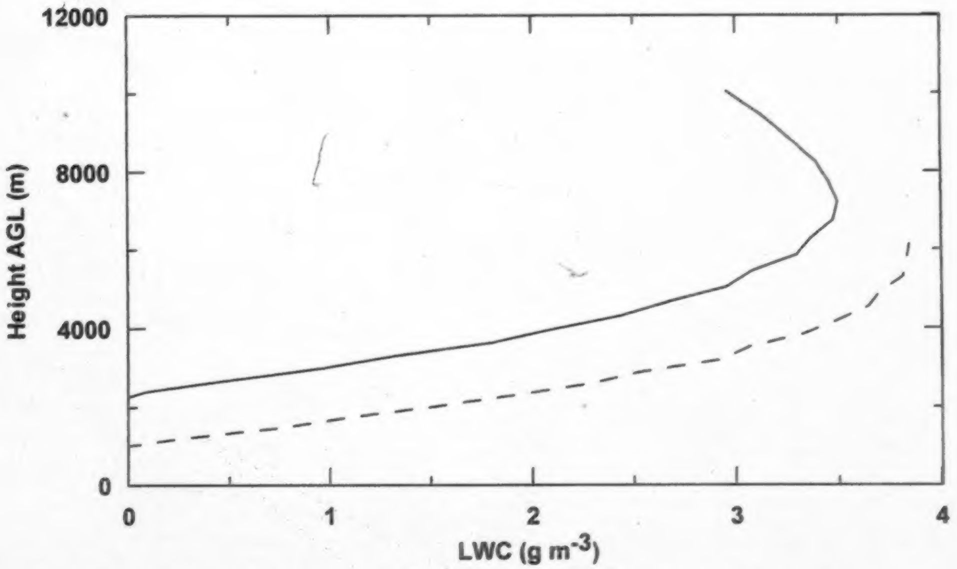

Figure 4.4: Model derived profiles of liquid water content (LWC) for 11 July 1985 (solid line) and 6 July 1984 (dashed line).

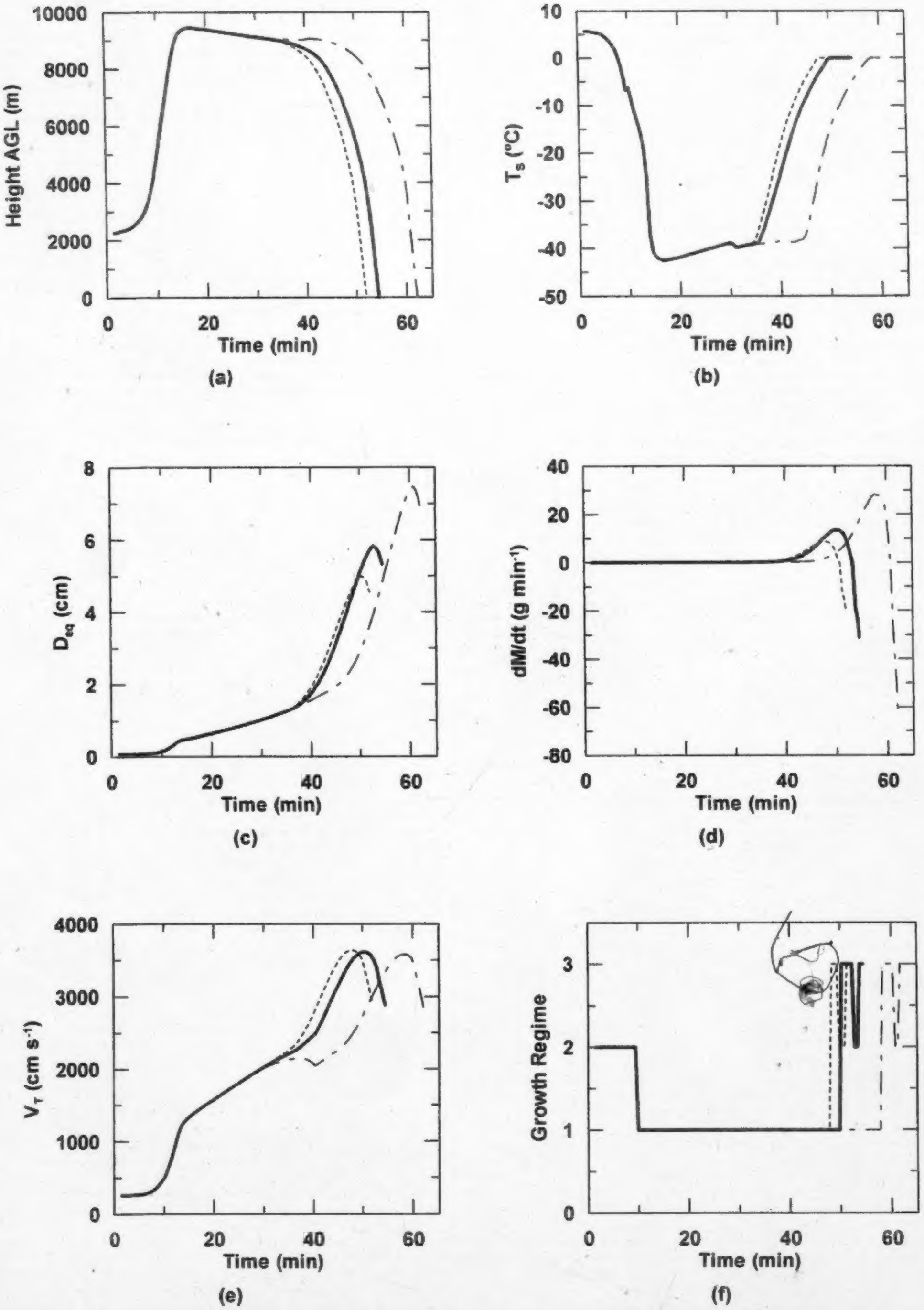

Figure 4.5: Growth time history of an oblate hailstone on 11 July 1985 for 3 different aspect ratios: α_c = 1 (dotted line), α_c = 0.77 (heavy black line), and α_c = 0.50 (dash-dotted line). Depicted are (a) Height (*Z*); (b) Hailstone temperature (T_S); (c) Equivalent diameter (D_{eq}); (d) Mass growth rate (*dM/dt*); (e) Terminal velocity (V_T); (f) Growth regime (1 = dry, 2 = wet, 3 = wet shedding).

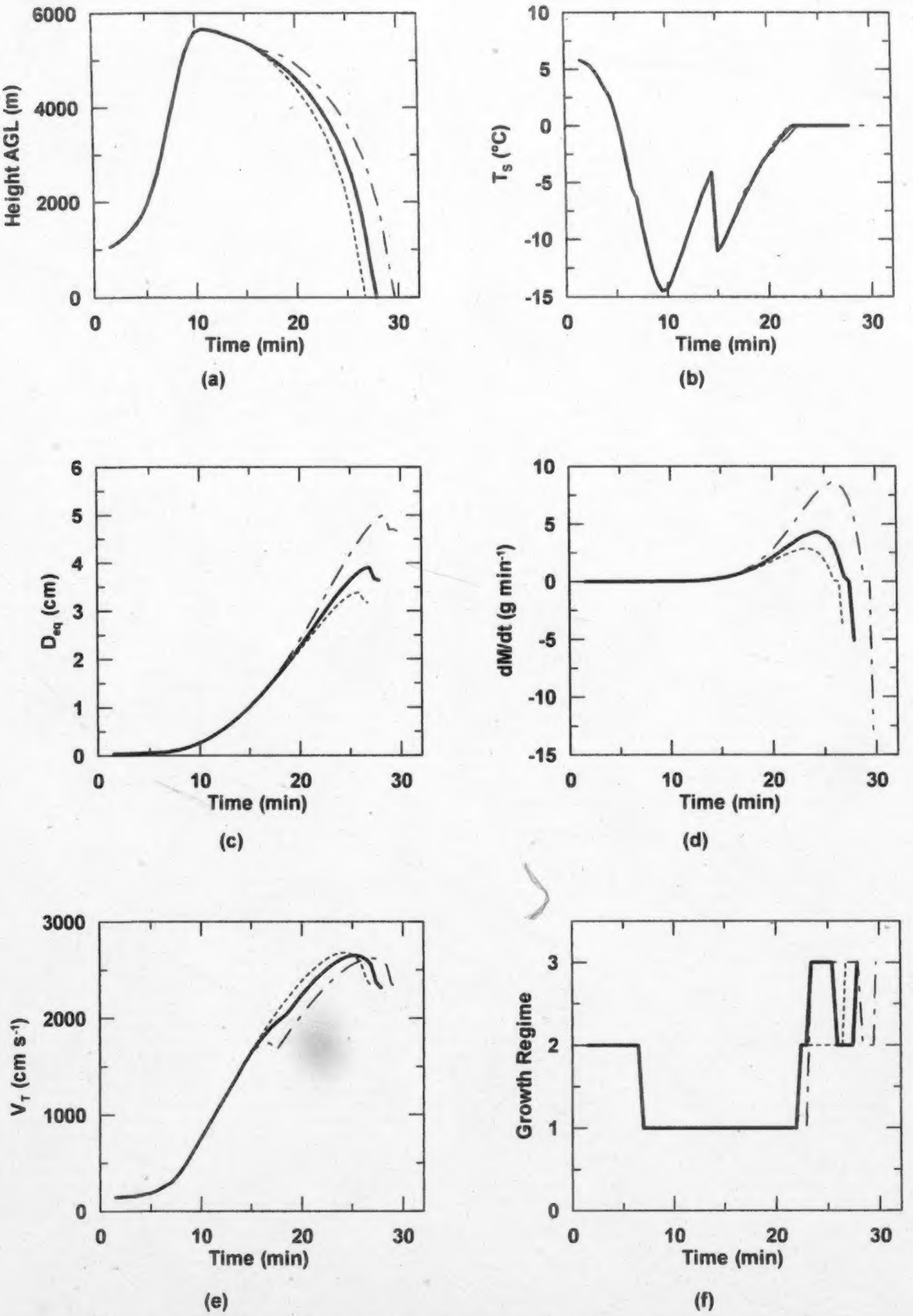

Figure 4.6: Growth time history of an oblate hailstone on 6 July 1984 for 3 different aspect ratios: $\alpha_c = 1$ (dotted line), $\alpha_c = 0.77$ (heavy black line), and $\alpha_c = 0.50$ (dash-dotted line). Depicted are (a) Height (*Z*); (b) Hailstone temperature (T_S); (c) Equivalent diameter (D_{eq}); (d) Mass growth rate (*dM/dt*); (e) Terminal velocity (V_T); (f) Growth regime (1 = dry, 2 = wet, 3 = wet shedding).

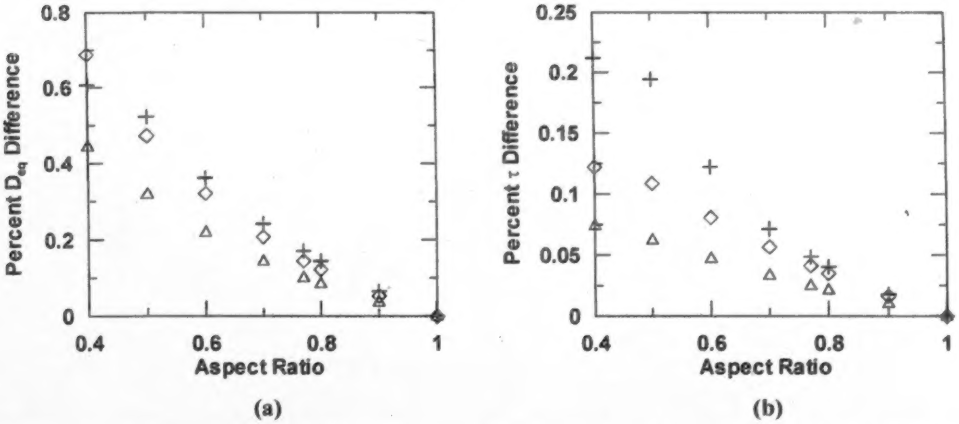

Figure 4.7: Percent increase in final equivalent diameter (a) and total growth time (b) as a function of aspect ratio for the two case study days: 11 July 1985 (crosses) and 6 July 1984 (diamonds). The corresponding average percent increases for all 20 severe hail days (triangles) are also shown.

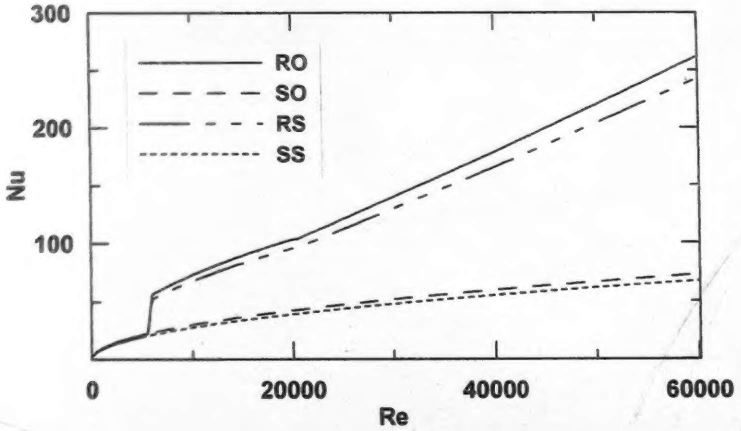

Figure 5.1: Nusselt number as a function of Reynolds number for 4 different types of hailstones: a rough oblate (RO) hailstone ($\alpha = 0.77$), a smooth oblate (SO) hailstone ($\alpha = 0.77$), a rough spherical (RS) hailstone and a smooth spherical (SS) hailstone. A Reynolds number of 10000 corresponds to an equivalent diameter of 1.2 cm for an ambient temperature of - 15°C, while a Reynolds number of 60000 corresponds to an equivalent diameter of 3.7 cm for the same ambient temperature.

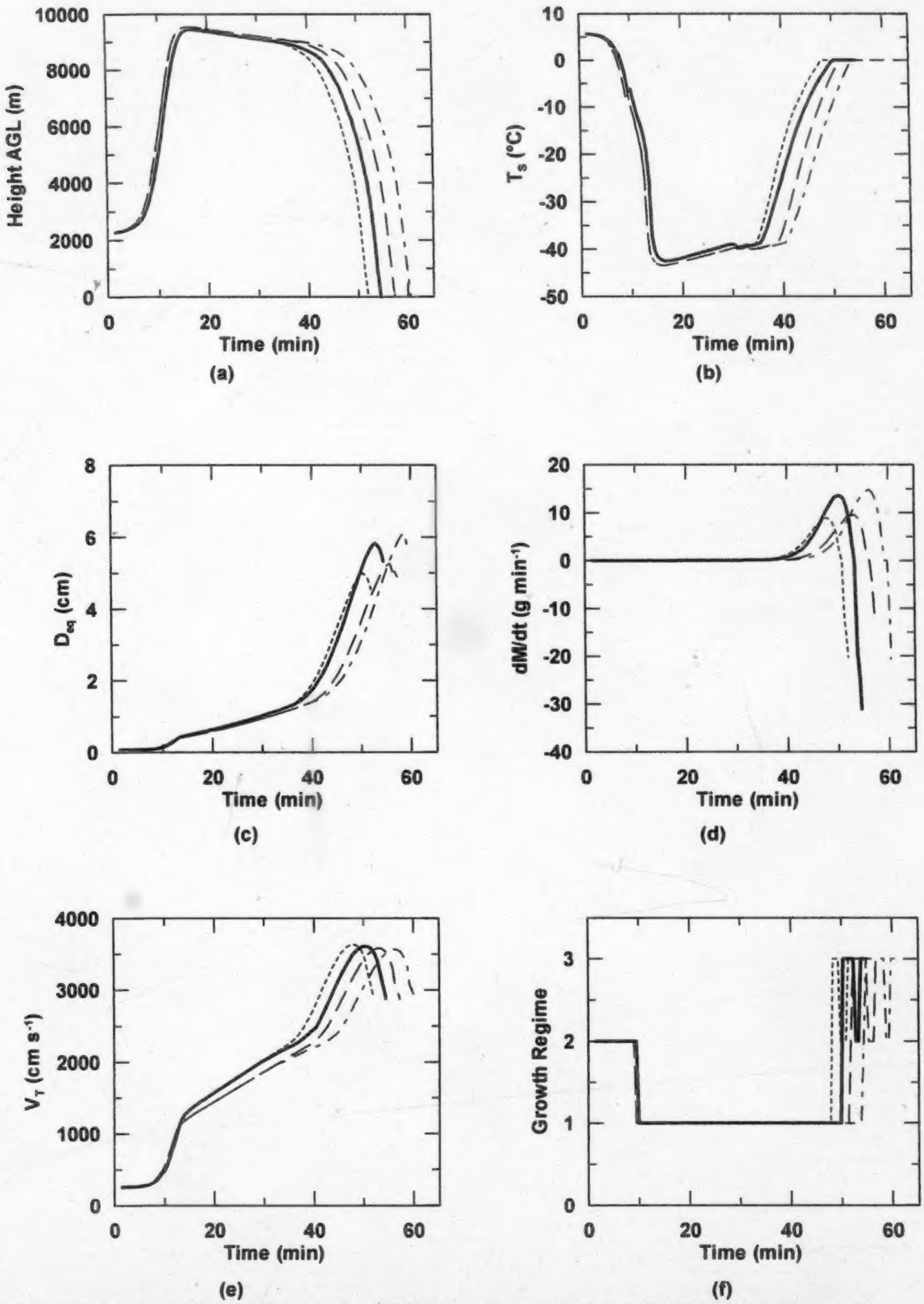

Figure 5.2: Growth time history of an oblate hailstone on 11 July 1985 for 4 cases: rough oblate (heavy solid line), rough spherical (dotted line), smooth oblate (dash-dotted line) and smooth spherical (dashed line). Depicted are (a) Height (*Z*); (b) Hailstone temperature (T_S); (c) Equivalent diameter (D_{eq}); (d) Mass growth rate (*dM/dt*); (e) Terminal velocity (V_T); (f) Growth regime (1 = dry, 2 = wet, 3 = wet shedding). For the oblate cases, hailstones are assumed to evolve to a constant aspect ratio of 0.77.

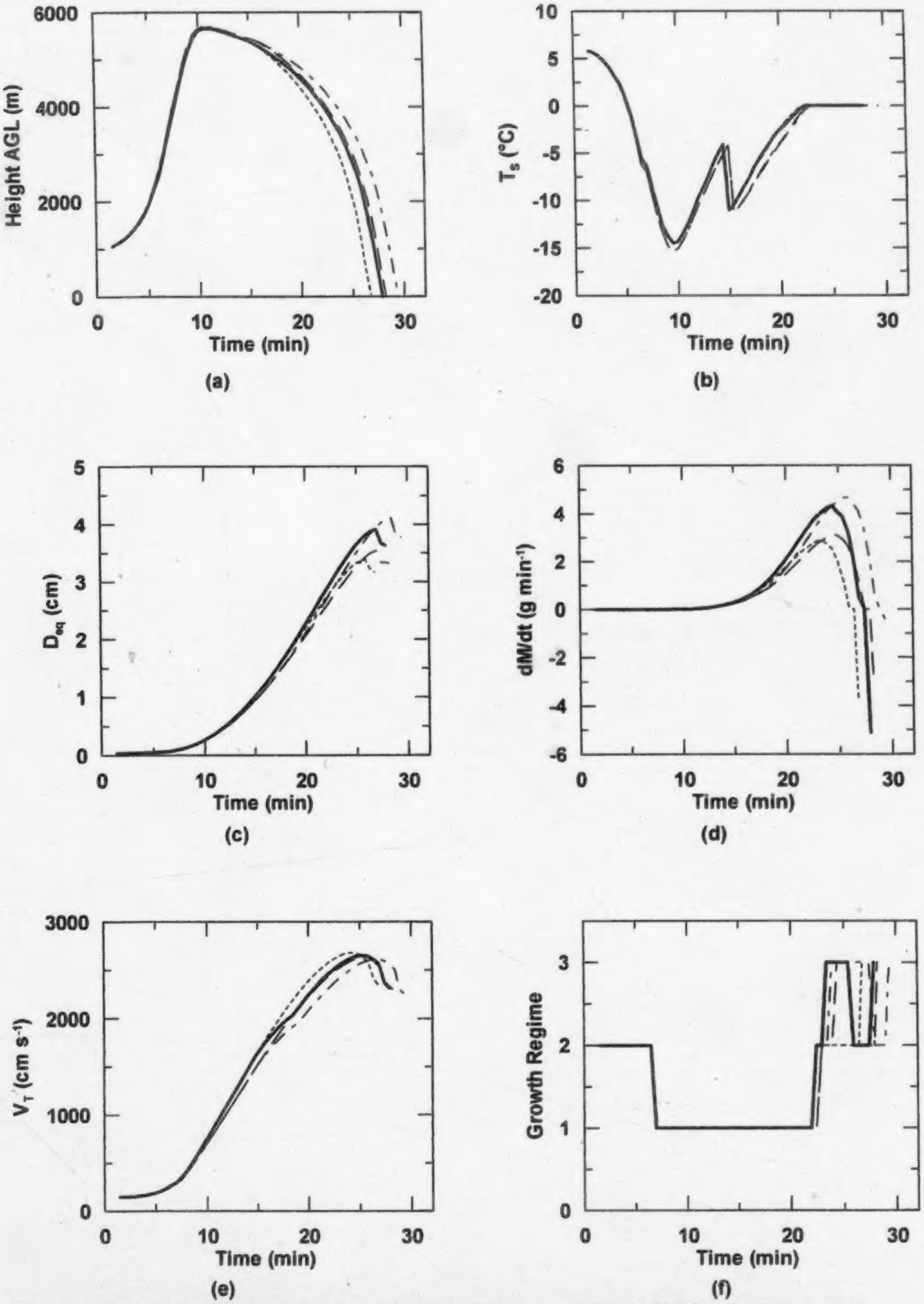

Figure 5.3: Growth time history of an oblate hailstone on 6 July 1984 for 4 cases: rough oblate (heavy solid line), rough spherical (dotted line), smooth oblate (dash-dotted line) and smooth spherical (dashed line). Depicted are (a) Height (*Z*); (b) Hailstone temperature (T_S); (c) Equivalent diameter (D_{eq}); (d) Mass growth rate (*dM/dt*); (e) Terminal velocity (V_T); (f) Growth regime (1 = dry, 2 = wet, 3 =wet shedding). For the oblate cases, hailstones are assumed to evolve to a constant aspect ratio of 0.77.

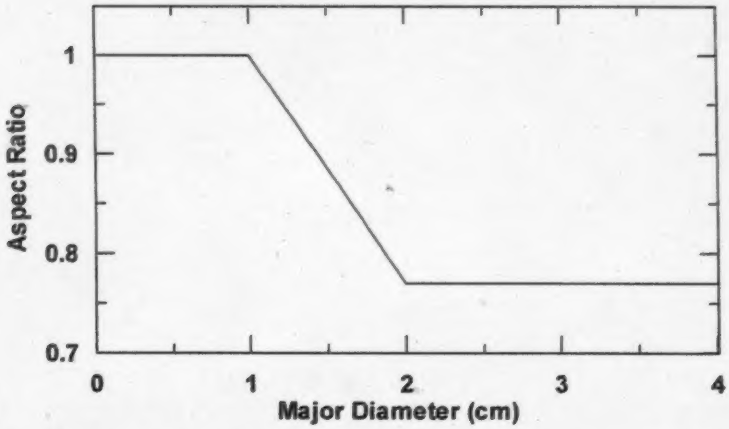

Figure 6.1: Aspect ratio as a function of hailstone major diameter for control values of D_1 = 1 cm, D_2 = 2 cm and α_c = 0.77.

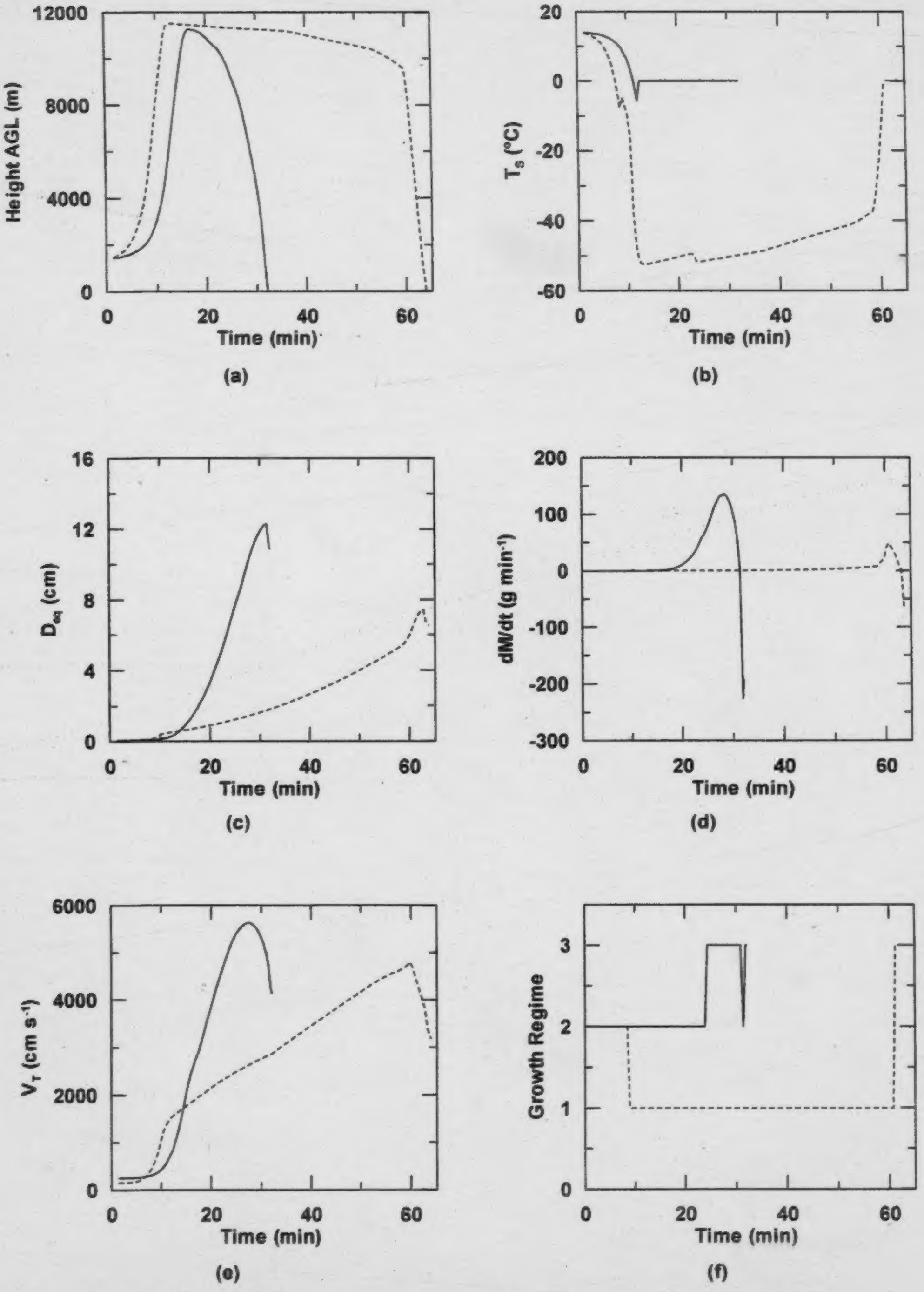

Figure 6.2: Growth time history of an average oblate hailstone on 28 July 1984 for 2 different embryo diameters: D_0 = 400 µm (dotted line) and D_0 = 700 µm (solid line). Depicted are (a) Height (Z); (b) Hailstone temperature (T_S); (c) Equivalent diameter (D_{eq}); (d) Mass growth rate (dM/dt); (e) Terminal velocity (V_T); (f) Growth regime (1 = dry, 2 = wet, 3 = wet shedding).

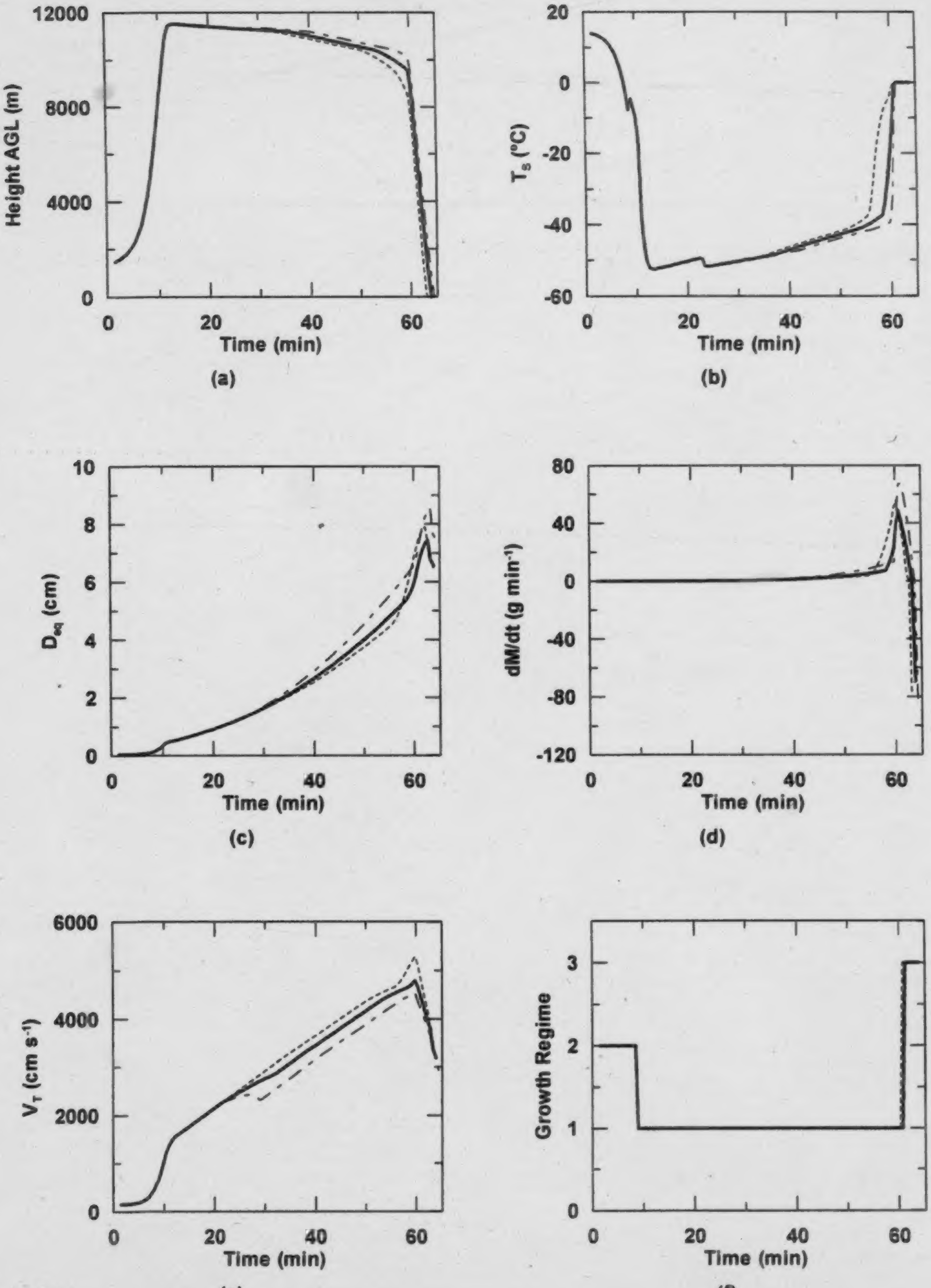

(a) (b)

(c) (d)

(e) (f)

Figure 6.3: Growth time history of an oblate hailstone on 28 July 1984 for 3 different aspect ratios: $\alpha_c = 1$ (dotted line), $\alpha_c = 0.77$ (heavy black line), and $\alpha_c = 0.50$ (dash-dotted line). Depicted are (a) Height (Z); (b) Hailstone temperature (T_S); (c) Equivalent diameter (D_{eq}); (d) Mass growth rate (dM/dt); (e) Terminal velocity (V_T); (f) Growth regime (1 = dry, 2 = wet, 3 = wet shedding). The embryo diameter is 400 μm and the storm duration is 60 minutes.

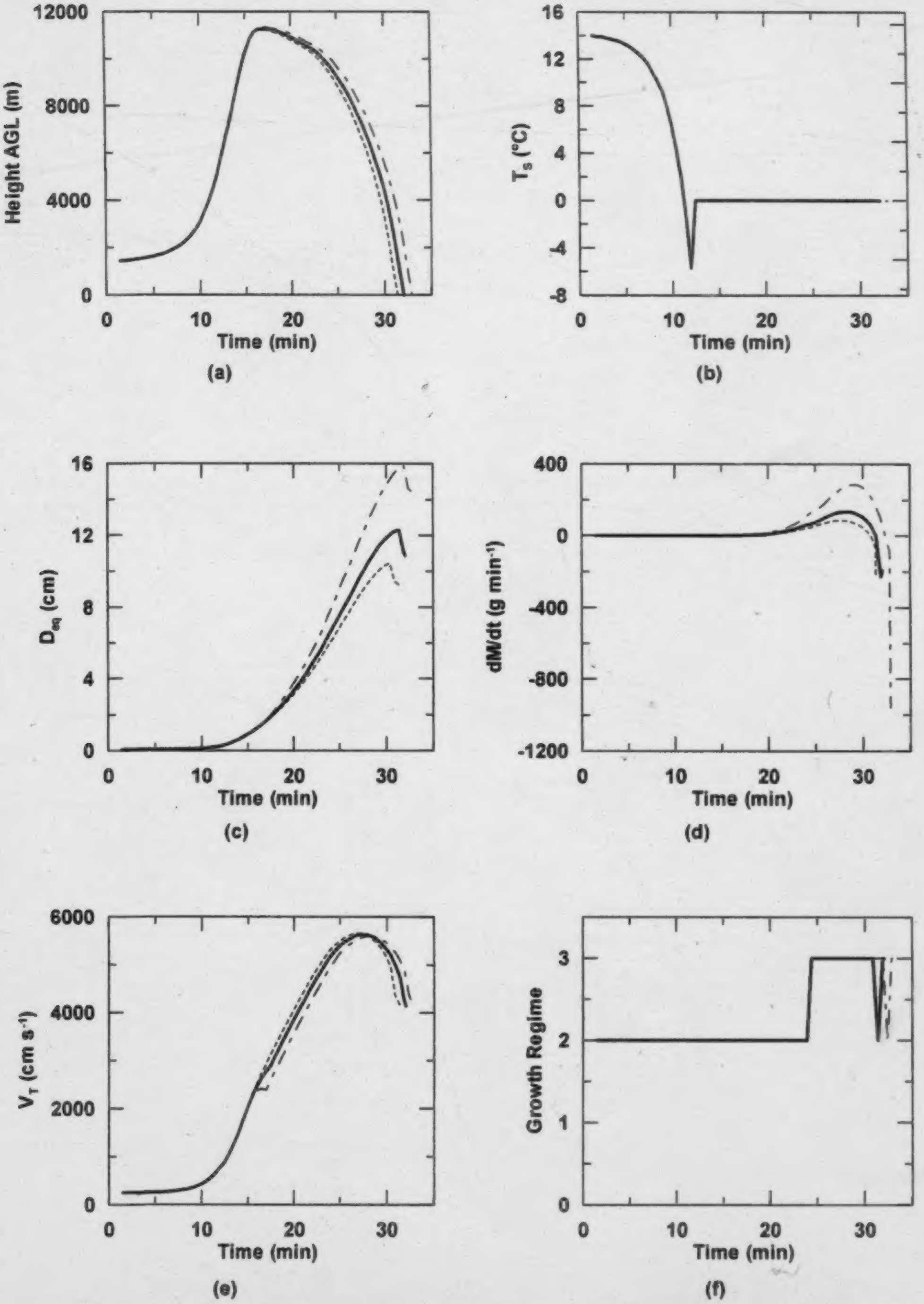

Figure 6.4: Growth time history of an oblate hailstone on 28 July 1984 for 3 different aspect ratios: $\alpha_c = 1$ (dotted line), $\alpha_c = 0.77$ (heavy black line), and $\alpha_c = 0.50$ (dash-dotted line). Depicted are (a) Height (*Z*); (b) Hailstone temperature (T_S); (c) Equivalent diameter (D_{eq}); (d) Mass growth rate (*dM/dt*); (e) Terminal velocity (V_T); (f) Growth regime (1 = dry, 2 = wet, 3 = wet shedding). The embryo diameter is 700 μm and the storm duration is 60 minutes.

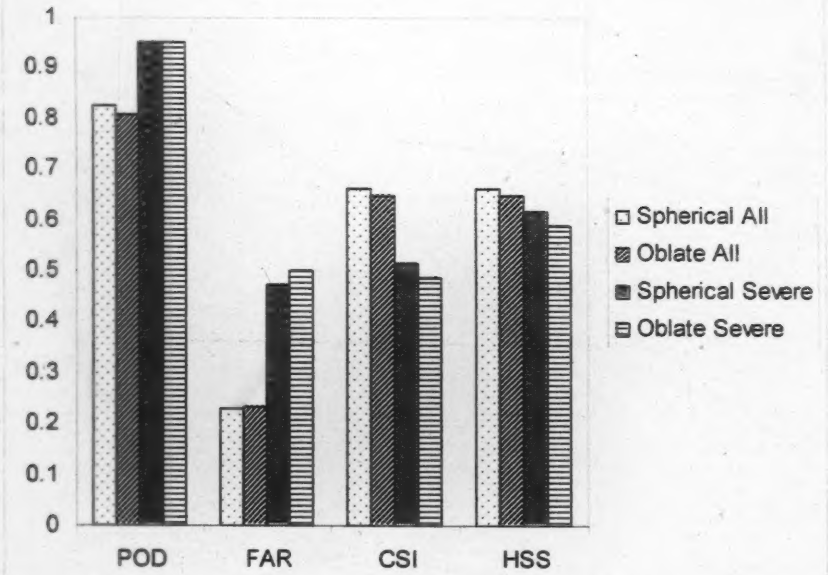

Figure 7.1: Summary of skill scores for the spherical and oblate versions of HC2 for 62 hail days ("All") and 20 severe hail days ("Severe") between 1983 and 1985.

TABLES

Table 4.1: Observed cloud parameters and maximum observed hail size along with cloud and hail model output from the control runs for our two case study days: 11 July 1985 and 6 July 1984.

	11-Jul-85	06-Jul-84
OBSERVED		
CAPE (J/kg)	761.2	454.1
Precipitable Water (cm)	2.18	1.49
Max. Radar Echo (dBZ)	60	50
CCL (m AGL)	2249	1514
Shear (s^{-1})	6.5E-03	5.7E-03
Bulk Richardson Number	7	3
Max. Observed Hail Size	Golfball	Golfball
CLOUD MODEL OUTPUT		
Max. Updraft Velocity (m/s)	27	19.7
Max. Liquid Water Content (g/m^3)	3.5	3.8
Cloud Base (m AGL)	2260	1010
Cloud Top (m AGL)	9415	5719
Duration (min)	60	46
HAIL MODEL OUTPUT		
Initial Embryo Diameter (μm)	700	400
Final Equivalent Spherical Diameter (cm)	5.3	3.9
Hailstone Size Category	Golfball	Golfball
Total Growth Time (min)	54.5	27.9

Table 4.2: Differences between the final maximum equivalent hailstone diameter (D_{eq}) and total growth time (τ) predicted by the oblate model (designated by D_{eq} and τ, respectively) and the corresponding parameters predicted by the model if the hailstone is assumed to remain spherical (designated by D_S and τ_S, respectively). The percent increases in equivalent diameter, total growth time, and kinetic energy (based on $K.E. \propto D_{eq}^4$) are also shown.

These percent increases are calculating by taking the differences between the oblate and spherical results and dividing by the spherical value.

Date (yyyymmdd)	D_{eq} - D_S (cm)	% D_{eq} Increase	τ - τ_S (min)	% τ Increase	% K.E. Increase
19830622	0.2	6.8%	0.4	0.7%	30.0%
19830624	-0.3	-4.2%	0.6	1.0%	-15.7%
19830706	1.2	17.3%	3.2	5.7%	89.0%
19830713	0.9	16.9%	3.5	6.9%	87.0%
19830721	0.2	6.6%	0.4	0.7%	28.9%
19830724	1.1	17.5%	0.8	2.1%	90.3%
19830803	0.2	3.7%	0.5	0.8%	15.6%
19830815	0.2	7.0%	0.4	0.6%	31.2%
19840625	0.5	15.9%	1.2	4.3%	80.2%
19840706	0.5	14.5%	1.1	4.1%	71.9%
19840712	1.0	17.0%	3.0	5.0%	87.4%
19840728	1.6	17.6%	0.6	2.1%	91.5%
19840806	0.3	7.5%	0.3	0.5%	33.8%
19840824	0.2	6.7%	0.4	0.7%	29.8%
19850623	0.0	0.8%	0.6	1.4%	3.4%
19850711	0.8	17.1%	2.5	4.9%	88.3%
19850712	0.3	11.1%	0.9	3.6%	52.4%
19850723	0.0	0.0%	0.1	0.5%	0.0%
19850804	0.2	7.3%	0.4	0.6%	32.3%
19850830	0.5	14.4%	0.9	3.5%	71.4%
Average	**0.5**	**10.1%**	**1.1**	**2.5%**	**49.9%**

Table 4.3: Final equivalent diameter (D_{eq}) at ground and total evolution time (τ) as a function of minimum aspect ratio (α_c) for (a) 11 July 1985 and (b) 6 July 1984. Also shown are the percent increase in D_{eq} compared to that of the final diameter attained by a spherical hailstone ($\%D_{eq} = (D_{eq}(\alpha_c) - D(\alpha = 1))/D(\alpha = 1)$), the percent increase in τ compared to that of the growth time of a spherical hailstone ($\%\tau = (\tau(\alpha_c) - \tau(\alpha = 1))/\tau(\alpha = 1)$), and the percent increase in kinetic energy (K.E.) compared to that of a spherical hailstone, assuming $K.E. \propto D_{eq}^4$. Control values are in boldface.

α_c	D_{eq} (cm)	τ (min)	% D_{eq} Increase	% τ Increase	% K.E. Increase
1.00	4.6	52.0	0.0%	0.0%	0.0%
0.90	4.9	52.9	6.6%	1.8%	29.1%
0.80	5.2	54.1	14.5%	4.1%	71.9%
0.77	**5.3**	**54.5**	**17.1%**	**4.9%**	**88.3%**
0.70	5.7	55.7	24.2%	7.2%	137.8%
0.60	6.2	58.4	36.3%	12.2%	244.8%
0.50	6.9	62.1	52.3%	19.4%	438.1%
0.40	7.3	63.0	60.7%	21.2%	566.2%

(a)

α_c	D_{eq} (cm)	τ (min)	% D_{eq} Increase	% τ Increase	% K.E. Increase
1.00	3.2	26.8	0.0%	0.0%	0.0%
0.90	3.3	27.2	5.4%	1.6%	23.2%
0.80	3.6	27.7	12.3%	3.5%	59.1%
0.77	**3.6**	**27.9**	**14.5%**	**4.1%**	**71.9%**
0.70	3.8	28.3	20.8%	5.7%	113.1%
0.60	4.2	28.9	32.2%	8.1%	205.2%
0.50	4.7	29.7	47.3%	10.9%	371.0%
0.40	5.4	30.0	68.8%	12.2%	711.3%

(b)

Table 4.4: Average final equivalent diameter at ground ($<D_{eq}>$) and average total evolution time ($<\tau>$) as a function of minimum aspect ratio (α_c) for all 20 severe hail days from 1983 to 1985. Also shown are the average percent increase in D_{eq} compared to that of the final diameter attained by a spherical hailstone ($\langle \%D_{eq} \rangle = \langle (D_{eq}(\alpha_c) - D(\alpha = 1))/D(\alpha = 1) \rangle$) and the average percent increase in τ compared to that of the growth time of a spherical hailstone ($\langle \%\tau \rangle = \langle (\tau(\alpha_c) - \tau(\alpha = 1))/\tau(\alpha = 1) \rangle$). The average percent increase in kinetic energy, K.E., has also been calculated (in the same manner as the other averages) assuming $K.E. \propto D_{eq}^4$. Control values are in boldface.

α_c	$<D_{eq}>$ (cm)	$<\tau>$ (min)	<% D_{eq}> Increase	<% τ> Increase	<% K.E.> Increase
1.00	4.3	47.7	0.0%	0.0%	0.0%
0.90	4.4	48.1	3.7%	1.0%	16.0%
0.80	4.7	48.6	8.5%	2.1%	40.6%
0.77	**4.7**	**48.7**	**10.1%**	**2.5%**	**49.9%**
0.70	4.9	49.1	14.4%	3.3%	76.8%
0.60	5.3	49.7	21.9%	4.7%	134.8%
0.50	5.8	50.3	31.8%	6.2%	237.3%
0.40	6.4	50.8	44.4%	7.4%	411.9%

Table 5.1: Comparison of selected results for experiments *RO*, *SO*, *RS* and *SS*. Final equivalent diameter (D_{eq}) and total growth time (τ) are shown for the two case study days (11 July 1985 and 6 July 1984).

Date	Experiment	D_{eq} (cm)	τ (min)
11/07/1985	*RO*	5.3	54.5
	SO	5.7	60.5
	RS	4.6	52.0
	SS	4.9	57.3
06/07/1984	*RO*	3.6	27.9
	SO	3.8	29.4
	RS	3.2	26.8
	SS	3.3	28.2

Table 5.2: Contributions of the total effect, the effect of roughness, the effect of oblateness, and the mutual interaction effect towards the final maximum equivalent diameter (D_{eq}) of a hailstone for each of the 20 severe hail days between 1983 and 1985. Values are in percentages and were derived using the factor separation technique. The averages of each of the four effects for all 20 severe hail days are also shown.

DATE	TOTAL EFFECT	PURE ROUGHNESS EFFECT	PURE OBLATENESS EFFECT	MUTUAL INTERACTION EFFECT
22/06/1983	13.36%	6.16%	6.51%	0.68%
24/06/1983	17.01%	22.11%	9.18%	-14.29%
06/07/1983	15.63%	-1.38%	12.59%	4.43%
13/07/1983	12.67%	-3.65%	15.28%	1.04%
21/07/1983	12.46%	5.54%	6.23%	0.69%
24/07/1983	15.81%	-1.40%	5.12%	12.09%
03/08/1983	14.45%	10.38%	8.13%	-4.06%
15/08/1983	12.04%	4.68%	7.02%	0.33%
25/06/1984	8.81%	-6.08%	14.29%	0.61%
06/07/1984	9.34%	-4.52%	13.86%	0.00%
12/07/1984	21.40%	3.77%	-9.76%	27.40%
28/07/1984	79.08%	52.22%	7.08%	19.77%
06/08/1984	13.24%	5.29%	7.35%	0.59%
24/08/1984	12.31%	5.22%	6.72%	0.37%
23/06/1985	23.20%	22.16%	4.12%	-3.09%
11/07/1985	9.00%	-6.95%	16.36%	-0.41%
12/07/1985	1.89%	-8.30%	11.32%	-1.13%
23/07/1985	3.74%	3.74%	0.00%	0.00%
04/08/1985	12.58%	4.97%	6.95%	0.66%
30/08/1985	8.31%	-5.34%	13.95%	-0.30%
AVERAGE	**15.82%**	**5.43%**	**8.11%**	**2.27%**

Table 5.3: Contributions of the total effect, the effect of roughness, the effect of oblateness, and the mutual interaction effect towards the total growth time (τ) of a hailstone for each of the 20 severe hail days between 1983 and 1985. Values are in percentages and were derived using the factor separation technique. The averages of each of the four effects for all 20 severe hail days are also shown.

DATE	TOTAL EFFECT	PURE ROUGHNESS EFFECT	PURE OBLATENESS EFFECT	MUTUAL INTERACTION EFFECT
22/06/1983	-0.31%	-1.01%	0.69%	0.00%
24/06/1983	-0.53%	-1.48%	0.42%	0.53%
06/07/1983	-3.83%	-9.00%	2.17%	3.01%
13/07/1983	-3.63%	-9.84%	4.84%	1.37%
21/07/1983	-0.29%	-0.95%	0.73%	-0.07%
24/07/1983	-32.96%	-34.33%	2.65%	-1.28%
03/08/1983	-0.46%	-1.22%	0.51%	0.25%
15/08/1983	-0.26%	-0.82%	0.64%	-0.08%
25/06/1984	-1.31%	-5.41%	4.38%	-0.28%
06/07/1984	-1.17%	-5.11%	4.22%	-0.28%
12/07/1984	-1.42%	-6.13%	2.06%	2.65%
28/07/1984	-49.91%	-50.93%	0.58%	0.44%
06/08/1984	-0.29%	-0.78%	0.57%	-0.08%
24/08/1984	-0.24%	-0.89%	0.62%	0.03%
23/06/1985	-1.49%	-2.88%	0.94%	0.46%
11/07/1985	-4.85%	-9.28%	5.51%	-1.08%
12/07/1985	-0.92%	-4.37%	3.73%	-0.28%
23/07/1985	-1.26%	-1.77%	0.51%	0.00%
04/08/1985	-0.30%	-0.89%	0.65%	-0.06%
30/08/1985	-1.20%	-4.51%	3.60%	-0.28%
AVERAGE	**-5.33%**	**-7.58%**	**2.00%**	**0.25%**

Table 6.1: Sensitivity experiments showing the effect of changing the major diameter at which the hailstone's aspect ratio begins to decrease (D_1) and the major diameter beyond which the hailstone's aspect ratio remains constant at 0.77 (D_2) for each of two severe hail days: 11 July 1985 and 6 July 1984. The averages for all severe hail days are also shown. Control values are in boldface.

		19850711		19840706		All Severe Days	
D_1 (cm)	D_2 (cm)	D_{eq} (cm)	τ (min)	D_{eq} (cm)	τ (min)	$\langle D_{eq} \rangle$ (cm)	$\langle \tau \rangle$ (min)
D_f	1.5	5.3	55.2	3.7	27.6	4.8	48.6
D_f	2.0	5.3	54.8	3.7	27.7	4.8	48.6
D_f	2.5	5.3	54.4	3.6	27.8	4.8	48.7
D_f	3.0	5.3	54.2	3.6	27.8	4.7	48.6
D_f	3.5	5.3	54.0	3.5	27.7	4.7	48.6
1.0	1.5	5.3	55.9	3.7	27.8	4.8	48.8
1.0	**2.0**	**5.3**	**54.5**	**3.6**	**27.9**	**4.7**	**48.7**
1.0	2.5	5.3	54.0	3.6	27.9	4.7	48.7
1.0	3.0	5.3	53.8	3.5	27.9	4.7	48.7
1.0	3.5	5.3	53.7	3.5	27.8	4.7	48.6
1.5	2.0	5.3	53.6	3.6	27.9	4.7	48.7
1.5	2.5	5.3	53.5	3.6	27.9	4.7	48.7
1.5	3.0	5.3	53.4	3.5	27.9	4.7	48.7
1.5	3.5	5.2	53.3	3.4	27.7	4.6	48.6
2.0	2.5	5.3	53.4	3.5	27.9	4.7	48.7
2.0	3.0	5.3	53.3	3.4	27.8	4.6	48.6
2.0	3.5	5.2	53.3	3.3	27.6	4.6	48.5

Table 6.2: Sensitivity experiments showing the effect of varying the collection efficiency of ice (E_i) on final equivalent diameter (D_{eq}) and total growth time (τ) of an average oblate hailstone for the two case study days (11 July 1985 and 6 July 1984) and for the averages of all severe hail days. Control values are highlighted in boldface.

	19850711		19840706		All Severe Hail Days	
E_i	D_{eq} (cm)	τ (min)	D_{eq} (cm)	τ (min)	D_{eq} (cm)	τ (min)
0.10	1.9	66.9	3.6	27.9	3.0	51.6
0.11	1.9	66.9	3.6	27.9	3.0	51.6
0.12	3.3	64.9	3.6	27.9	3.3	51.1
0.13	4.2	63.8	3.6	27.9	3.4	50.9
0.14	5.0	62.9	3.6	27.9	3.6	50.7
0.15	5.4	61.9	3.6	27.9	3.8	50.4
0.16	5.4	60.4	3.6	27.9	4.1	50.1
0.17	5.3	58.7	3.6	27.9	4.3	49.8
0.18	5.3	57.2	3.6	27.9	4.5	49.5
0.19	5.3	55.8	3.6	27.9	4.6	49.1
0.20	**5.3**	**54.5**	**3.6**	**27.9**	**4.7**	**48.7**
0.21	5.3	53.4	3.6	27.9	4.9	48.4
0.22	5.3	52.3	3.6	27.9	5.1	48.0
0.23	5.3	51.4	3.6	27.9	5.3	47.6
0.24	5.3	50.5	3.6	27.9	5.4	47.2
0.25	5.3	49.6	3.6	27.9	5.5	46.8

Table 6.3: Sensitivity experiments showing the effect of varying the median volume cloud droplet radius (r_d) on final equivalent diameter (D_{eq}) and total growth time (τ) of an average oblate hailstone for the two case study days (11 July 1985 and 6 July 1984) and for the averages of all severe hail days. Control values are highlighted in boldface.

	19850711		19840706		All Severe Hail Days	
r_d (μm)	D_{eq} (cm)	τ (min)	D_{eq} (cm)	τ (min)	D_{eq} (cm)	τ (min)
20.4	5.2	55.1	3.6	28.6	4.5	50.6
25.5	**5.3**	**54.5**	**3.6**	**27.9**	**4.7**	**48.7**
30.6	5.4	54.1	3.7	27.5	4.8	48.6

Table 6.4: Sensitivity experiments showing the effect of varying the hailstone ice density (ρ_H) on final equivalent diameter (D_{eq}) and total growth time (τ) of an average oblate hailstone for the two case study days (11 July 1985 and 6 July 1984) and for the averages of all severe hail days. Control values are highlighted in boldface.

	19850711		19840706		All Severe Hail Days	
ρ_H (g cm^{-3})	D_{eq} (cm)	τ (min)	D_{eq} (cm)	τ (min)	D_{eq} (cm)	τ (min)
0.80	6.0	56.3	4.1	28.0	5.1	50.6
0.85	5.7	55.4	3.9	28.0	4.9	50.4
0.90	**5.3**	**54.5**	**3.6**	**27.9**	**4.7**	**48.7**

Table 6.5: Sensitivity experiments showing the effect of varying the initial embryo diameter (D_0) on final equivalent diameter (D_{eq}) and total growth time (τ) of an average oblate hailstone for the two case study days (11 July 1985 and 6 July 1984) as well as for 28 July 1984. The chosen control values for each case are highlighted in boldface. The embryo diameter for each severe hail day was chosen to both maximize final equivalent diameter while minimizing total growth time.

	19850711		19840706		19840728	
D_0 (μm)	D_{eq} (cm)	τ (min)	D_{eq} (cm)	τ (min)	D_{eq} (cm)	τ (min)
100	1.9	66.8	3.6	29.8	4.3	65.2
200	4.2	63.8	3.6	28.4	5.4	64.6
300	5.4	61.9	3.6	27.9	5.9	64.2
400	5.3	59.3	**3.6**	**27.9**	6.5	63.9
500	5.3	57.1	3.6	28.0	7.4	63.5
600	5.3	55.4	3.6	28.5	8.0	63.3
700	**5.3**	**54.5**	3.6	29.3	**10.9**	**32.1**
800	5.3	56.2	3.6	31.2	10.9	35.3

Table 6.6: Comparison of the final diameter at ground (D), hailstone size category and total growth time (τ) for (spherical) hailstones evolving under the HAILCAST shedding and terminal velocity schemes and for spherical hailstones evolving under the HC2 shedding and terminal velocity schemes. All HC2 runs were done using the control parameter values for HAILCAST in order to facilitate easy comparison. The observed hail size category and corresponding representative diameter are also shown for each severe hail day. (P = PEA, GR = GRAPE, W = WALNUT, G = GOLFBALL, >G = >GOLFBALL).

	Observed		HAILCAST			HC2 Spherical (H1 parameter values)		
Date (yyyymmdd)	D (cm)	Size Category	D (cm)	Size Category	τ (min)	D (cm)	Size Category	τ (min)
19830622	2.7	W	2.3	W	57.9	2.7	W	57.5
19830624	2.7	W	4.7	G	64.0	5.9	>G	63.7
19830706	4.3	G	4.3	G	60.0	7.2	>G	55.9
19830713	2.7	W	4.4	G	56.5	5.6	>G	52.0
19830721	2.7	W	2.2	W	55.4	2.7	W	54.9
19830724	4.3	G	5.4	>G	56.5	6.3	>G	54.7
19830803	4.3	G	3.4	G	64.8	4.3	G	64.5
19830815	4.3	G	2.2	W	65.7	2.9	W	65.3
19840625	2.7	W	2.7	W	27.7	3.1	W	27.3
19840706	4.3	G	2.9	W	26.9	3.2	W	26.4
19840712	2.7	W	4.4	G	63.4	5.9	>G	62.2
19840728	6.4	>G	5.3	G	63.7	7.6	>G	62.9
19840806	4.3	G	2.6	W	65.5	3.2	W	65.2
19840824	2.7	W	2.0	GR	66.5	2.5	W	66.1
19850623	4.3	G	1.5	GR	43.0	1.7	GR	42.1
19850711	4.3	G	3.9	G	62.7	4.6	G	58.4
19850712	2.7	W	1.6	GR	25.4	2.5	W	23.5
19850723	2.7	W	1.1	P	23.8	1.2	P	23.2
19850804	6.4	>G	2.1	GR	66.6	2.8	W	66.1
19850830	2.7	W	3.0	W	27.2	3.3	W	26.3

Table 6.7: The difference in final hail diameter and total growth time of the HC2 and HAILCAST terminal velocity/shedding schemes. The abbreviation H2 refers to HC2 predictions and H1 refers to HAILCAST predictions. Also shown are the percent increases in final diameter and total growth time when our model (HC2) is used compared with the original HAILCAST. The averages for all 20 severe hail days are shown, and our case study days are highlighted in boldface.

Date (yyyymmdd)	$D_{H2} - D_{H1}$ (cm)	% D Increase	$\tau_{H2} - \tau_{H1}$ (min)	% τ Increase
19830622	0.4	17.2%	-0.4	-0.7%
19830624	1.2	26.2%	-0.3	-0.5%
19830706	2.8	64.7%	-4.2	-6.9%
19830713	1.2	26.0%	-4.5	-7.9%
19830721	0.5	24.9%	-0.5	-0.8%
19830724	0.9	16.6%	-1.8	-3.2%
19830803	0.9	27.5%	-0.3	-0.5%
19830815	0.6	28.3%	-0.4	-0.6%
19840625	0.4	13.9%	-0.4	-1.4%
19840706	**0.3**	**11.5%**	**-0.5**	**-1.9%**
19840712	1.5	33.6%	-1.2	-1.8%
19840728	2.2	41.9%	-0.8	-1.2%
19840806	0.7	27.1%	-0.3	-0.5%
19840824	0.5	25.9%	-0.4	-0.6%
19850623	0.2	11.3%	-1.0	-2.2%
19850711	**0.6**	**16.0%**	**-4.3**	**-6.8%**
19850712	0.9	59.6%	-1.9	-7.6%
19850723	0.1	8.3%	-0.6	-2.5%
19850804	0.8	36.1%	-0.5	-0.7%
19850830	0.3	8.3%	-0.9	-3.5%
AVERAGE	**0.9**	**26.2%**	**-1.3**	**-2.6%**

Table 7.1: Fractional difference, f_D, between a hailstone's major diameter and its equivalent diameter, as a function of aspect ratio, α.

α	1.00	0.90	0.80	0.70	0.60	0.50	0.40
f_D	0.0%	3.6%	7.7%	12.6%	18.6%	26.0%	35.7%

Table 7.2: Differences in hailstone size category that result when major diameter, D, is used to classify hailstones instead of equivalent diameter, D_{eq}. For an oblate hailstone with an aspect ratio of 0.77 and for one with an aspect ratio of 0.50, the major diameter is calculated for hailstones with equivalent diameters that represent the average of each size category, and then again for those with equivalent diameters that represent the upper limit of each size category. Then, a new size category is assigned to each oblate hailstone, based on its major diameter.

		α=0.77		α=0.50	
Category	**D_{eq} (cm)**	**D (cm)**	**New Category**	**D (cm)**	**New Category**
Shot	0.2	0.2	Shot	0.3	Shot
	0.4	0.4	Pea	0.5	Pea
Pea	0.8	0.9	Pea	1.0	Pea
	1.2	1.3	Grape	1.5	Grape
Grape	1.7	1.8	Grape	2.1	Walnut
	2.0	2.2	Walnut	2.5	Walnut
Walnut	2.7	2.9	Walnut	3.3	Golfball
	3.2	3.5	Golfball	4.0	Golfball
Golfball	4.3	4.6	Golfball	5.4	> Golfball
	5.3	5.8	>Golfball	6.7	>Golfball

Table 7.3: Summary of maximum equivalent diameter at ground predicted by the spherical and oblate versions of HC2 compared to the actual size categories (given as ranges of equivalent diameter values in cm) observed on the 20 severe hail days between 1983 and 1985.

Date (dd/mm/yyyy)	Observed Size Range (cm)	Oblate Model	Spherical Model
		D_{eq} (cm)	D (cm)
22/06/1983	2.1 - 3.3	3.3	3.1
24/06/1983	2.1 - 3.3	6.9	7.2
06/07/1983	3.3 - 5.3	8.4	7.1
13/07/1983	2.1 - 3.3	6.5	5.6
21/07/1983	2.1 - 3.3	3.3	3.1
24/07/1983	3.3 - 5.3	7.5	6.4
03/08/1983	3.3 - 5.3	5.1	4.9
15/08/1983	3.3 - 5.3	3.4	3.1
25/06/1984	2.1 - 3.3	3.6	3.1
06/07/1984	3.3 - 5.3	3.6	3.2
12/07/1984	2.1 - 3.3	7.1	6.1
28/07/1984	≥ 5.3	10.9	9.2
06/08/1984	3.3 - 5.3	3.9	3.6
24/08/1984	2.1 - 3.3	3.0	2.8
23/06/1985	3.3 - 5.3	2.4	2.4
11/07/1985	3.3 - 5.3	5.3	4.6
12/07/1985	2.1 - 3.3	2.7	2.4
23/07/1985	2.1 - 3.3	1.1	1.1
04/08/1985	≥ 5.3	3.4	3.2
30/08/1985	2.1 - 3.3	3.7	3.2
AVERAGE		**4.7**	**4.3**

Table 7.4: 2 × 2 contingency tables used to derive the skill scores of hail forecasts for the oblate and spherical versions of HC2 for 62 hail days.

		HC2 OBLATE		HC2 SPHERICAL	
		Forecast		Forecast	
		Hail	No Hail	Hail	No Hail
Observed	Hail	50 (H)	12 (M)	51 (H)	11 (M)
	No Hail	15 (FA)	83 (N)	15 (FA)	83 (N)

Table 7.5: Skill scores the HC2 spherical and oblate hail models for 62 hail days and for 20 severe hail days between 1983 and 1985.

	All Hail Days		Severe Hail Days	
	Oblate	Spherical	Oblate	Spherical
POD	0.81	0.82	0.95	0.95
FAR	0.23	0.23	0.50	0.47
CSI	0.65	0.66	0.49	0.51
HSS	0.65	0.66	0.59	0.62

Table 7.6: Hail-size forecast performance of the HC2 spherical and oblate model versions for 62 hail days and 20 severe hail days between 1983 and 1985.

	Hail Days		Severe Hail Days	
Hail Size Category	**Oblate (%)**	**Spherical (%)**	**Oblate (%)**	**Spherical (%)**
Correct	31%	34%	45%	50%
Within one	63%	63%	80%	75%
One too small	11%	15%	10%	15%
Two or more too small	19%	19%	5%	10%
One too large	21%	15%	25%	10%
Two or more too large	18%	18%	15%	15%